NASA CR-72377

SEVENTH QUARTERLY REPORT

ELECTROCHEMICAL CHARACTERIZATION OF NONAQUEOUS SYSTEMS FOR SECONDARY BATTERY APPLICATION

November 1967 - January 1968

by

M. Shaw, O. A. Paez, D. A. Lufkin, A. H. Remanick

prepared for

NATIONAL AERONAUTICS AND SPACE ADMINISTRATION

February 16, 1968

CONTRACT NAS 3-8509

Technical Management
Space Power Systems Division
National Aeronautics and Space Administration
Lewis Research Center, Cleveland, Ohio
Mr. Robert B. King

NARMCO RESEARCH AND DEVELOPMENT DIVISION

OF

WHITTAKER CORPORATION
3540 Aero Court
San Diego, California 92123

TABLE OF CONTENTS

CYCLIC VOLTAMMOGRAMS

LIST OF TABLES

LIST OF FIGURES*

* Other than Cyclic Voltammograms

ELECTROCHEMICAL CHARACTERIZATION OF NONAQUEOUS SYSTEMS FOR SECONDARY BATTERY APPLICATION

by

M. Shaw, O. A. Paez, A. H. Remanick, D. A. Lufkin

ABSTRACT

Multisweep cyclic voltammograms have now been obtained for over 950 systems comprising silver, copper, nickel, cobalt, zinc, cadmium, molybdenum, indium, iron, vanadium, chromium, and manganese electrodes in acetonitrile, butyrolactone, dimethylformamide, and propylene carbonate solutions of chlorides, perchlorates, and fluorides. This completes the screening of the positive plate - electrolyte combinations. Twenty-four systems are recommended on the basis of their electrochemical characteristics at the molecular level of the electrode reaction.

SUMMARY

The electrochemical characterization of nonaqueous battery systems by multisweep cyclic voltammetry has been continued. Cyclic voltammograms are now available on over 950 systems comprising silver, copper, nickel, cobalt, zinc, cadmium, molybdenum, indium, iron, vanadium, chromium, and manganese in chloride, perchlorate, and fluoride solutions of acetonitrile, butyrolactone, dimethylformamide, and propylene carbonate. Solutes consist primarily of $AlCl_3$, LiCl, $MgCl_2$, $CaCl_2$, $Mg(ClO_4)_2$, $LiClO_4$, MgF_2, $LiPF_6$, KPF_6, $Mg(PF_6)_2$, $Ca(PF_6)_2$, $LiBF_4$, $Mg(BF_4)_2$, and $Ca(BF_4)_2$.

During this reporting period, cyclic voltammograms were obtained on fluorinated electrodes of zinc, cadmium, indium, and iron. In general, iron fluoride systems exhibited only anodic peaks or none at all. Although indium fluoride gave both anodic and cathodic peaks, the peak displacement was usually in excess of 0.5 v.

A list of twenty-four recommended systems is presented. In order to lessen this to a workable number, a micro-compatability test was devised, consisting of the potentiostatic discharge of electrodes after various periods of wet stand time following a sweep charge. Evidence exists that this test may not be valid, because apparent loss of discharge capacity on stand cannot be explained by electrode dissolution in the electrolyte.

INTRODUCTION

The purpose of this program is to conduct a molecular level screening by the cyclic voltammetric method on a large number of electrochemical systems in nonaqueous electrolytes, and to characterize them as to their suitability for use in high energy density secondary batteries.

Since the release and storage of energy in a battery is initiated at the molecular level of the reaction, and therefore dependent on the charge and mass transfer processes, it is essential that screening be conducted at this level, in order to eliminate those systems whose electrode processes are inadequate for secondary battery operation.

I. CYCLIC VOLTAMMETRY

A. ANALYSIS OF CYCLIC VOLTAMMOGRAMS

Table I lists the conductivities of the solutions used in preparing the electrochemical systems screened during this quarter. The systems screened are shown in Tables II and III, representing a total of 97 systems. To date, cyclic voltammograms have been obtained for over 950 different positive-electrolyte combinations.

Curve analysis was accomplished by dividing all systems into two major groups:

1. Systems involving chloride and perchlorate electrolytes.
2. Systems involving fluoride electrolytes.

Each main group was then subdivided according to the identity of the working electrode. Each of these subgroups was further broken down according to the identity of the solvent portion of the solution. The cyclic voltammograms are then discussed in terms of the total solution. This classification facilitates data analysis, and has permitted a more significant correlation among the electrochemical systems.

Except in those cases where the metal is converted to a cathodic material prior to assembly in the measuring cell, the working electrode is the base metal itself. During the voltage sweep, the metal is oxidized to some anodic product which serves as the cathode subsequently reduced during the cathodic portion of the sweep. Each sweep cycle thus corresponds to a charge-discharge cycle. In the absence of complicating factors, it is assumed that chloride cathodes would be formed in chloride electrolytes, and fluoride cathodes in fluoride electrolytes.

Each cyclic voltammogram is identified by a CV number and labelled according to the electrochemical system, sweep rate, temperature, and zero reference representing the open circuit voltage (ocv) of the working electrode with respect to the indicated reference electrode. The current axis is in units of ma/cm^2, each unit being of variable scale depending on the X-Y recorder sensitivity setting. A maximum sensitivity of 0.1 $ma/cm^2/cm$ division has been established to avoid exaggerating the current background of poor systems. The sweep is always in a clockwise direction, the potential becoming more positive to the right. Positive currents represent anodic (charge) reactions, and negative currents represent cathodic (discharge) reactions. The voltage axis units are relative to the ocv so that voltage units are in terms of electrode polarization.

For comparative purposes, current density magnitude is classified according to very high (more than 300 ma/cm^2), high (100-300 ma/cm^2), medium high (50-100 ma/cm^2), medium low (10-50 ma/cm^2), low (1-10 ma/cm^2), and very low (less than 1 ma/cm^2).

Analysis is based on the cyclic voltammograms obtained at the lowest sweep rate, 40 mv/sec, except where additional information is required from the higher sweep rate curves to aid in the analysis.

TABLE I

ELECTROLYTE CONDUCTIVITY*

Electrolyte	Molality m	Conductivity $ohm^{-1} cm^{-1}$
Dimethylformamide-$LiClO_4$	1.0	2.6×10^{-2}
Dimethylformamide-KPF_6	0.75	2.1×10^{-2}
Dimethylformamide-$Mg(ClO_4)_2$	0.75	2.0×10^{-2}
Dimethylformamide-$AlCl_3$+LiCl	0.5 (1)	1.0×10^{-2}
Dimethylformamide-$LiPF_6$	0.5	9.0×10^{-3}
Dimethylformamide-LiCl	0.5	7.7×10^{-3}
Dimethylformamide-$LiBF_4$	0.5	7.3×10^{-3}
Dimethylformamide-$MgCl_2$	0.5	7.0×10^{-3}
Propylene carbonate-$LiClO_4$	1.0	5.8×10^{-3}
Propylene carbonate-$AlCl_3$+$LiClO_4$	0.5 (1)	5.6×10^{-3}
Propylene carbonate-KPF_6	0.75	4.5×10^{-3}
Dimethylformamide-$CaCl_2$	<0.25 (s)	5.3×10^{-3}
Propylene carbonate-$LiBF_4$	0.5	2.9×10^{-3}
Propylene carbonate-$Ca(PF_6)_2$	<0.5 (s)	2.8×10^{-3}
Dimethylformamide-$Mg(PF_6)_2$	<0.5 (s)	2.8×10^{-3}
Dimethylformamide-$Mg(BF_4)_2$	<0.5 (s)	2.4×10^{-3}
Propylene carbonate-$Mg(PF_6)_2$	<0.25 (s)	2.4×10^{-3}
Dimethylformamide-PF_5	0.5	2.2×10^{-3}
Dimethylformamide-$Ca(PF_6)_2$	<0.5 (s)	1.9×10^{-3}
Dimethylformamide-$Ca(BF_4)_2$	<0.5 (s)	1.9×10^{-3}
Propylene carbonate-LiCl+$LiClO_4$	(2)	1.4×10^{-3}
Propylene carbonate-PF_5	0.5	1.3×10^{-3}
Propylene carbonate-$Ca(BF_4)_2$	<0.5 (s)	8.2×10^{-4}
Propylene carbonate-$Mg(BF_4)_2$	<0.25 (s)	7.3×10^{-4}
Dimethylformamide-BF_3	<0.5 (s)	7.0×10^{-4}
Propylene carbonate-$CaCl_2$	<0.25 (s)	6.9×10^{-4}

* In order of decreasing conductivity
(s) Saturated
(1) Concentration with respect to each salt
(2) 0.05 m $LiClO_4$, saturated with LiCl

TABLE II

ELECTROCHEMICAL SYSTEMS SCREENED

CHLORIDE AND PERCHLORATE ELECTROLYTES

Solvent / Solute	Dimethylformamide	Propylene carbonate
$LiCl$	ZnF_2, CdF_2, InF_3, FeF_3	
$LiCl+LiClO_4$		ZnF_2, CdF_2, InF_3, FeF_3
$LiClO_4$	ZnF_2, CdF_2, InF_3, FeF_3	ZnF_2, CdF_2, InF_3, FeF_3
$MgCl_2$	ZnF_2, CdF_2, InF_3	
$Mg(ClO_4)_2$	ZnF_2, CdF_2, InF_3, FeF_3	
$CaCl_2$	ZnF_2, CdF_2, InF_3, FeF_3	ZnF_2, CdF_2, InF_3, FeF_3
$AlCl_3+LiCl$	ZnF_2, CdF_2, InF_3, FeF_3	
$AlCl_3+LiClO_4$		ZnF_2, CdF_2, InF_3, FeF_3

TABLE III

ELECTROCHEMICAL SYSTEMS SCREENED

FLUORIDE ELECTROLYTES

Solvent / Solute	Dimethylformamide	Propylene carbonate
PF_5	ZnF_2, CdF_2, FeF_3	ZnF_2, CdF_2, InF_3, FeF_3
KPF_6	ZnF_2, CdF_2, InF_3, FeF_3	
$LiPF_6$	ZnF_2, CdF_2, InF_3, FeF_3	ZnF_2, CdF_2, InF_3
$Mg(PF_6)_2$	ZnF_2, CdF_2, InF_3	ZnF_2, InF_3, FeF_3
$Ca(PF_6)_2$	ZnF_2, CdF_2, InF_3, FeF_3	ZnF_2, CdF_2, InF_3, FeF_3
BF_3	ZnF_2, CdF_2, InF_3, FeF_3	
$LiBF_4$	ZnF_2, CdF_2, InF_3, FeF_3	ZnF_2, CdF_2, InF_3, FeF_3
$Mg(BF_4)_2$	ZnF_2, CdF_2	ZnF_2, CdF_2, InF_3, FeF_3
$Ca(BF_4)_2$	ZnF_2, CdF_2, InF_3, FeF_3	ZnF_2, CdF_2, InF_3, FeF_3

a. Systems Involving Chloride and Perchlorate Electrolytes

(1) Zinc Fluoride Electrode

(a) Dimethylformamide solutions

The cyclic voltammogram for zinc fluoride in $LiClO_4$ solution is shown in Figure 1 (CV-3700). The curve is similar to that for the base metal (Ref. 1, p. 38) obtained earlier except that peak current densities are about twice as large in the present case.

Zinc fluoride in $Mg(ClO_4)_2$ solution shows a single, sharp, medium low anodic peak and a broad low current density cathodic peak. The shape of the curve is significantly different from that of zinc metal in this electrolyte, and the peak current densities are less by an order of magnitude. The cyclic voltammogram is shown in Figure 2 (CV-3670).

Zinc fluoride electrodes in $AlCl_3$+LiCl solution show broad, high anodic peaks and medium low cathodic peaks. The anodic area is one hundred times larger than the cathodic area. Earlier work on zinc metal indicated anodic voltage overload. This suggests that fluorination reduces the effective surface decreasing the extent of the anodic reaction. The results for zinc fluoride in LiCl solution are similar to those in $AlCl_3$+LiCl solution. Earlier work indicated that zinc metal in LiCl solution results in current overload due to extensive anodic activity. Similar behavior results for zinc fluoride in $MgCl_2$ solution. Tests on zinc fluoride electrodes in $CaCl_2$ solution result in anodic voltage overload. Cathodic current was negligible.

(b) Propylene carbonate solutions

The cyclic voltammogram for zinc fluoride in $AlCl_3$+$LiClO_4$ solution shows low cathodic activity and an anodic peak of medium low current density. Similar results were obtained for the base metal in previous work. Low anodic, and very low cathodic activity, are observed for zinc fluoride in LiCl+$LiClO_4$ solution. Similar results are obtained in $LiClO_4$ and $CaCl_2$ solutions.

(2) Cadmium Fluoride Electrode

(a) Dimethylformamide solutions

The cyclic voltammogram for cadmium fluoride in $LiClO_4$ solution shows broad multi-peak anodic and cathodic activity in the low current density range. Anodic and cathodic areas are equal. Earlier work with cadmium metal indicated very high anodic and cathodic current densities. Similar results are observed in $Mg(ClO_4)_2$ solution, in that very low anodic and cathodic activity results for the fluorinated metal, whereas the metal itself shows very high activity.

Cadmium fluoride in LiCl solutions shows very low anodic and cathodic peaks compared with very high anodic and medium high cathodic activity for cadmium metal alone. Low anodic and cathodic activity is found in $MgCl_2$ and $AlCl_3$+LiCl solutions, which is comparable to the behavior of cadmium metal. The curve for cadmium fluoride in $CaCl_2$ solution shows very low anodic and cathodic activity. Earlier work on the base metal shows high anodic and cathodic peaks.

(b) Propylene carbonate solutions

Cadmium fluoride electrodes in $LiClO_4$ and in $CaCl_2$ solutions show very low electrochemical activity, compared with current overload in $LiClO_4$ and voltage overload in $CaCl_2$ solutions for cadmium metal. Cadmium fluoride in LiCl+$LiClO_4$ solution shows low anodic and cathodic activity. Curves are not reproducible and the current decreases on cycling. Low anodic and cathodic activity had also been found for cadmium metal. Cadmium fluoride electrodes in $AlCl_3$+$LiClO_4$ solution show very low anodic and cathodic activity, whereas curves for cadmium metal obtained previously show peaks in the medium high range.

(3) Indium Fluoride Electrode

(a) Dimethylformamide solutions

Indium fluoride shows excessive anodic dissolution in $LiClO_4$ solution. The

solution turned black at about the third cycle, and the anodic current increased rapidly to greater than 300 ma/cm^2, at which time it dropped to a low value. Examination revealed that the working electrode had dissolved and fallen off. Indium fluoride in $Mg(ClO_4)_2$ solution shows high anodic and low, broad cathodic peaks. The curve is similar to that obtained earlier for indium metal. In LiCl and $CaCl_2$ solutions, the curves for indium fluoride show decreasing cathodic peak height with decreasing sweep rate, indicating soluble cathodic reactants. Similar results were obtained with indium metal in these electrolytes. Indium fluoride in $MgCl_2$ solution shows very high anodic and medium low cathodic current densities. Sweep rate behavior was not obtained because of anodic voltage overload at the high sweep rate.

Indium fluoride in $AlCl_3$+LiCl solution shows high anodic activity over a broad voltage range and low cathodic activity. Sweep rate behavior indicates soluble cathodic reactants.

(b) Propylene carbonate solutions

The cyclic voltammogram for indium fluoride in $LiClO_4$ solution is shown in Figure 3 (CV-3665). The curve is almost identical to that for the base metal (Ref. 1, p. 49). Broad, single anodic and cathodic peaks with 1 volt separation between them are observed in each case. The peak currents for the fluorinated electrode fall in the medium high anodic and medium low cathodic current range, and are twenty percent lower than obtained for indium metal. Voltage overload is obtained in LiCl+$LiClO_4$ solution in both the anodic and cathodic directions. The curve for indium fluoride in $AlCl_3$+$LiClO_4$ solution is almost identical to that obtained previously for indium metal. The cyclic voltammogram for the fluoride electrode is shown in Figure 4 (CV-3799). Sharp, medium low anodic peak, and broad, low cathodic peaks, occur for both metal and fluoride systems. Indium fluoride electrodes in $CaCl_2$ solutions result in anodic voltage overload, the cathodic sweep was not recorded. The base metal indicated anodic and cathodic voltage overload.

(4) Iron Fluoride Electrode

(a) Dimethylformamide solutions

Iron fluoride in $LiClO_4$ solution shows very low anodic and cathodic activity. Earlier work with iron metal showed a sharp, high anodic peak and negligible cathodic activity (Ref. 1, p. 50). Iron fluoride in LiCl, $CaCl_2$, $Mg(ClO_4)_2$, and $AlCl_3$+$LiClO_4$ solutions show very low anodic and cathodic activity. These results are significantly different from those obtained for the corresponding iron metal systems, where anodic activity in the medium low to very high range was indicated.

(b) Propylene carbonate solutions

Iron fluoride in $LiClO_4$ solution shows very low anodic and cathodic activity, which is comparable to behavior of iron metal. Iron fluoride electrodes in $CaCl_2$, LiCl+$LiClO_4$ and $AlCl_3$+$LiClO_4$ solutions show very low anodic and cathodic activity. Similar results were reported earlier for iron metal in these electrolytes.

b. Systems Involving Fluoride Electrolytes

(1) Zinc Fluoride Electrode

(a) Dimethylformamide solutions

Results on zinc fluoride in PF_5 solution show sharp anodic and cathodic peaks, increasing steadily with cycling until voltage overload occurred. A cyclic voltammogram obtained prior to instrument overload is shown in Figure 5 (CV-3971). Voltage overload with very high anodic and cathodic currents densities was reported earlier with zinc metal. The cyclic voltammogram for zinc fluoride in $LiPF_6$ solution is shown in Figure 6 (CV-3599). The curve shows a single medium low anodic and cathodic peaks separated by about 400 mv, and a coulombic ratio of 0.16. Peak heights for zinc electrodes in this electrolyte (Ref. 1, p. 54) are twenty times larger than that found for the fluorinated metal.

The sweep curve for the system, ZnF_2/DMF-KPF_6 shows sharp, very high anodic and cathodic peaks with only 30 mv separation. The curve is shown in Figure 7 (CV-3684). A steady increase in peak height occurs during the preliminary phase of the cycling (i.e., first ten cycles). The curve is similar to that reported earlier (Ref. 1, p. 52) for zinc metal in this electrolyte.

Broad, medium low, anodic and cathodic peaks with 700 mv separation result for zinc fluoride electrodes in $Ca(PF_6)_2$ solution. Peak heights for zinc metal were larger by a factor of ten. Low anodic and very low cathodic peaks result in $Mg(PF_6)_2$ solution, compared with voltage overload obtained for the base metal.

The curve for zinc fluoride in BF_3 solution shows a broad, high anodic peak and multiple cathodic peaks of medium high range and poor reproducibility. Similar curves of medium low range are obtained in $LiBF_4$ and $Mg(BF_4)_2$ solutions. Zinc fluoride in $Ca(BF_4)_2$ solution shows a broad, medium low anodic peak and multiple cathodic peaks with poor reproducibility. The current density of the highest cathodic peak falls in the high range and occurs 700 mv negative to the anodic peak.

As reported earlier, voltage overload was obtained for zinc metal in BF_3, $Mg(BF_4)_2$ and $Ca(BF_4)_2$ solutions, whereas zinc metal in $LiBF_4$ solution gave peaks larger than that of the fluorinated metal by a factor of ten.

(b) Propylene carbonate solutions

The cyclic voltammogram for zinc fluoride in PF_5 solution is shown in Figure 8 (CV-3763). The curve shows sharp anodic and cathodic peaks of medium high and medium low current density respectively. This is significantly different from that obtained with zinc metal where broad peaks and lower current densities were observed. Zinc fluoride in KPF_6 solution shows a single anodic and two cathodic peaks of medium low current density. Earlier results with zinc metal in this electrolyte showed single sharp, medium high, anodic and cathodic peaks.

The curves for zinc fluoride electrodes in $LiPF_6$ solutions show irreproducible, medium low anodic and cathodic peaks spread over a half volt range. Zinc metal in this electrolyte shows single anodic and cathodic peaks with very high current density. Better reproducibility is observed in $Mg(PF_6)_2$ solution where single anodic and cathodic peaks of medium low current density, and 0.2 volt peak-to-peak separation are observed. The cyclic voltammogram for this system is shown in Figure 9 (CV-3812), for comparison with that of metal (Ref. 2, p. 29) where broader peaks and higher currents are obtained. Zinc fluoride in $Ca(PF_6)_2$ solution results in broad peaks of low anodic and very low cathodic activity. Zinc fluoride electrodes in $LiBF_4$ solution result in single, low anodic and cathodic peaks whereas the base metal gave currents larger by an order of magnitude. In $Ca(BF_4)_2$ solution, zinc fluoride electrodes give broad, medium low anodic and low cathodic peaks. Very low anodic and cathodic activity and no peaks result for zinc fluoride in $Mg(BF_4)_2$ solutions. Voltage overload had resulted earlier with zinc metal.

(2) Cadmium Fluoride Electrode

(a) Dimethylformamide solutions

Cadmium fluoride in PF_5 solution causes voltage overload for both anodic and cathodic sweeps, with very high current densities. Results from previous work on cadmium metal show broad, high anodic, and medium low cathodic peaks.

Cadmium fluoride in hexafluorophosphate solutions shows, generally, medium low to very low anodic and cathodic activity. In $LiPF_6$ solution, low anodic and medium low cathodic peaks with more than 1 volt peak to peak separation, result. Least activity occurs in KPF_6 solution with very low anodic and cathodic current and no peak formation. Low anodic and cathodic peaks result in $Mg(PF_6)_2$ and $Ca(PF_6)_2$ solutions. Cadmium metal in these systems resulted in both anodic and cathodic current overload. Similar low current curves result for cadmium fluoride electrodes in tetrafluoroborate solutions. Generally, multiple anodic and single

cathodic peaks are observed. Earlier work on the metal indicated very high anodic and cathodic activity.

(b) Propylene carbonate solutions

Cathodic voltage overload results for cadmium fluoride in $LiPF_6$ solution. Previous results on cadmium metal in this electrolyte indicate current overload. Cadmium fluoride in KPF_6 solution results in very low anodic and cathodic peaks. In $Ca(PF_6)_2$ solution the curve shows a sharp, high anodic peak and a broad cathodic peak in the medium low range. Cadmium fluoride in PF_5 solution results in voltage overload. Very low anodic and cathodic peaks result for $LiBF_4$ and $Ca(BF_4)_2$ solutions, where earlier work on the base metal resulted in voltage overload. Cadmium fluoride in $Mg(BF_4)_2$ solution results in voltage overload, similar to that obtained for the base metal.

(3) Indium Fluoride Electrode

(a) Dimethylformamide solutions

Indium fluoride in $Ca(PF_6)_2$ solution shows high anodic and cathodic activity spread over the 2-volt scan. The sweep curve shows a single, broad anodic peak, and a broad, medium low cathodic peak, followed by a steady increase in cathodic current, which continues to the negative extreme of the sweep. Examination revealed that the electrode diameter was reduced to half its original size. The solution showed black discoloration, and a dark deposit had settled to the bottom of the cell. Indium fluoride in BF_3, $LiPF_6$, and $Mg(PF_6)_2$ solutions result in anodic voltage overload. Earlier work with indium metal showed voltage overload with very high anodic and cathodic currents in these electrolytes, except for $LiPF_6$ solution, where very high anodic activity was indicated (Ref. 2, p. 32).

Indium fluoride in KPF_6 solution shows a very high anodic and a medium high cathodic peak. Sweep rate behavior indicates formation of a soluble

anodic product. Similar results were recorded earlier for indium metal. Indium fluoride in $LiBF_4$ solution results in voltage overload. Examination of the working electrode revealed that its diameter was reduced to one-third of its original size. In $Ca(BF_4)_2$ solutions, indium fluoride shows very high anodic and medium low cathodic activity. Voltage overload results at the fast sweep rate. Indium metal had earlier shown voltage overload at all sweep rates.

(b) Propylene carbonate solutions

The curve for indium fluoride electrodes in PF_5 solution shows broad, high anodic and cathodic peaks with 0.6 v separation. Examination of the electrode revealed a black reaction product on its surface and a reduction of its diameter. The curve is shown in Figure 10 (CV-3770). Previous work on indium metal failed to show any peaks, and the current densities fell in the medium low range.

Indium fluoride electrodes in KPF_6 solution result in voltage overload. In this system, voltage overload occurred after several cycles during which time anodic and cathodic peak heights were increasing. Previous work on the metal also showed voltage overload.

The cyclic voltammogram for indium fluoride in $Ca(PF_6)_2$ is shown in Figure 11 (CV-3882). The curve shows broad, medium high anodic, and high cathodic peaks, separated by 0.65 v. The coulombic ratio (cathodic to anodic peak area) is 0.90. Similar results were observed in $Mg(PF_6)_2$ solution but with less reproducibility. Earlier work on indium metal in these electrolytes indicate anodic and cathodic voltage overload, with very high currents. Indium fluoride in $LiBF_4$ solution shows broad, medium high anodic and medium low cathodic peaks. Similar results (but at higher current densities) were reported for indium metal (Ref. 2, p. 34). Anodic voltage overload results for indium fluoride in $Mg(BF_4)_2$ and $Ca(BF_4)_2$ solutions. Results observed for the base metal indicated anodic and cathodic voltage overload with very high anodic and cathodic currents.

(4) Iron Fluoride Electrodes

(a) Dimethylformamide solutions

Iron fluoride electrodes in PF_5, $LiPF_6$, $Ca(PF_6)_2$, BF_3 and $LiBF_4$ solutions show very low anodic and cathodic activity. These results are significantly different from those for the base metal in these electrolytes where generally high or very high anodic activity is indicated. The cyclic voltammogram for a typical system (FeF_3/PC-$LiBF_4$) is shown in Figure 12 (CV-3913).

Iron fluoride electrodes in KPF_6 solution shows no peaks and only very low anodic and cathodic activity. Earlier work on iron metal gave current densities four times larger. Iron fluoride electrodes in $Ca(BF_4)_2$ solution show a single, low anodic peak and very low cathodic activity, compared with earlier data on iron metal which showed very high anodic activity.

(b) Propylene carbonate solutions

The curve for iron fluoride in PF_5 solution shows very low anodic and cathodic activity, comparable with results obtained on iron metal. Results in propylene carbonate for indium fluoride in hexafluorophosphate and tetrafluoroborate solutions are the same as in dimethylformamide. The anodic and cathodic currents are in the very low range. Tests were made on solutions of hexafluorophosphate and tetrafluoroborate salts of lithium, magnesium, and calcium.

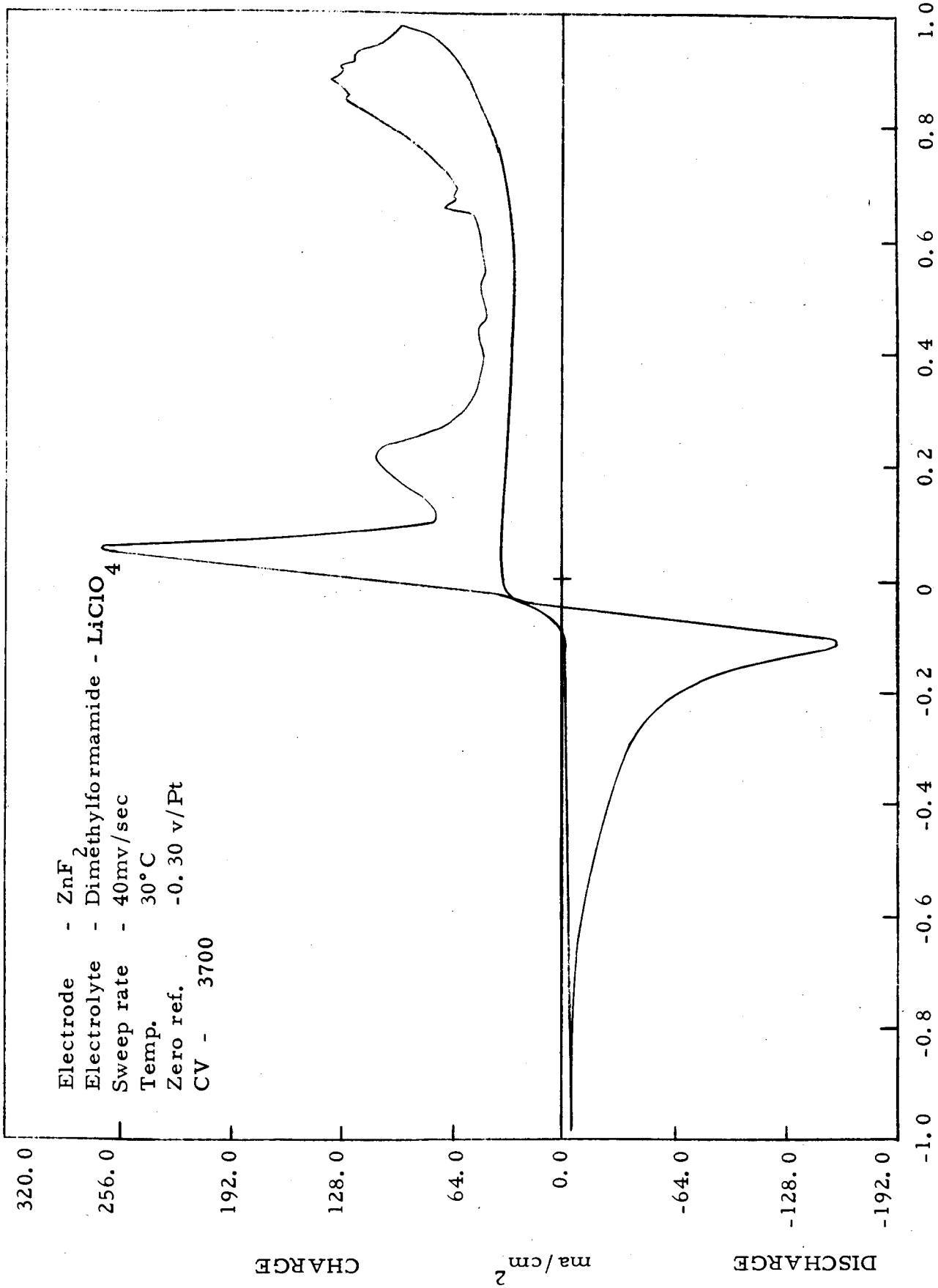
Electrode - ZnF_2
Electrolyte - Dimethylformamide - $LiClO_4$
Sweep rate - 40mv/sec
Temp. 30° C
Zero ref. -0.30 v/Pt
CV - 3700
320.0
256.0
192.0
128.0
64.0
0.0
-64.0
-128.0
-192.0
CHARGE
DISCHARGE
ma/cm^2
-1.0
-0.8
-0.6
-0.4
-0.2
0
0.2
0.4
0.6
0.8
1.0
VOLTS POLARIZATION

Figure 1

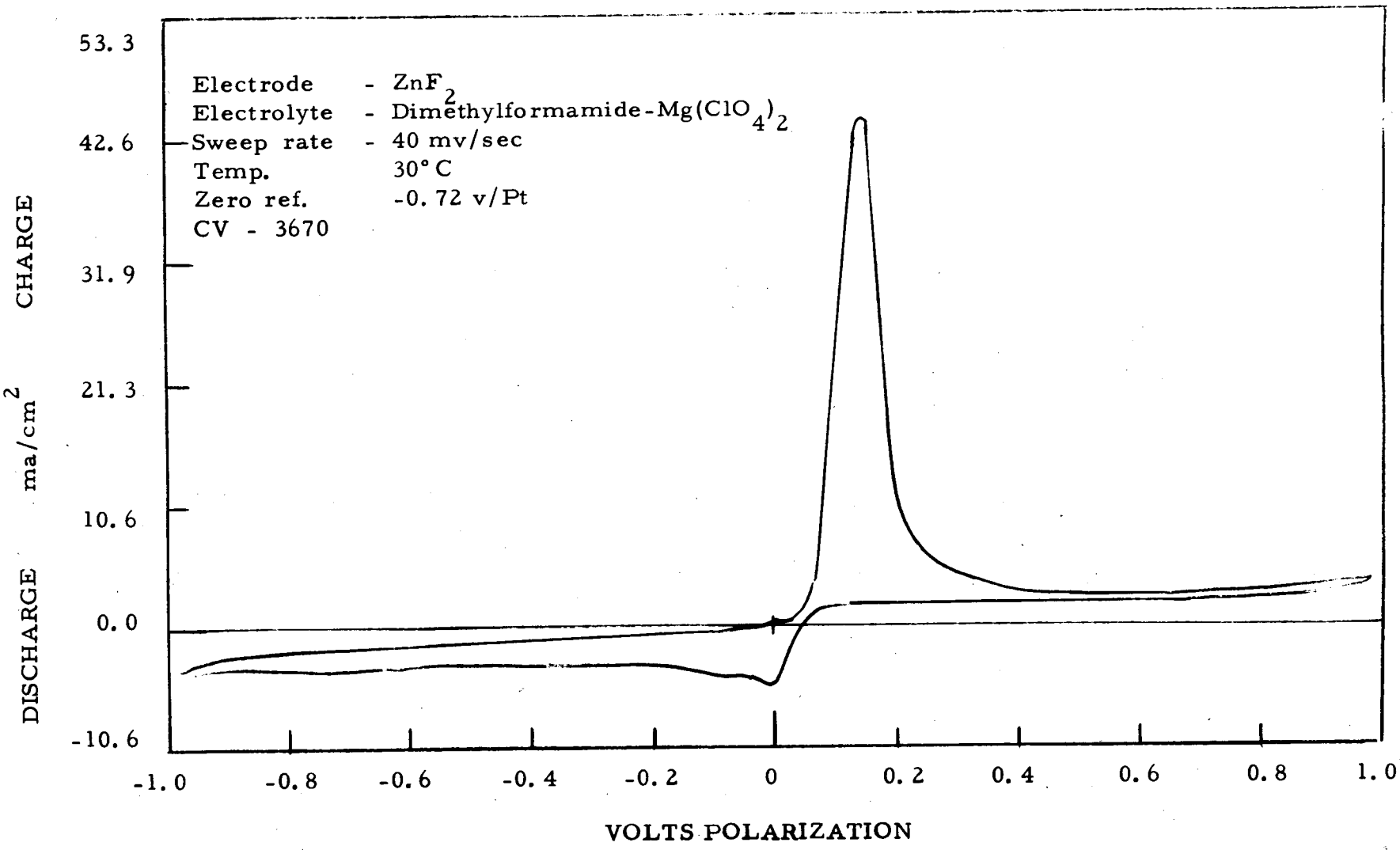
Electrode - ZnF_2
Electrolyte - Dimethylformamide-$Mg(ClO_4)_2$
Sweep rate - 40 mv/sec
Temp. 30° C
Zero ref. -0.72 v/Pt
CV - 3670
53.3
42.6
31.9
21.3
10.6
0.0
-10.6
DISCHARGE ma/cm^2 CHARGE
-1.0
-0.8
-0.6
-0.4
-0.2
0
0.2
0.4
0.6
0.8
1.0
VOLTS POLARIZATION

Figure 2

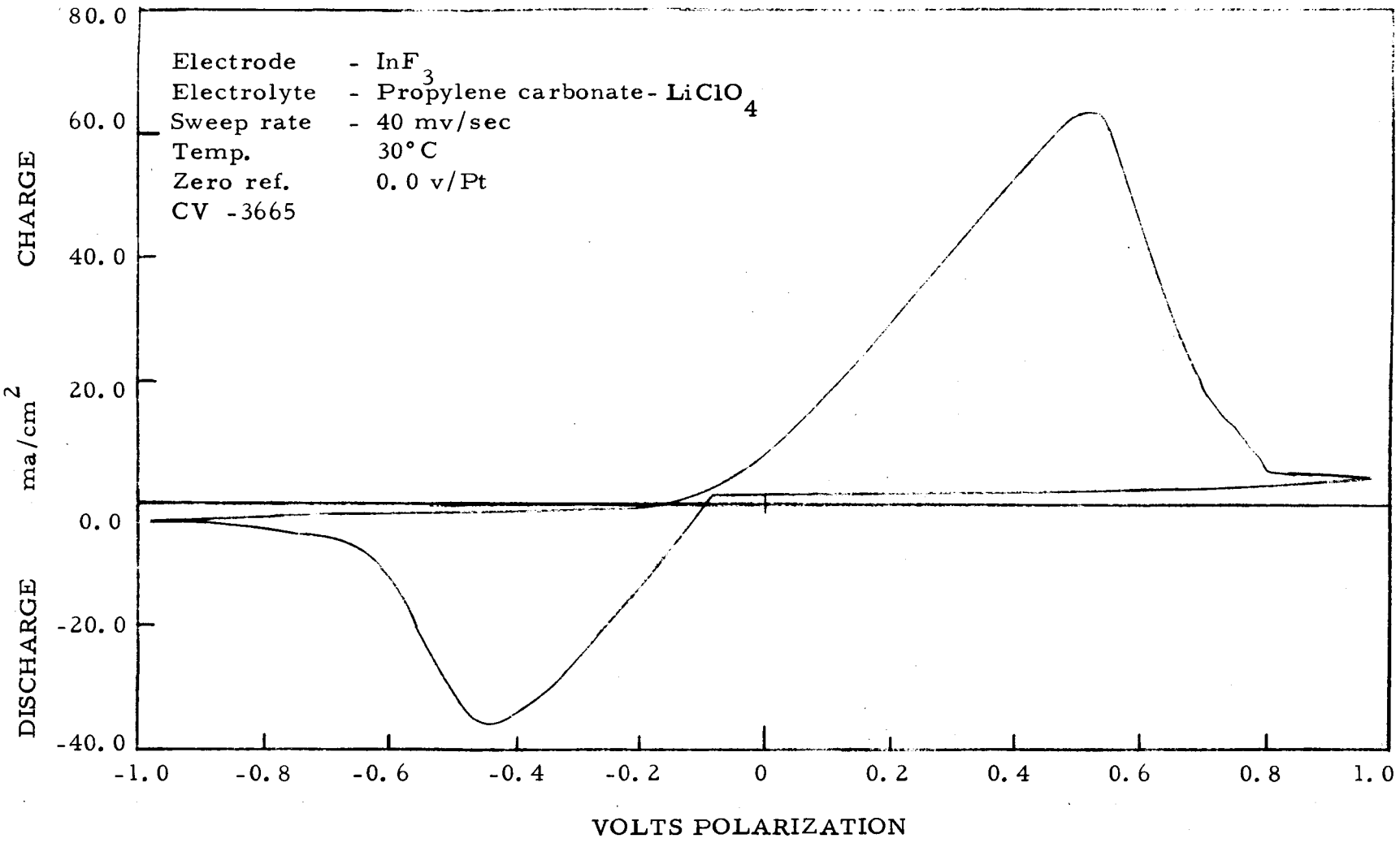
Electrode - InF_3
Electrolyte - Propylene carbonate - $LiClO_4$
Sweep rate - 40 mv/sec
Temp. 30°C
Zero ref. 0.0 v/Pt
CV -3665
80.0
60.0
40.0
20.0
0.0
-20.0
-40.0
CHARGE
DISCHARGE
ma/cm^2
-1.0
-0.8
-0.6
-0.4
-0.2
0
0.2
0.4
0.6
0.8
1.0
VOLTS POLARIZATION

Figure 3

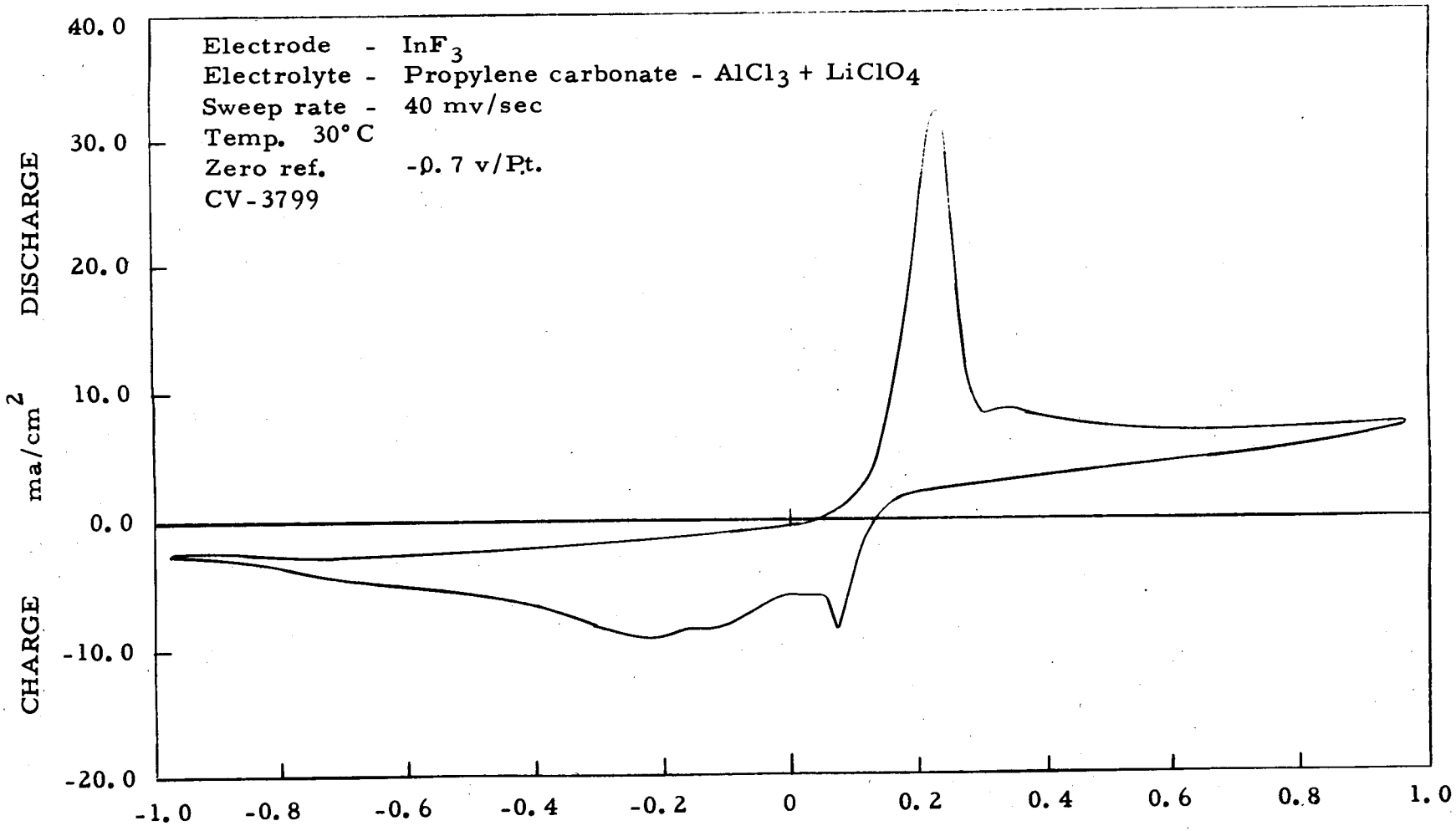
Electrode - InF_3
Electrolyte - Propylene carbonate - $AlCl_3 + LiClO_4$
Sweep rate - 40 mv/sec
Temp. 30° C
Zero ref. -0.7 v/Pt.
CV-3799
DISCHARGE
CHARGE
ma/cm^2
40.0
30.0
20.0
10.0
0.0
-10.0
-20.0
-1.0
-0.8
-0.6
-0.4
-0.2
0
0.2
0.4
0.6
0.8
1.0
VOLTS POLARIZATION

Figure 4

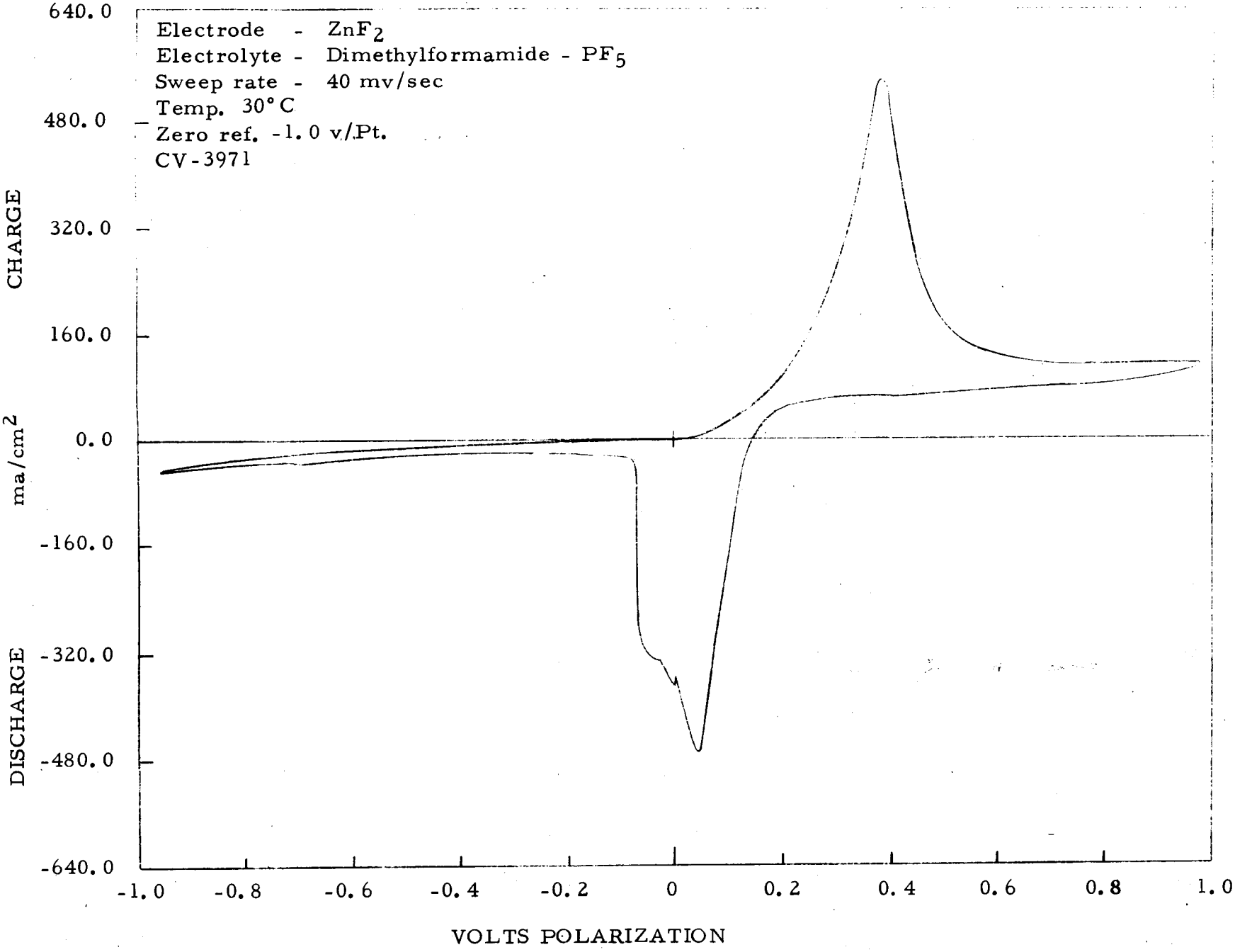
Electrode - ZnF_2
Electrolyte - Dimethylformamide - PF_5
Sweep rate - 40 mv/sec
Temp. 30°C
Zero ref. -1.0 v/Pt.
CV-3971
640.0
480.0
320.0
160.0
0.0
-160.0
-320.0
-480.0
-640.0
CHARGE
DISCHARGE
ma/cm²
-1.0
-0.8
-0.6
-0.4
-0.2
0
0.2
0.4
0.6
0.8
1.0
VOLTS POLARIZATION

Figure 5

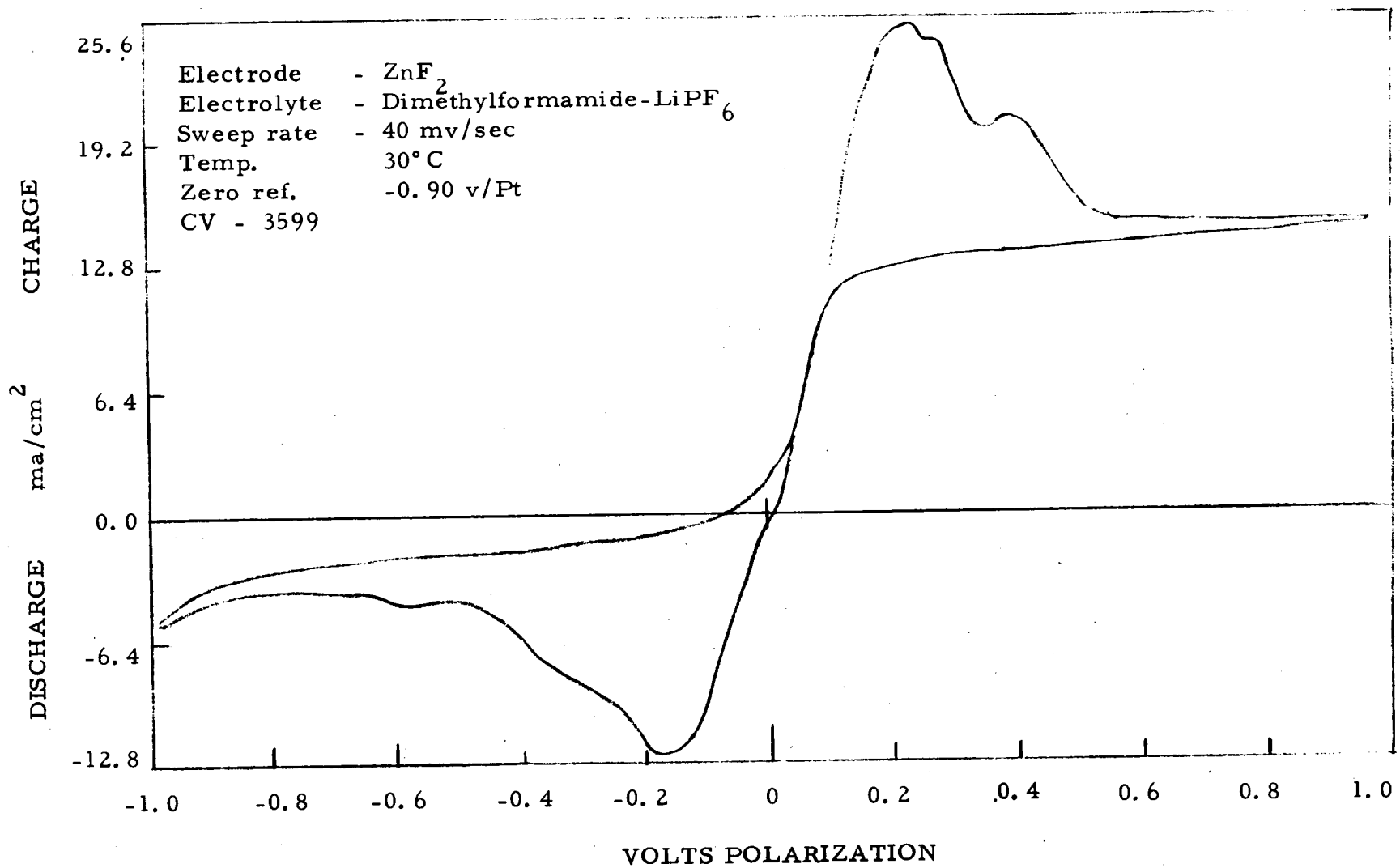
Electrode - ZnF_2
Electrolyte - Dimethylformamide-$LiPF_6$
Sweep rate - 40 mv/sec
Temp. 30° C
Zero ref. -0.90 v/Pt
CV - 3599
25.6
19.2
12.8
6.4
0.0
-6.4
-12.8
CHARGE
DISCHARGE
ma/cm^2
-1.0
-0.8
-0.6
-0.4
-0.2
0
0.2
0.4
0.6
0.8
1.0
VOLTS POLARIZATION

Figure 6

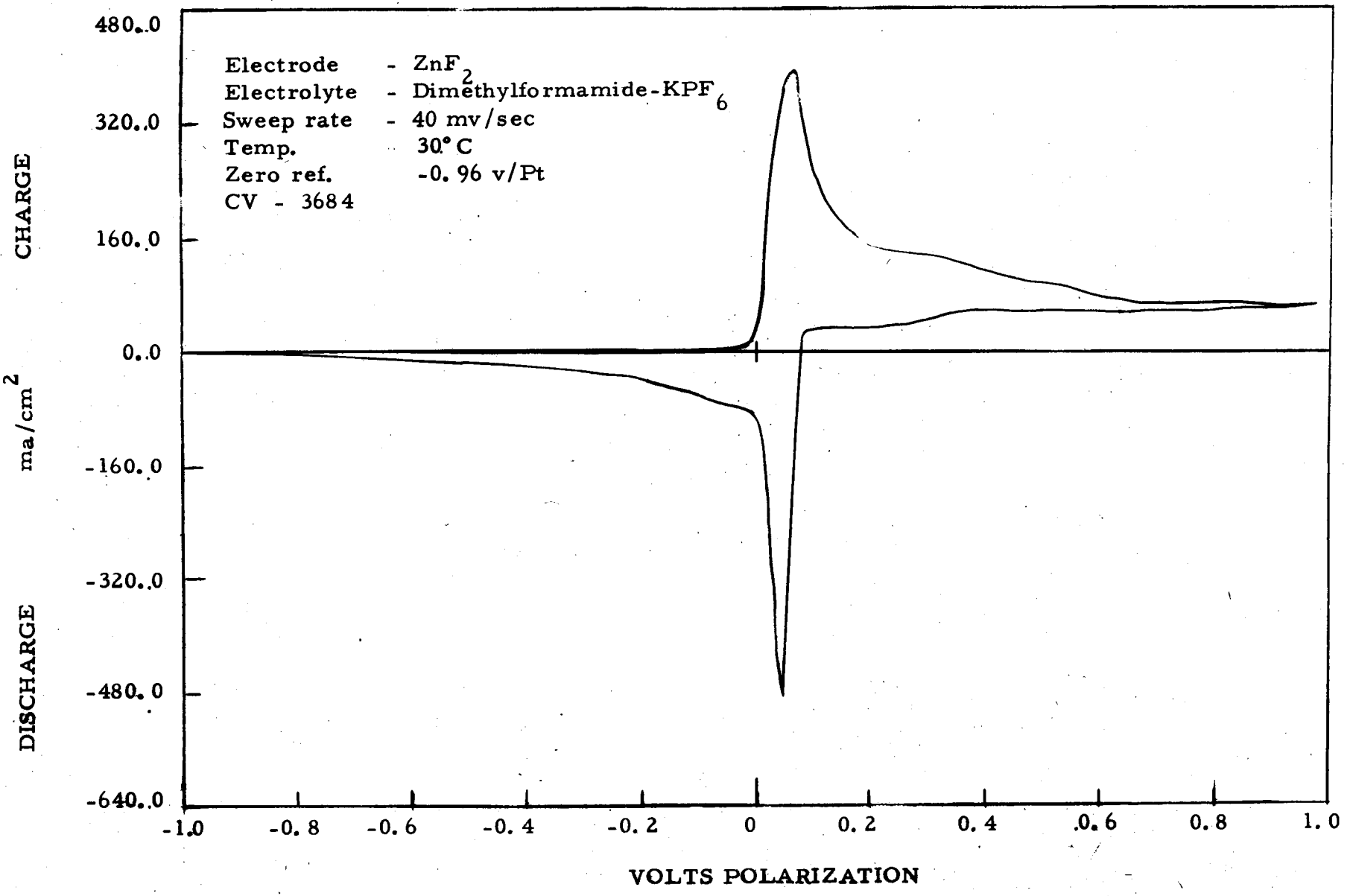
Electrode - ZnF_2
Electrolyte - Dimethylformamide-KPF_6
Sweep rate - 40 mv/sec
Temp. 30° C
Zero ref. -0.96 v/Pt
CV - 3684
480.0
320.0
160.0
0.0
-160.0
-320.0
-480.0
-640.0
CHARGE
DISCHARGE
ma/cm^2
-1.0
-0.8
-0.6
-0.4
-0.2
0
0.2
0.4
0.6
0.8
1.0
VOLTS POLARIZATION

Figure 7

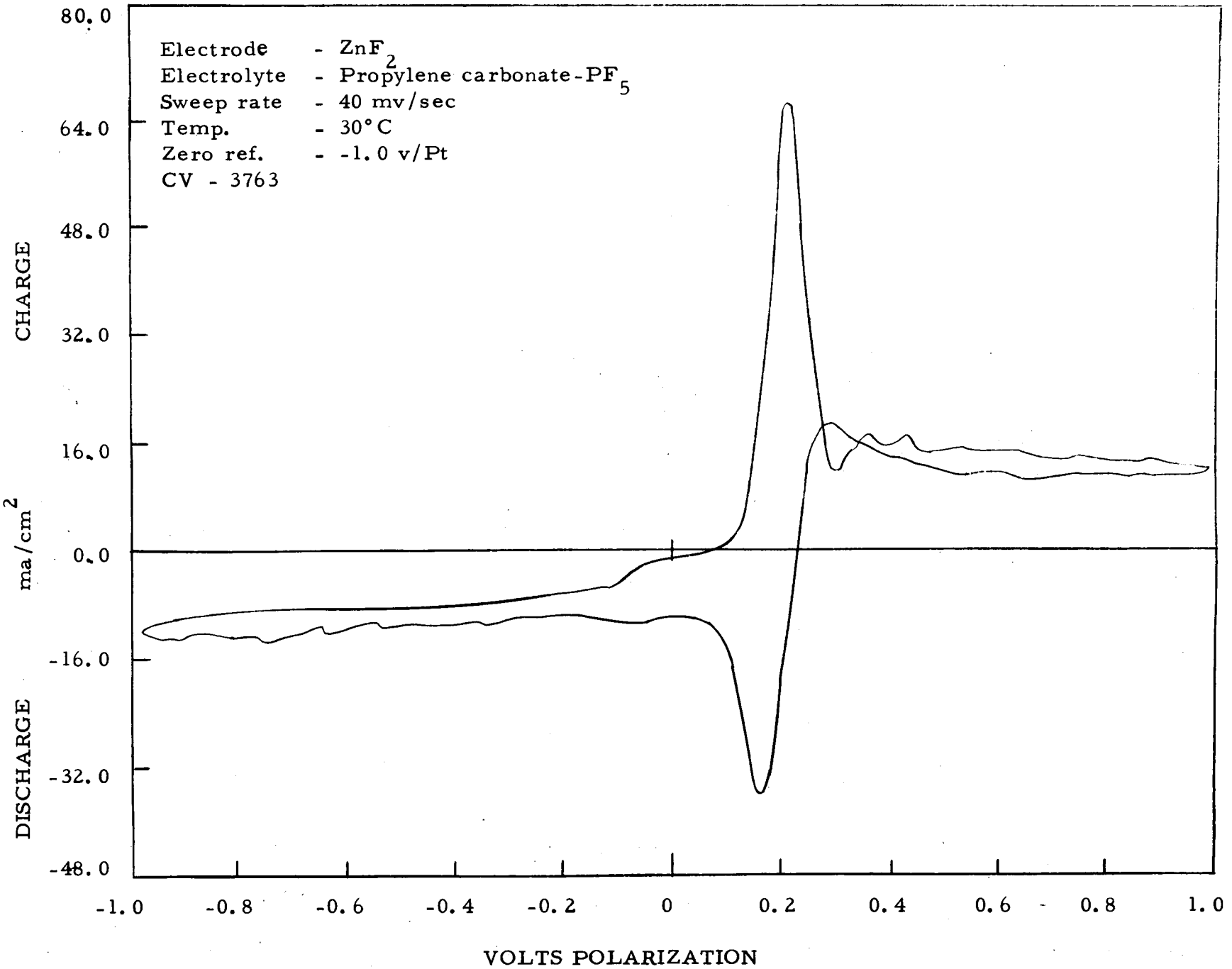
Electrode - ZnF_2
Electrolyte - Propylene carbonate-PF_5
Sweep rate - 40 mv/sec
Temp. - 30°C
Zero ref. - -1.0 v/Pt
CV - 3763
80.0
64.0
48.0
32.0
16.0
0.0
-16.0
-32.0
-48.0
CHARGE
DISCHARGE
ma/cm^2
-1.0
-0.8
-0.6
-0.4
-0.2
0
0.2
0.4
0.6
0.8
1.0
VOLTS POLARIZATION

Figure 8

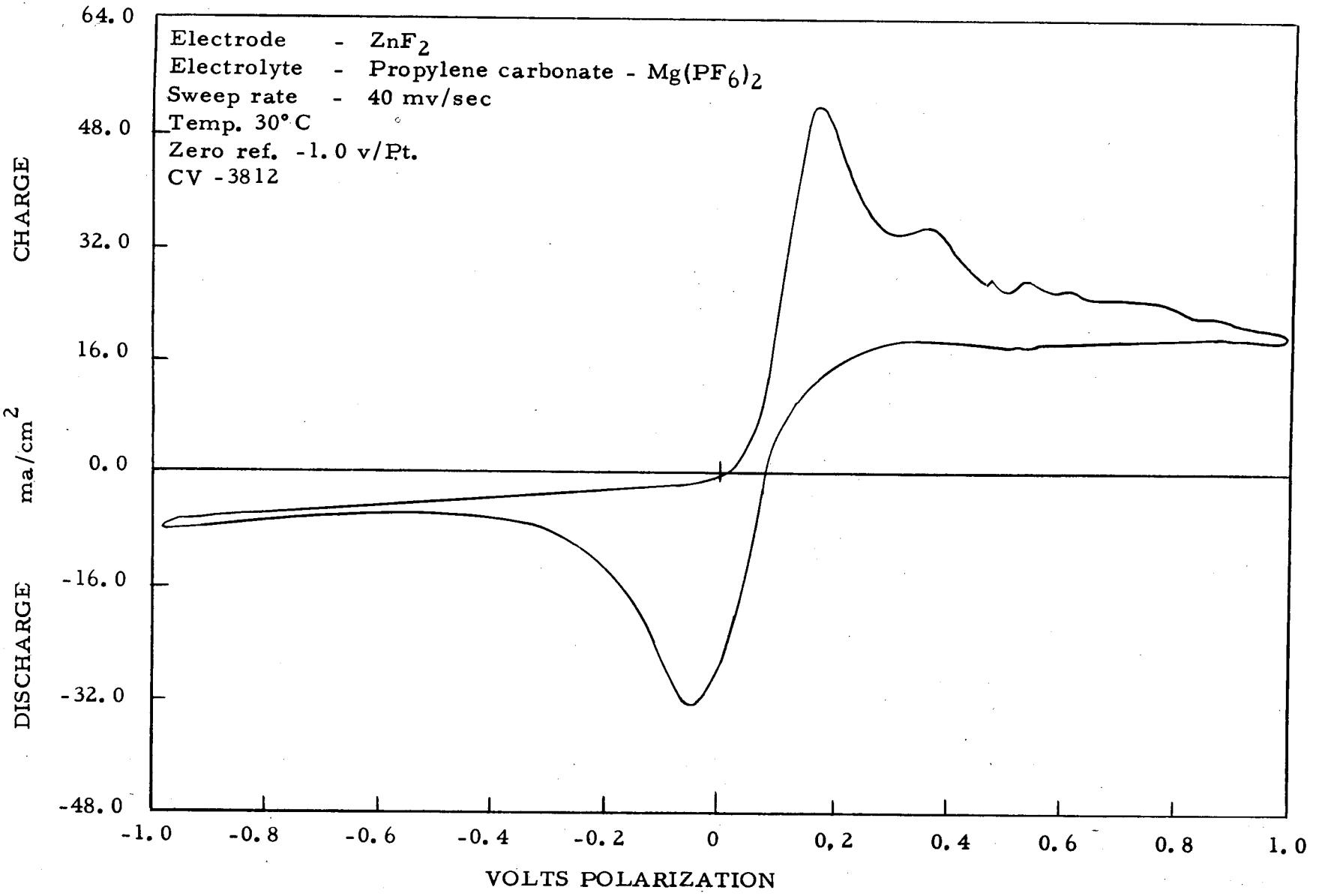
Electrode - ZnF_2
Electrolyte - Propylene carbonate - $Mg(PF_6)_2$
Sweep rate - 40 mv/sec
Temp. 30° C
Zero ref. -1.0 v/Pt.
CV -3812
64.0
48.0
32.0
16.0
0.0
-16.0
-32.0
-48.0
CHARGE
DISCHARGE
ma/cm^2
-1.0
-0.8
-0.6
-0.4
-0.2
0
0,2
0.4
0.6
0.8
1.0
VOLTS POLARIZATION

Figure 9

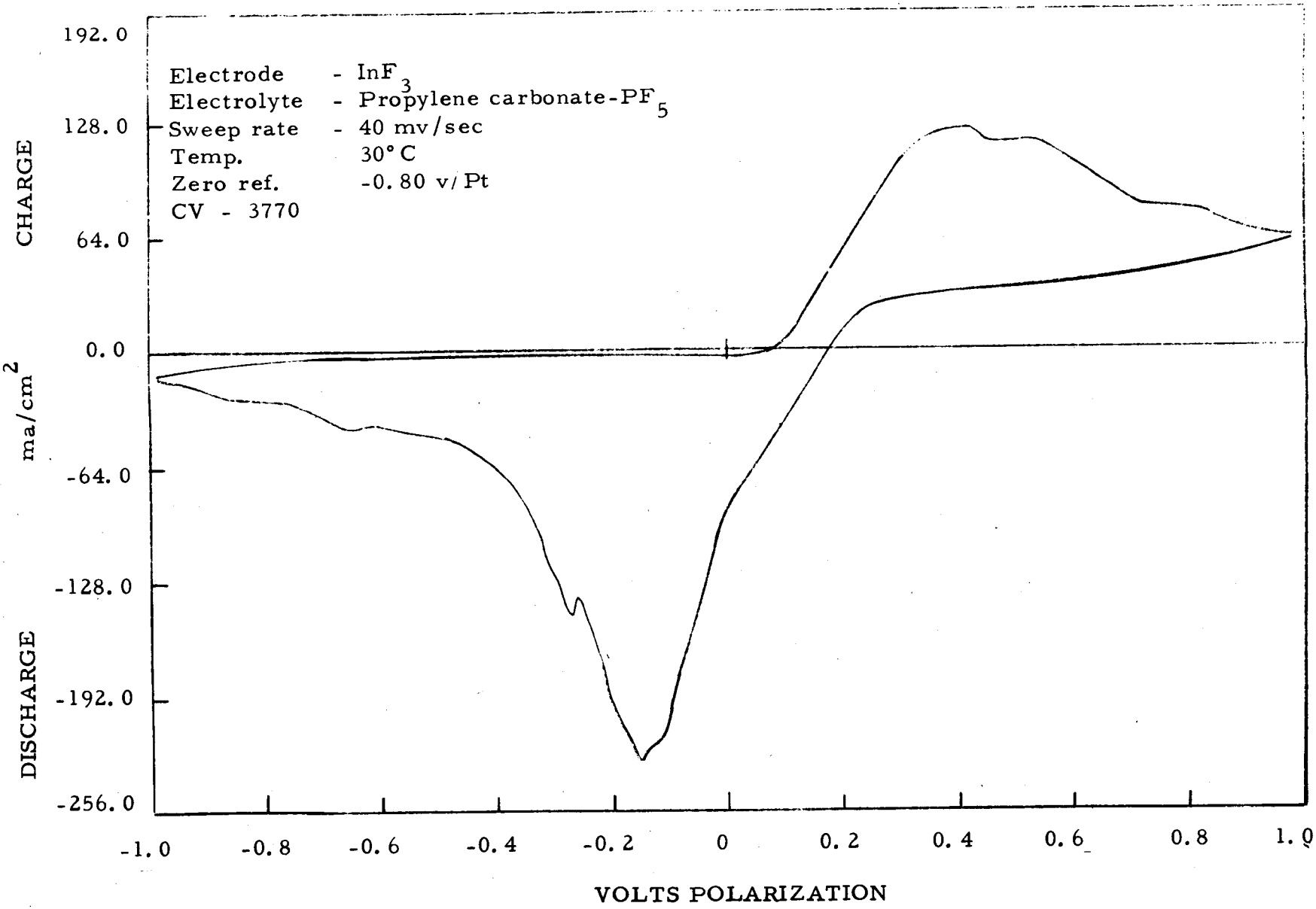
Electrode - InF_3
Electrolyte - Propylene carbonate-PF_5
Sweep rate - 40 mv/sec
Temp. 30° C
Zero ref. -0.80 v/Pt
CV - 3770
192.0
128.0
64.0
0.0
-64.0
-128.0
-192.0
-256.0
CHARGE
DISCHARGE
ma/cm^2
-1.0
-0.8
-0.6
-0.4
-0.2
0
0.2
0.4
0.6
0.8
1.0
VOLTS POLARIZATION

Figure 10

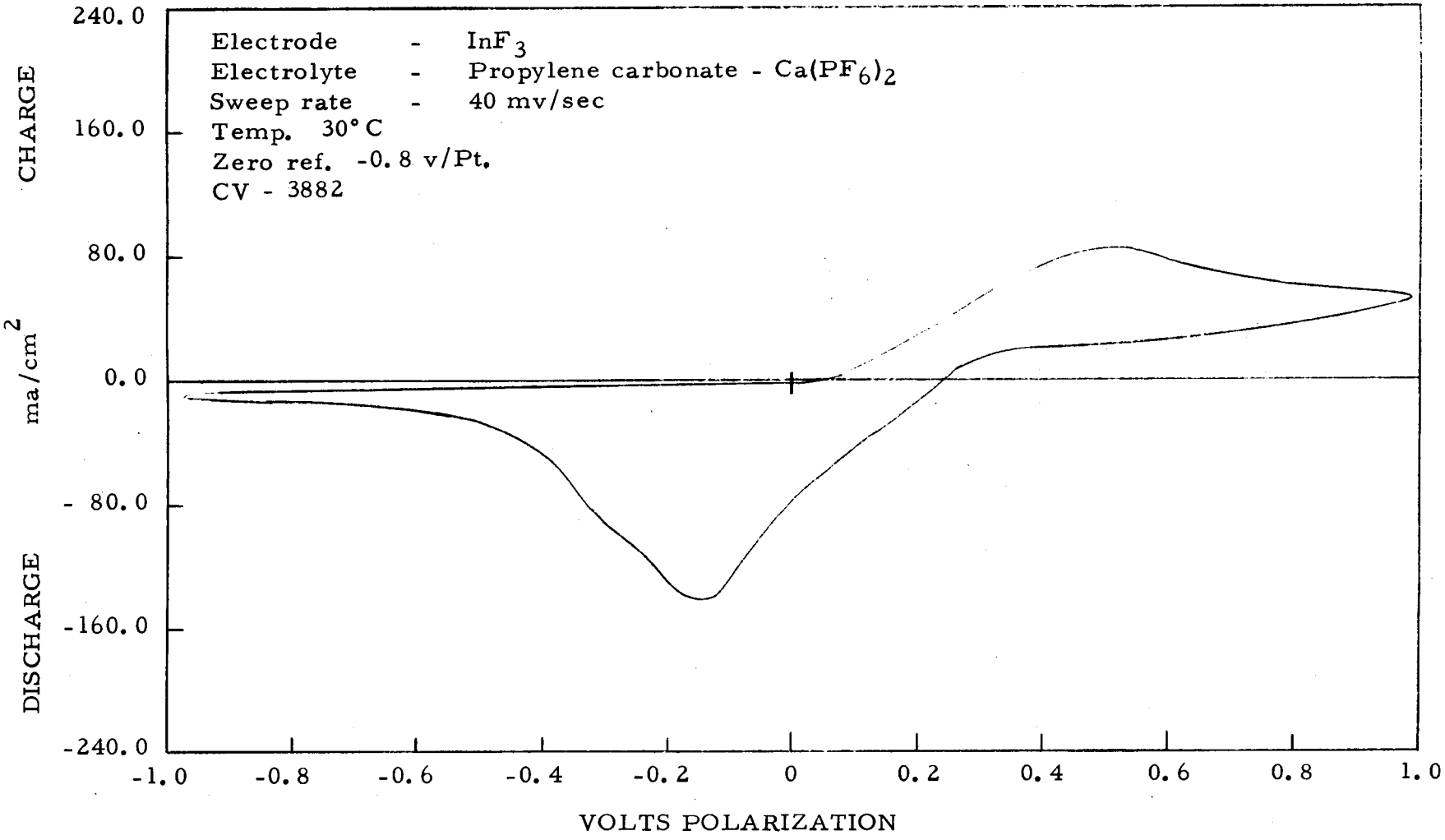
Electrode - InF_3
Electrolyte - Propylene carbonate - $Ca(PF_6)_2$
Sweep rate - 40 mv/sec
Temp. 30° C
Zero ref. -0.8 v/Pt.
CV - 3882
CHARGE
DISCHARGE
ma/cm^2
240.0
160.0
80.0
0.0
- 80.0
-160.0
-240.0
-1.0
-0.8
-0.6
-0.4
-0.2
0
0.2
0.4
0.6
0.8
1.0
VOLTS POLARIZATION

Figure 11

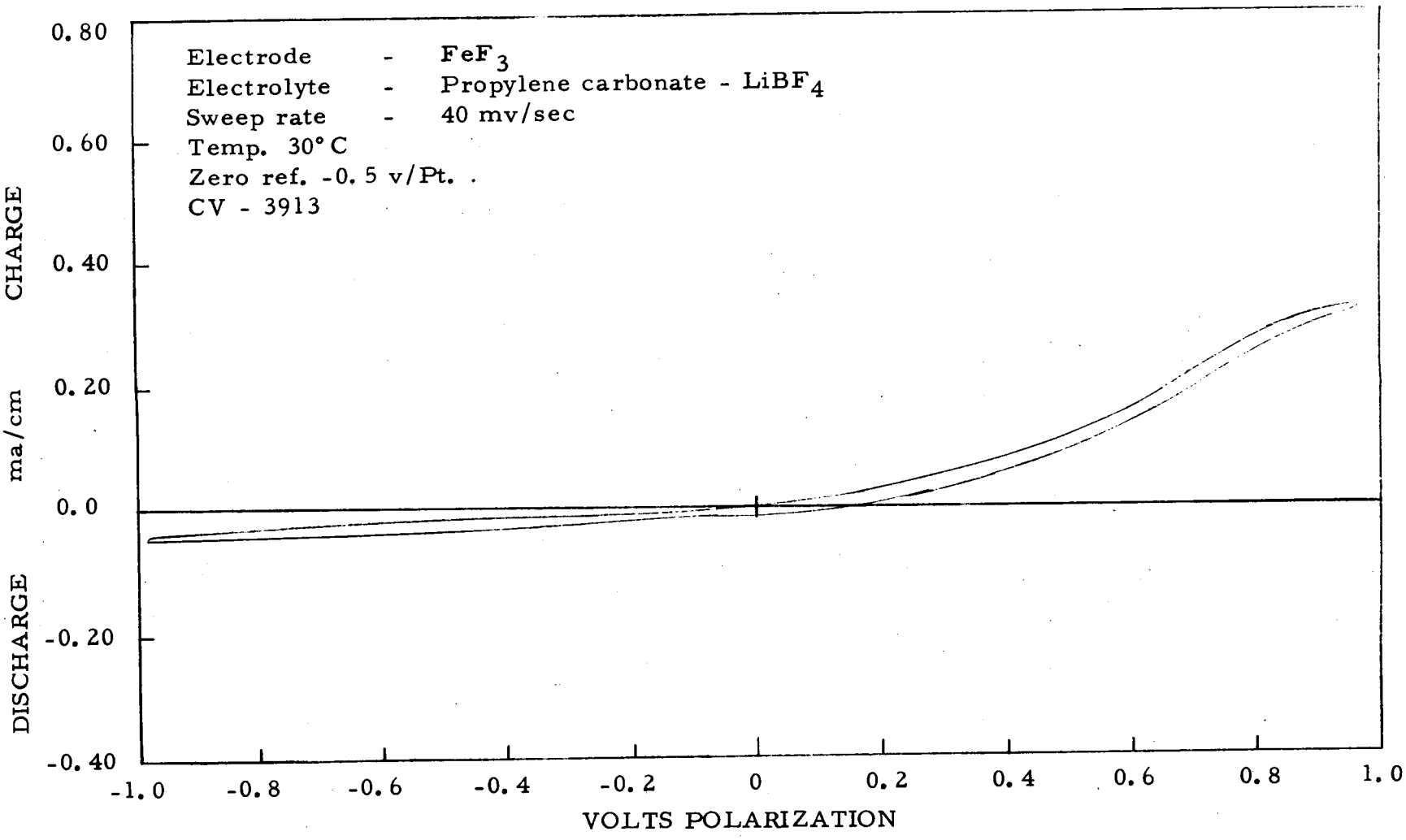
Electrode - FeF_3
Electrolyte - Propylene carbonate - $LiBF_4$
Sweep rate - 40 mv/sec
Temp. 30° C
Zero ref. -0.5 v/Pt.
CV - 3913
0.80
0.60
0.40
0.20
0.0
-0.20
-0.40
CHARGE
DISCHARGE
ma/cm 2
-1.0
-0.8
-0.6
-0.4
-0.2
0
0.2
0.4
0.6
0.8
1.0
VOLTS POLARIZATION

Figure 12

B. TABLES OF CYCLIC VOLTAMMETRIC DATA

Included in this section are tables listing parameters derived from the cyclic voltammograms. These parameters are as follows:

1. Sweep index - This is a relative figure of merit taking into account peak heights, sweep rate, and discharge capacity. This parameter is described in more detail in an earlier report (Ref. 3, p. 80).

2. Peak current density range - Relative magnitude of peak currents classified according to page 2.

3. ΔV_p - Peak-to-peak displacement in volts of charge and discharge reactions giving a measure of overall electrode reversibility, or in more practical terms, a measure of suitability of the electrochemical system for second battery application.

4. Coulombic ratio - Ratio of cathodic to anodic peak area. Values significantly in excess of unity for the pre-formed electrodes (chlorinated and fluorinated metals) are indicative of the contribution of the original cathodic material to the discharge reaction independent of the material formed by the preceding charge sweep.

5. Discharge capacity - Measure of discharge utilization per unit area of electrode surface, when compared with the coulombic ratio except for values of the latter greater than unity.

Also included are tables listing the systems causing voltage and current overload of the instrumentation preventing recordable voltammograms as well as those systems failing to exhibit either anodic or cathodic peaks. In cases of solutions having varying molality, the concentrations are included with the designated system. The concentration of all solutions are listed in Table I.

TABLE IV

SYSTEMS CAUSING VOLTAGE OVERLOAD
OF INSTRUMENTATION

Systems	CV	Max. Anod. C. D. ma/cm^2	Max. Cath. C. D. ma/cm^2
ZnF_2/DMF-PF_5	3971	440	480
ZnF_2/DMF-$CaCl_2$	3942	4000	nil
CdF_2/DMF-PF_5	3972	1200	1600
CdF_2/PC-PF_5	3530	1600	nr*
CdF_2/PC-$LiPF_6$	3964	40	2000
CdF_2/PC-$Mg(BF_4)_2$	3749	56	120
InF_3/DMF-$LiPF_6$	3862	3200	150
InF_3/DMF-$Mg(PF_6)_2$	3861	2000	1400
InF_3/DMF-BF_3	3930	4800	3200
InF_3/DMF-$LiBF_4$	3611	3200	320
InF_3/PC-KPF_6	3776	1600	440
InF_3/PC-$Mg(BF_4)_2$	3924	40	nr*
InF_3/PC-$Ca(BF_4)_2$	3936	4800	nr*
InF_3/PC-$LiCl+LiClO_4$	3694	450	320
InF_3/PC-$CaCl_2$	3875	40	nr*

* - Not recorded

DMF - Dimethylformamide

PC - Propylene carbonate

TABLE V

PEAK CURRENT DENSITY RANGE
CHLORIDE AND PERCHLORATE ELECTROLYTES

System	CV	Anodic	Cathodic
ZnF_2/DMF-LiCl	3565	low	low
ZnF_2/DMF-$LiClO_4$	3700	high	high
ZnF_2/DMF-$MgCl_2$	3624	medium high	low
ZnF_2/DMF-$Mg(ClO_4)_2$	3670	medium low	low
ZnF_2/DMF-$AlCl_3$+LiCl	3712	high	medium low
ZnF_2/PC-$LiClO_4$	3660	very low	very low
ZnF_2/PC-LiCl+$LiClO_4$	3687	low	very low
ZnF_2/PC-$AlCl_3$+$LiClO_4$	3787	medium low	low
CdF_2/DMF-$LiClO_4$	3706	low	very low
CdF_2/DMF-$MgCl_2$	3629	very low	very low
CdF_2/DMF-$CaCl_2$	3944	very low	very low
CdF_2/DMF-$Mg(ClO_4)_2$	3668	very low	very low
CdF_2/DMF-$AlCl_3$+LiCl	3718	very low	very low
CdF_2/PC-LiCl+$LiClO_4$	3695	low	low
CdF_2/PC-$AlCl_3$+$LiClO_4$	3798	very low	very low
InF_3/DMF-$LiClO_4$	3711	very high	high
InF_3/DMF-$Mg(ClO_4)_2$	3852	high	medium low
InF_3/DMF-LiCl	3839	medium high	low
InF_3/DMF-$MgCl_2$	3631	very high	medium low
InF_3/DMF-$AlCl_3$+LiCl	3724	high	low
InF_3/PC-$LiClO_4$	3665	medium high	medium low
InF_3/PC-$AlCl_3$+$LiClO_4$	3804	medium low	medium low

DMF - Dimethylformamide

PC - Propylene carbonate

TABLE VI

PEAK CURRENT DENSITY RANGE
FLUORIDE ELECTROLYTES

System	CV	Anodic	Cathodic
ZnF_2/DMF-PF_5	3971	very high	very high
ZnF_2/DMF-$LiPF_6$	3599	medium low	low
ZnF_2/DMF-KPF_6	3684	very high	very high
ZnF_2/DMF-$Mg(PF_6)_2$	3555	low	very low
ZnF_2/DMF-$Ca(PF_6)_2$	3583	medium low	medium low
ZnF_2/DMF-$LiBF_4$	3604	medium low	medium low
ZnF_2/DMF-$Mg(BF_4)_2$	3545	medium low	medium low
ZnF_2/DMF-$Ca(BF_4)_2$	3637	high	very high
ZnF_2/DMF-BF_3	3573	high	medium high
ZnF_2/PC-KPF_6	3750	medium low	medium low
ZnF_2/PC-$Mg(PF_6)_2$	3812	medium high	medium high
ZnF_2/PC-$Ca(PF_6)_2$	3636	low	very low
ZnF_2/PC-PF_5	3763	medium high	medium low
ZnF_2/PC-$LiPF_6$	3958	medium low	medium low
ZnF_2/PC-$LiBF_4$	3731	low	low
ZnF_2/PC-$Ca(BF_4)_2$	3594	medium low	low
CdF_2/DMF-$LiPF_6$	3524	low	medium low
CdF_2/DMF-$Ca(PF_6)_2$	3589	low	low
CdF_2/DMF-$LiBF_4$	3610	low	very low
CdF_2/DMF-$Mg(BF_4)_2$	3550	low	low
CdF_2/DMF-$Ca(BF_4)_2$	3642	low	low
CdF_2/DMF-BF_3	3578	low	low
CdF_2/PC-KPF_6	3762	very low	very low
CdF_2/PC-$Ca(PF_6)_2$	3540	high	medium low
CdF_2/PC-$LiBF_4$	3742	very low	very low
CdF_2/PC-$Ca(BF_4)_2$	3535	low	very low
InF_3/DMF-KPF_6	3675	very high	medium high

DMF - Dimethylformamide

PC - Propylene carbonate

TABLE VI (Cont'd.)

System	CV	Anodic	Cathodic
InF_3/DMF-$Ca(PF_6)_2$	3895	high	high
InF_3/DMF-$Ca(BF_4)_2$	3644	medium low	medium low
InF_3/PC-PF_5	3770	high	high
InF_3/PC-$Mg(PF_6)_2$	3919	high	high
InF_3/PC-$Ca(PF_6)_2$	3882	medium high	high
InF_3/PC-$LiBF_4$	3907	medium high	medium low
FeF_3/DMF-$LiBF_4$	3919	very low	very low

DMF - Dimethylformamide

PC - Propylene carbonate

TABLE VII

SWEEP INDEX*

System	CV	Anodic	Cathodic
		$ohm^{-1}cm^{-2}$	$ohm^{-1}cm^{-2}$
ZnF_2/DMF-$LiClO_4$	3700	-	85.1
ZnF_2/DMF-$Mg(ClO_4)_2$	3670	22.5	0.6
ZnF_2/DMF-PF_5	3971	137.	206.
ZnF_2/DMF-$LiPF_6$	3599	1.8	1.7
ZnF_2/DMF-KPF_6	3684	92.3	559.
ZnF_2/PC-PF_5	3763	183.	5.6
ZnF_2/PC-$Mg(PF_6)_2$	3812	6.2	6.3
InF_3/PC-$LiClO_4$	3665	12.8	9.0
InF_3/PC-PF_5	3770	142.	55.8
InF_3/PC-$Ca(PF_6)_2$	3882	10.4	31.0

DMF - Dimethylformamide

PC - Propylene carbonate

$$* \frac{(\text{peak c. d.})^2 \times 100}{\text{sweep rate} \times \text{coul/cm}^2}$$

TABLE VIII

ΔV_p, COULOMBIC RATIO, AND DISCHARGE CAPACITY

System	CV	ΔV_p*	Coul. ** Ratio	Disch. Capac. coul/cm^2
ZnF_2/DMF-$LiClO_4$	3700	0.17	0.24	0.75
ZnF_2/DMF-$Mg(ClO_4)_2$	3670	0.14	0.42	0.09
ZnF_2/DMF-PF_5	3971	0.34	0.52	2.70
ZnF_2/DMF-$LiPF_6$	3599	0.40	0.16	0.14
ZnF_2/DMF-KPF_6	3684	0.01	0.26	1.10
ZnF_2/DMF-$Mg(PF_6)_2$	3555	0.40	-	-
ZnF_2/DMF-$Ca(PF_6)_2$	3583	0.65	-	-
ZnF_2/PC-LiCl+$LiClO_4$	3687	0.90	-	-
ZnF_2/PC-$LiPF_6$	3958	0.15	-	-
ZnF_2/PC-KPF_6	3750	0.35	0.78	0.32
ZnF_2/PC-$Mg(PF_6)_2$	3812	0.20	0.37	0.40
ZnF_2/PC-$Ca(PF_6)_2$	3636	0.40	-	-
ZnF_2/PC-PF_5	3763	0.05	0.97	0.58
CdF_2/DMF-$Mg(ClO_4)_2$	3668	0.45	-	-
CdF_2/DMF-$Ca(PF_6)_2$	3589	0.50	-	-
CdF_2/DMF-$Ca(BF_4)_2$	3642	0.50	-	-
CdF_2/PC-KPF_6	3762	0.80	-	-
CdF_2/PC-$Ca(PF_6)_2$	3540	0.80	2.4	0.09
CdF_2/PC-$LiBF_4$	3742	0.60	-	-
CdF_2/PC-$Ca(BF_4)_2$	3535	0.60	-	-
InF_3/DMF-KPF_6	3675	0.19	-	-
InF_3/DMF-$Ca(PF_6)_2$	3895	0.50	-	-
InF_3/DMF-$Ca(BF_4)_2$	3644	0.70	-	-
InF_3/DMF-$CaCl_2$	3951	0.70	-	-
InF_3/PC-$LiClO_4$	3665	0.95	0.44	0.36

* Voltage separating anodic to cathodic peaks

** Ratio of cathodic to anodic peak areas

DMF - Dimethylformamide

PC - Propylene carbonate

TABLE VIII (Cont'd.)

System	CV	ΔV^*_p	Coul. ** Ratio	Disch. Capac. $\frac{\text{coul}}{\text{cm}^2}$
InF_3/PC-$AlCl_3$+$LiClO_4$	3799	-	0.73	0.22
InF_3/PC-PF_5	3770	0.55	0.85	2.31
InF_3/PC-$Ca(PF_6)_2$	3882	0.65	0.90	1.67
InF_3/PC-$LiBF_4$	3907	0.70	-	-

* Voltage separating anodic to cathodic peaks

** Ratio of cathodic to anodic peak areas

DMF - Dimethylformamide

PC - Propylene carbonate

TABLE IX

SYSTEMS EXHIBITING ANODIC PEAK ONLY*

System	CV	Peak Current Density Range
CdF_2/DMF-LiCl	3570	very low
CdF_2/DMF-$Mg(PF_6)_2$	3560	low (a)
CdF_2/PC-$AlCl_3$+$LiClO_4$	3798	very low
FeF_3/DMF-$LiPF_6$	3863	very low
FeF_3/DMF-$AlCl_3$+LiCl	3869	low
FeF_3/DMF-$Ca(PF_6)_2$	3902	very low
FeF_3/DMF-$Ca(BF_4)_2$	3649	low
FeF_3/PC-$Ca(BF_4)_2$	3937	very low
FeF_3/PC-PF_5	3778	very low
FeF_3/PC-$Mg(PF_6)_2$	3826	very low
FeF_3/PC-$Ca(PF_6)_2$	3889	very low
FeF_3/PC-$AlCl_3$+$LiClO_4$	3806	very low

* Maximum cathodic current density in very low range (<1 ma/cm^2) unless otherwise noted.

(a) Maximum cathodic current density in low range

DMF - Dimethylformamide

PC - Propylene carbonate

TABLE X

SYSTEMS EXHIBITING NO PEAKS*

System	CV
ZnF_2/PC-$Mg(BF_4)_2$	3743
ZnF_2/PC-$CaCl_2$	3616
CdF_2/DMF-KPF_6	3682
CdF_2/PC-$LiClO_4$	3650
CdF_2/PC-$CaCl_2$	3619
FeF_3/DMF-LiCl	3846
FeF_3/DMF-$LiClO_4$	3783
FeF_3/DMF-$Mg(ClO_4)_2$	3856
FeF_3/DMF-$CaCl_2$	3953
FeF_3/DMF-PF_5	3972
FeF_3/DMF-KPF_6	3679
FeF_3/DMF-BF_3	3931
FeF_3/PC-LiCl+$LiClO_4$	3833
FeF_3/PC-$LiClO_4$	3653
FeF_3/PC-$LiPF_6$	3965
FeF_3/PC-$CaCl_2$	3877
FeF_3/PC-$LiBF_4$	3913
FeF_3/PC-$Mg(BF_4)_2$	3925

* Maximum current density in very low range (<1 ma/cm^2) unless otherwise noted.

DMF - Dimethylformamide

PC - Propylene carbonate

II. RECOMMENDED SYSTEMS

A total of 950 positive-electrolyte combinations have now been electrochemically characterized by multisweep cyclic voltammetry. Twenty-four of these have been recommended for further study. The systems are listed in Table XI, and the cyclic voltammograms are shown in Figures 13 - 36. Recommendation was based on the height, shape, and displacement of the peaks. Sharp, high current density peaks displaced only a few millivolts from each other represent the ideal case. The value of the sweep index gives a relative measure of peak shape, so all recommended systems will have high index values.

Weighting these 24 systems according to order of peak current density, and in excess of 450 ma/cm^2, ten best systems have been selected, and are listed in Table XII. Being more restrictive, the 5 best systems are li sted in Table XIII. These have been chosen on the basis of having <u>all</u> parameters, i. e., peak current density, peak displacement, and cathodic sweep index, within the first best of ten. The systems are shown in the order of decreasing discharge current density, but this same sequence is obtained by listing the systems in order of increasing total weighted parameters (e. g. CV-1525 is 2nd best in ΔV_p, 1st in cathodic peak c. d., 1st in anodic peak c. d. and 2nd best in cathodic sweep index, giving 2-1-1-2 or a total of 6. In comparison, CV-2675 is 9-10-8-9 or 36).

TABLE XI

RECOMMENDED POSITIVE-ELECTROLYTE SYSTEMS*

CV	System
959	$Zn/PC-KPF_6$
992	$Zn/BL-KPF_6$
997	$Cd/BL-KPF_6$
1048	$Zn/DMF-KPF_6$ (a)
1053	$Cd/DMF-KPF_6$
1081	$AgO/BL-LiCl+AlCl_3$
1419	$CuF_2/PC-LiClO_4$
1491	$AgF_2/PC-LiBF_4$
1525	$CuF_2/DMF-LiPF_6$
1614	$CuF_2/PC-LiPF_6$
1999	$CuCl_2/PC-LiClO_4$
2208	$CuCl_2/BL-AlCl_3$
2236	$CuCl_2/DMF-LiCl+LiClO_4$
2300	$CuCl_2/DMF-LiPF_6$
2454	$CuCl_2/AN-LiPF_6$
2652	$Zn/DMF-KPF_6$ (b)
2675	$Zn/DMF-LiClO_4$
2690	$Cd/DMF-LiClO_4$
2733	$Zn/DMF-LiPF_6$
2739	$Zn/AN-LiClO_4$
2751	$Cu/AN-LiPF_6+KPF_6$
3273	$Cd/DMF-LiBF_4$
3684	$ZnF_2/DMF-KPF_6$
3700	$ZnF_2/DMF-LiClO_4$

* In order of measurement

BL - Butyrolactone
DMF - Dimethylformamide
PC - Propylene carbonate
AN - Acetonitrile

(a) 0.75 m KPF_6

(b) 2.0 m KPF_6

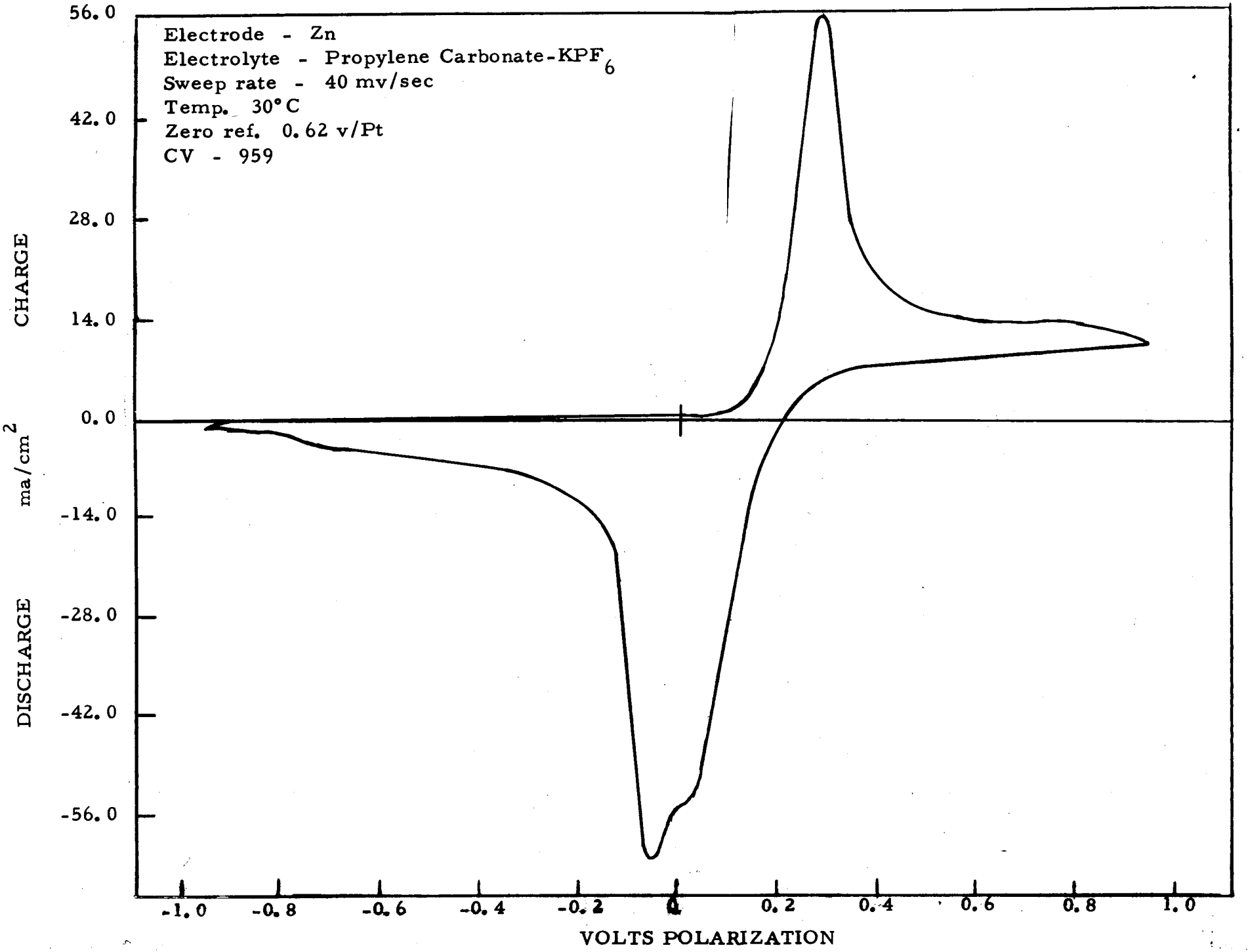
Electrode - Zn
Electrolyte - Propylene Carbonate-KPF6
Sweep rate - 40 mv/sec
Temp. 30°C
Zero ref. 0.62 v/Pt
CV - 959
56.0
42.0
28.0
14.0
0.0
-14.0
-28.0
-42.0
-56.0
CHARGE
DISCHARGE
ma/cm2
-1.0
-0.8
-0.6
-0.4
-0.2
0
0.2
0.4
0.6
0.8
1.0
VOLTS POLARIZATION

Figure 13

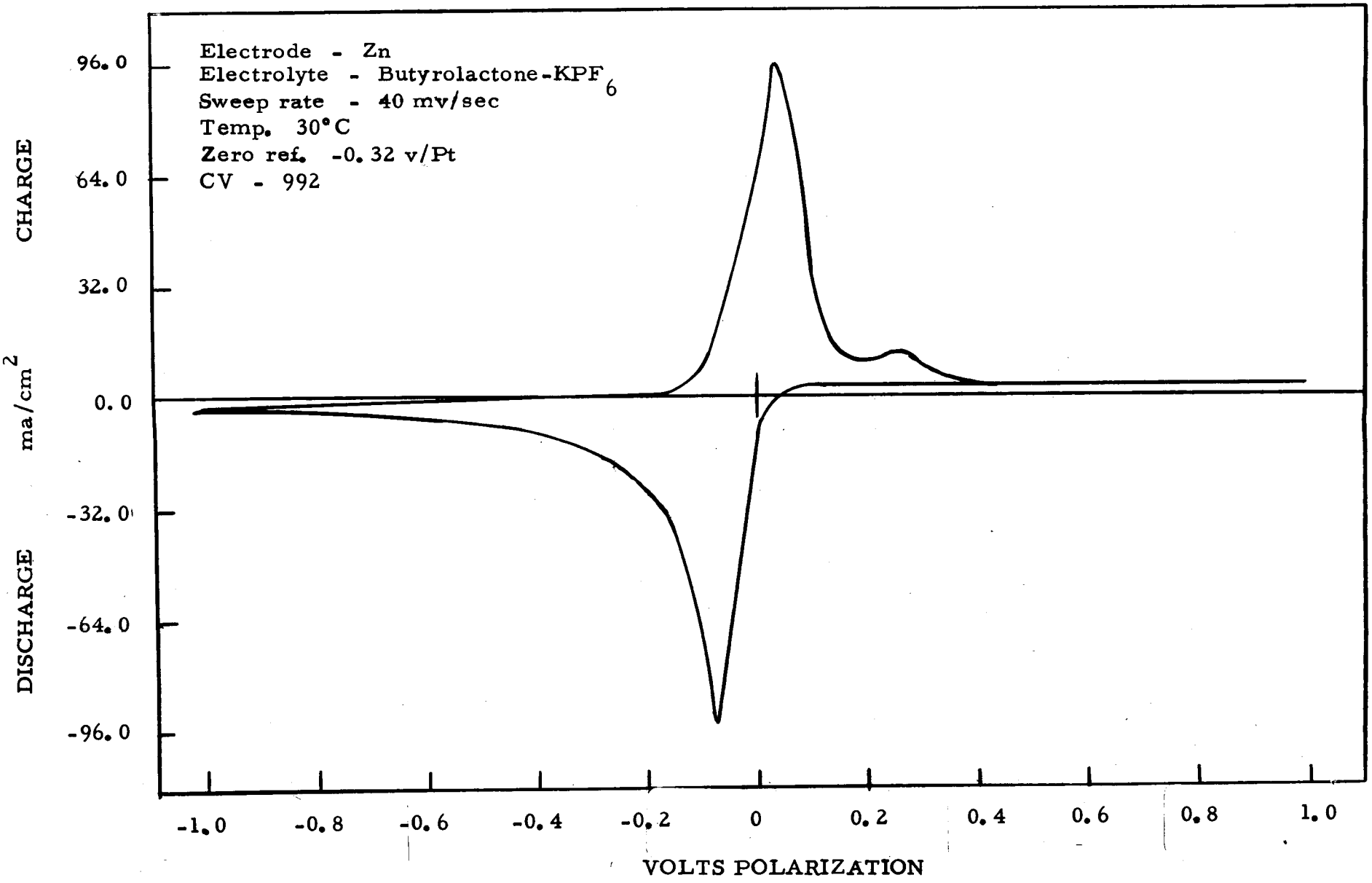
Electrode - Zn
Electrolyte - Butyrolactone-KPF6
Sweep rate - 40 mv/sec
Temp. 30°C
Zero ref. -0.32 v/Pt
CV - 992
96.0
64.0
32.0
0.0
-32.0
-64.0
-96.0
CHARGE
DISCHARGE
ma/cm2
-1.0
-0.8
-0.6
-0.4
-0.2
0
0.2
0.4
0.6
0.8
1.0
VOLTS POLARIZATION

Figure 14

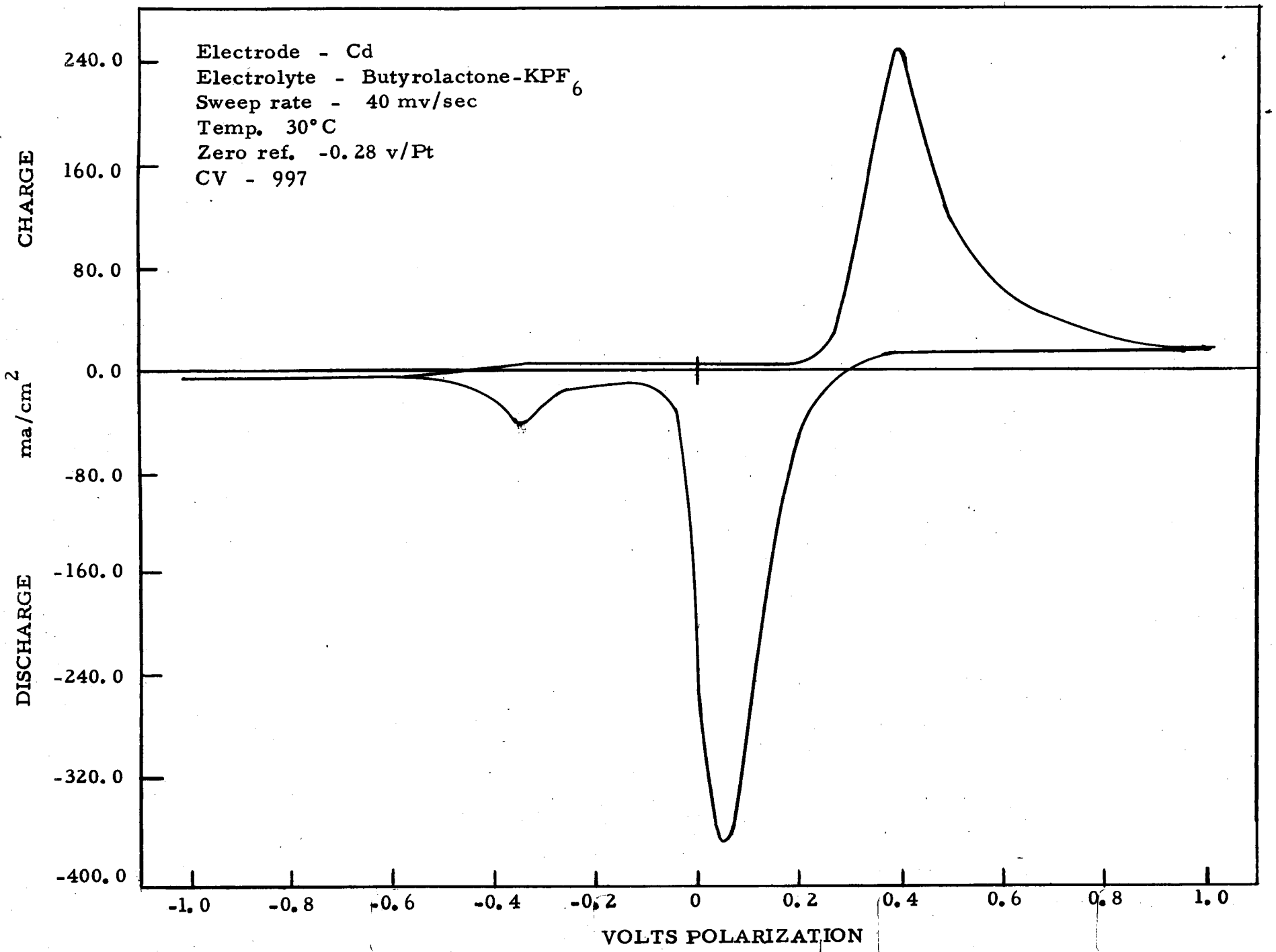
Electrode - Cd
Electrolyte - Butyrolactone-KPF6
Sweep rate - 40 mv/sec
Temp. 30°C
Zero ref. -0.28 v/Pt
CV - 997
CHARGE
DISCHARGE
ma/cm2
240.0
160.0
80.0
0.0
-80.0
-160.0
-240.0
-320.0
-400.0
-1.0
-0.8
-0.6
-0.4
-0.2
0
0.2
0.4
0.6
0.8
1.0
VOLTS POLARIZATION

Figure 15

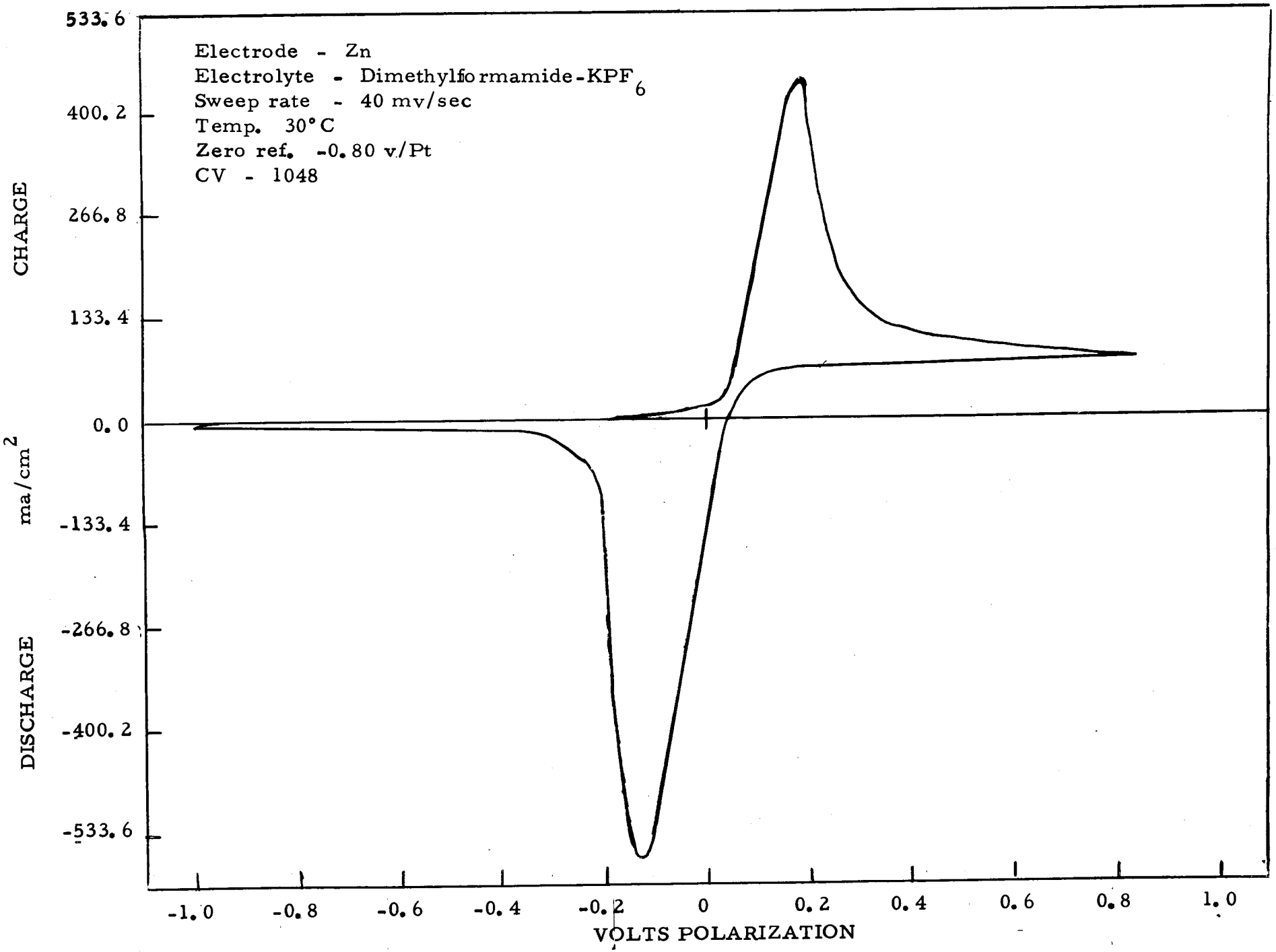
Electrode - Zn
Electrolyte - Dimethylformamide-KPF_6
Sweep rate - 40 mv/sec
Temp. 30°C
Zero ref. -0.80 v/Pt
CV - 1048
533.6
400.2
266.8
133.4
0.0
-133.4
-266.8
-400.2
-533.6
CHARGE
DISCHARGE
ma/cm^2
-1.0
-0.8
-0.6
-0.4
-0.2
0
0.2
0.4
0.6
0.8
1.0
VOLTS POLARIZATION

Figure 16

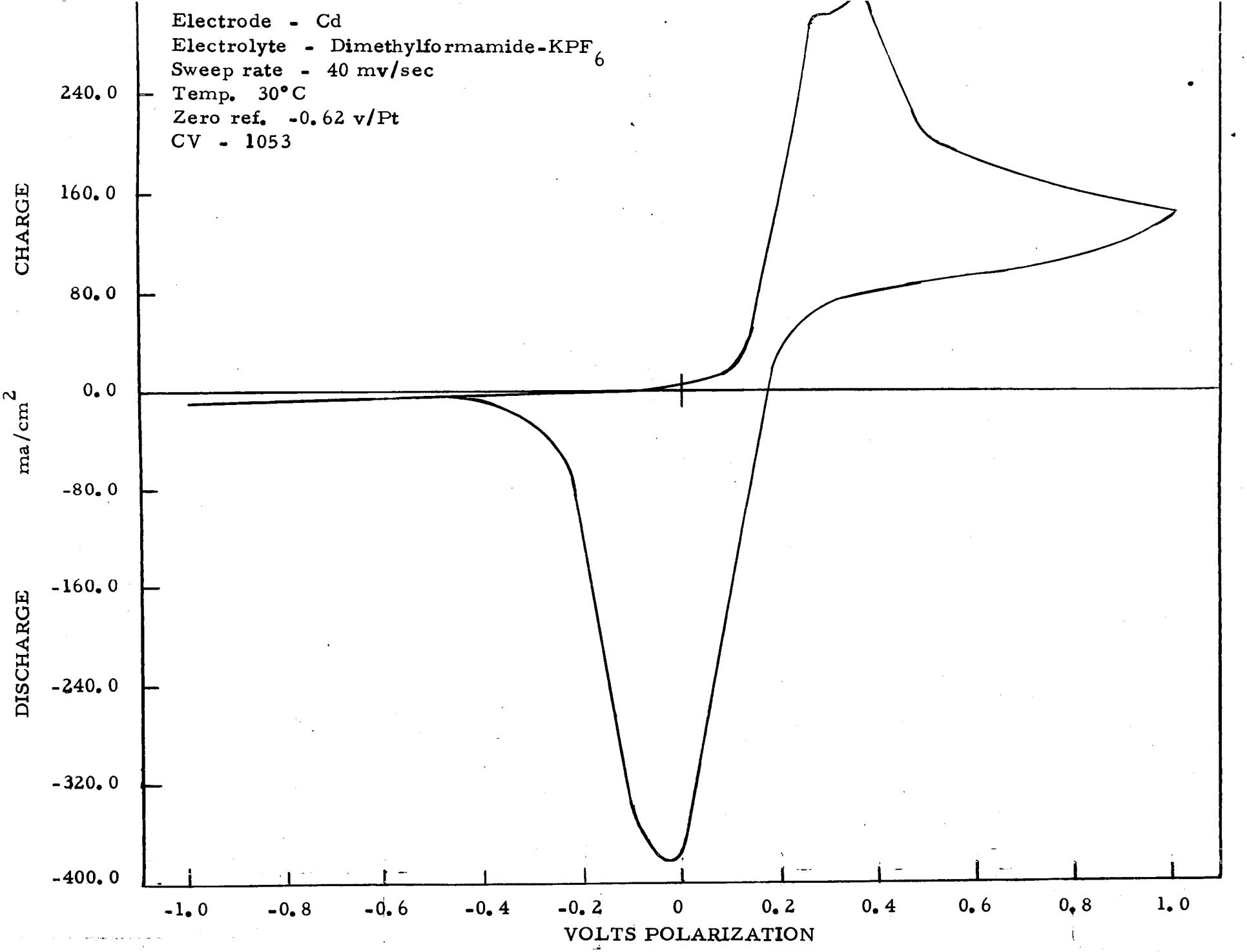
Electrode - Cd
Electrolyte - Dimethylformamide-KPF6
Sweep rate - 40 mv/sec
Temp. 30°C
Zero ref. -0.62 v/Pt
CV - 1053
240.0
160.0
80.0
0.0
-80.0
-160.0
-240.0
-320.0
-400.0
CHARGE
DISCHARGE
ma/cm2
-1.0
-0.8
-0.6
-0.4
-0.2
0
0.2
0.4
0.6
0.8
1.0
VOLTS POLARIZATION

Figure 17

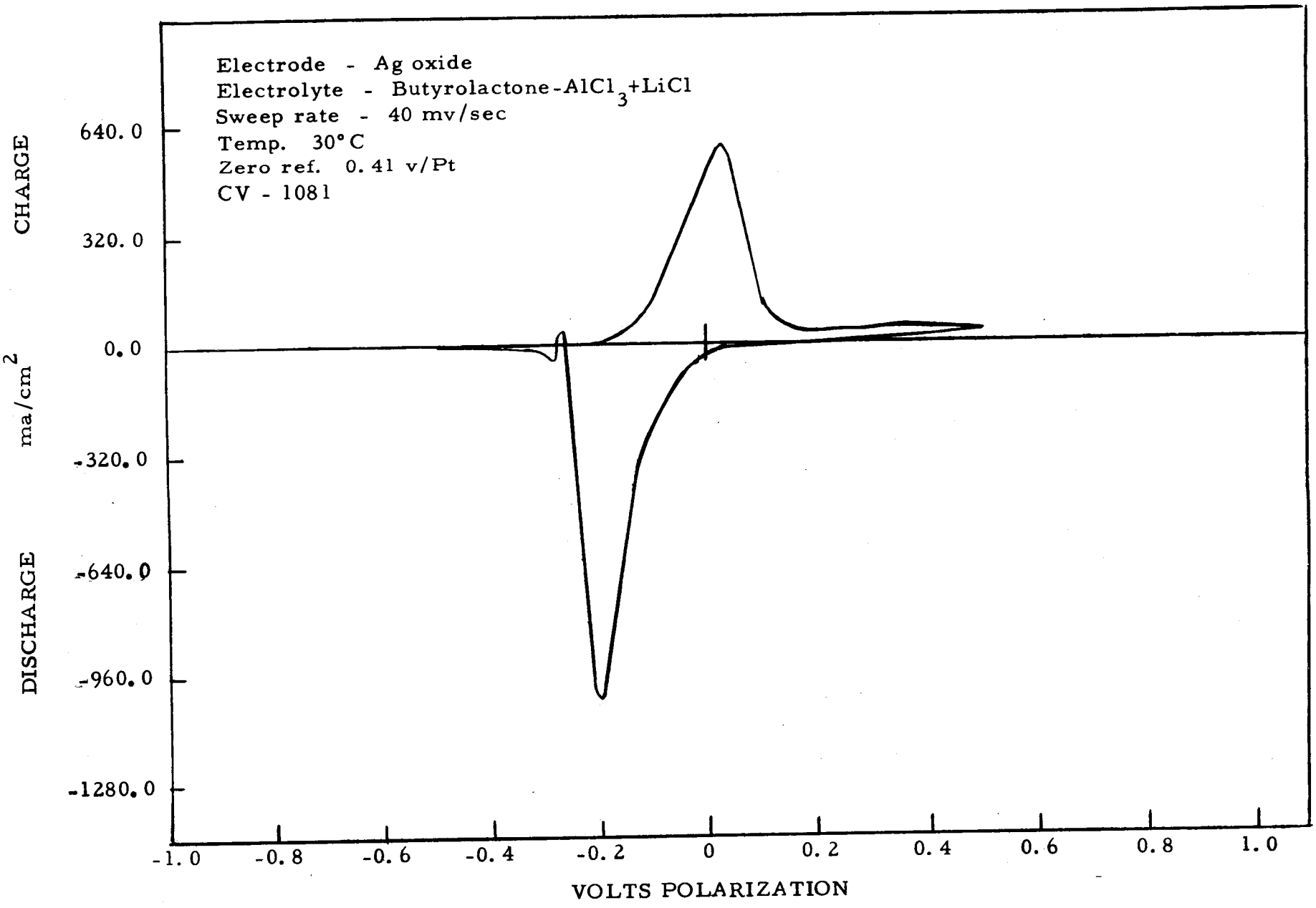
Electrode - Ag oxide
Electrolyte - Butyrolactone-AlCl3+LiCl
Sweep rate - 40 mv/sec
Temp. 30°C
Zero ref. 0.41 v/Pt
CV - 1081
CHARGE
DISCHARGE
ma/cm2
640.0
320.0
0.0
-320.0
-640.0
-960.0
-1280.0
-1.0
-0.8
-0.6
-0.4
-0.2
0
0.2
0.4
0.6
0.8
1.0
VOLTS POLARIZATION

Figure 18

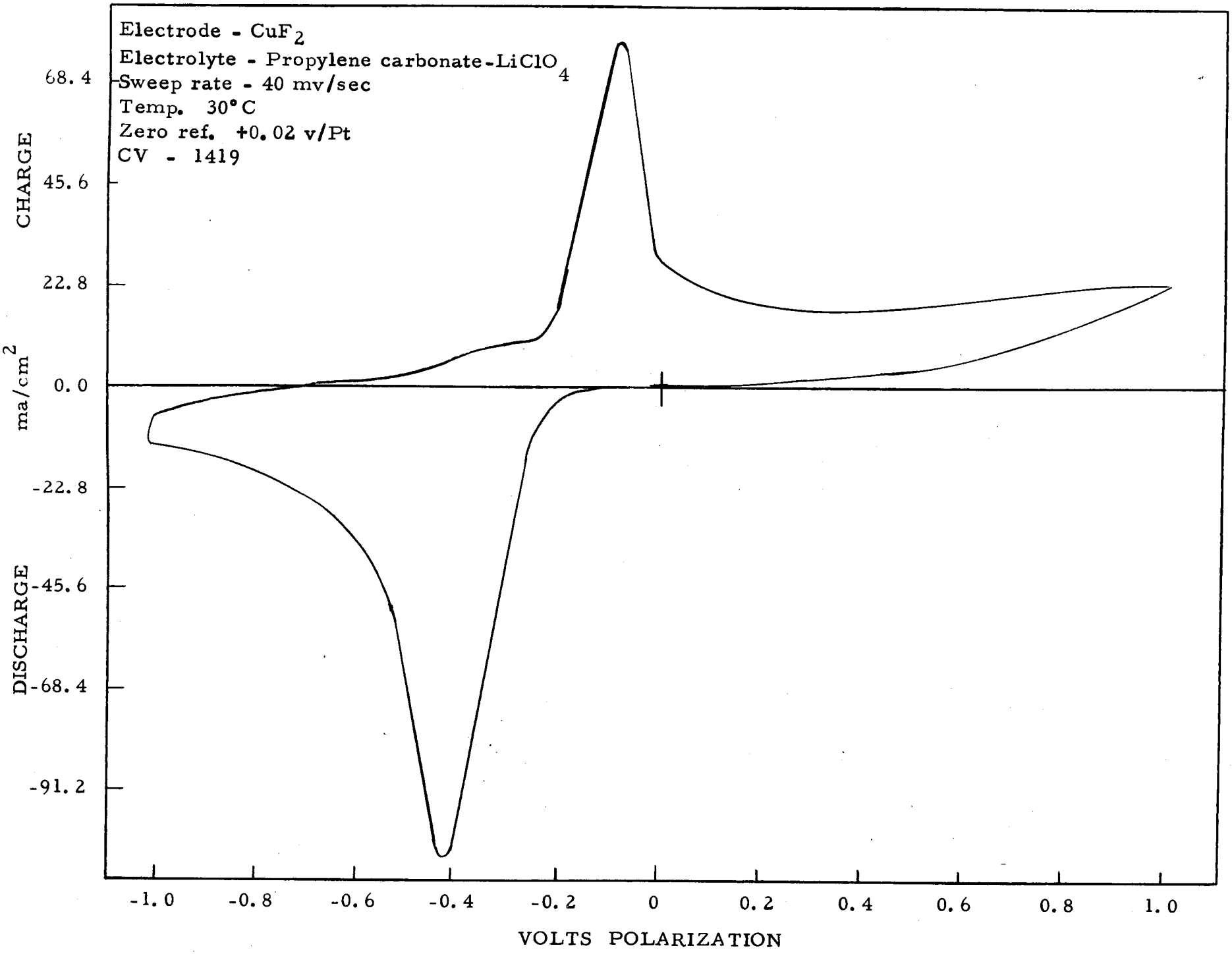
Electrode - CuF_2
Electrolyte - Propylene carbonate-$LiClO_4$
Sweep rate - 40 mv/sec
Temp. 30°C
Zero ref. +0.02 v/Pt
CV - 1419
68.4
45.6
22.8
0.0
-22.8
-45.6
-68.4
-91.2
CHARGE
DISCHARGE
ma/cm^2
-1.0
-0.8
-0.6
-0.4
-0.2
0
0.2
0.4
0.6
0.8
1.0
VOLTS POLARIZATION

Figure 19

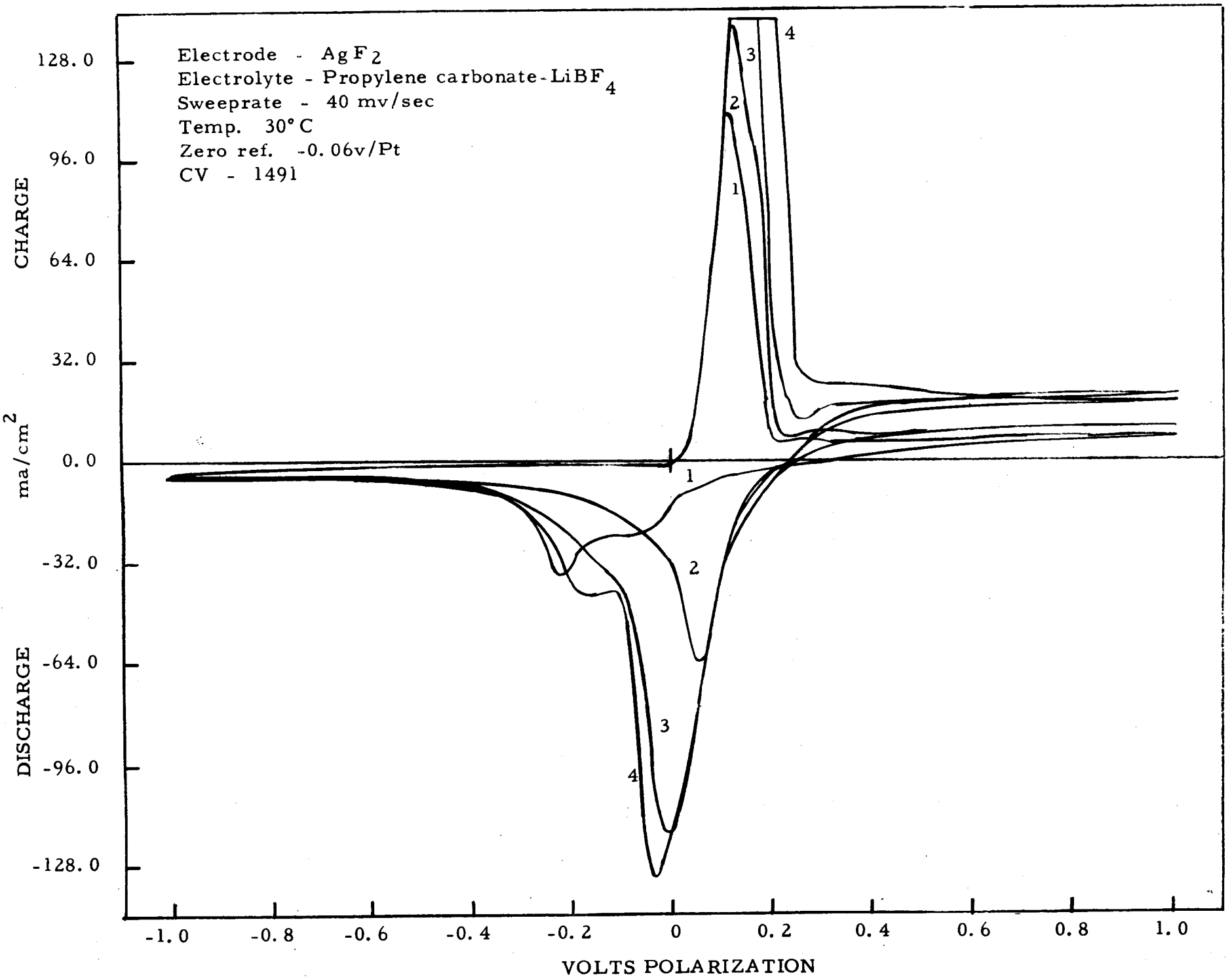
Electrode - AgF_2
Electrolyte - Propylene carbonate-$LiBF_4$
Sweeprate - 40 mv/sec
Temp. 30° C
Zero ref. -0.06v/Pt
CV - 1491
128.0
96.0
64.0
32.0
0.0
-32.0
-64.0
-96.0
-128.0
CHARGE
DISCHARGE
ma/cm^2
1
2
3
4
-1.0
-0.8
-0.6
-0.4
-0.2
0
0.2
0.4
0.6
0.8
1.0
VOLTS POLARIZATION

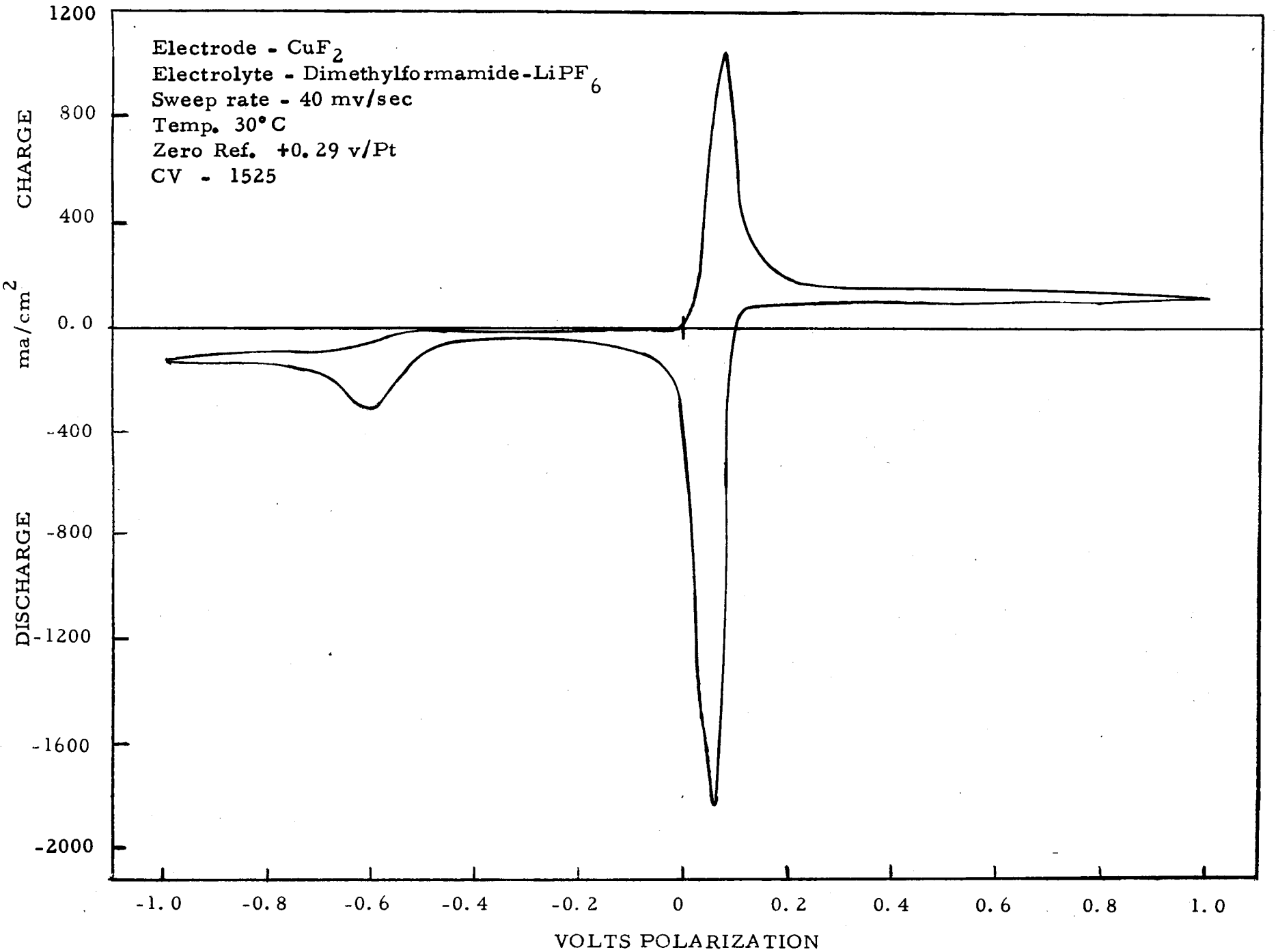
Electrode - CuF_2
Electrolyte - Dimethylformamide-$LiPF_6$
Sweep rate - 40 mv/sec
Temp. 30° C
Zero Ref. +0.29 v/Pt
CV - 1525
CHARGE
DISCHARGE
ma/cm^2
1200
800
400
0.0
-400
-800
-1200
-1600
-2000
-1.0
-0.8
-0.6
-0.4
-0.2
0
0.2
0.4
0.6
0.8
1.0
VOLTS POLARIZATION

Figure 21

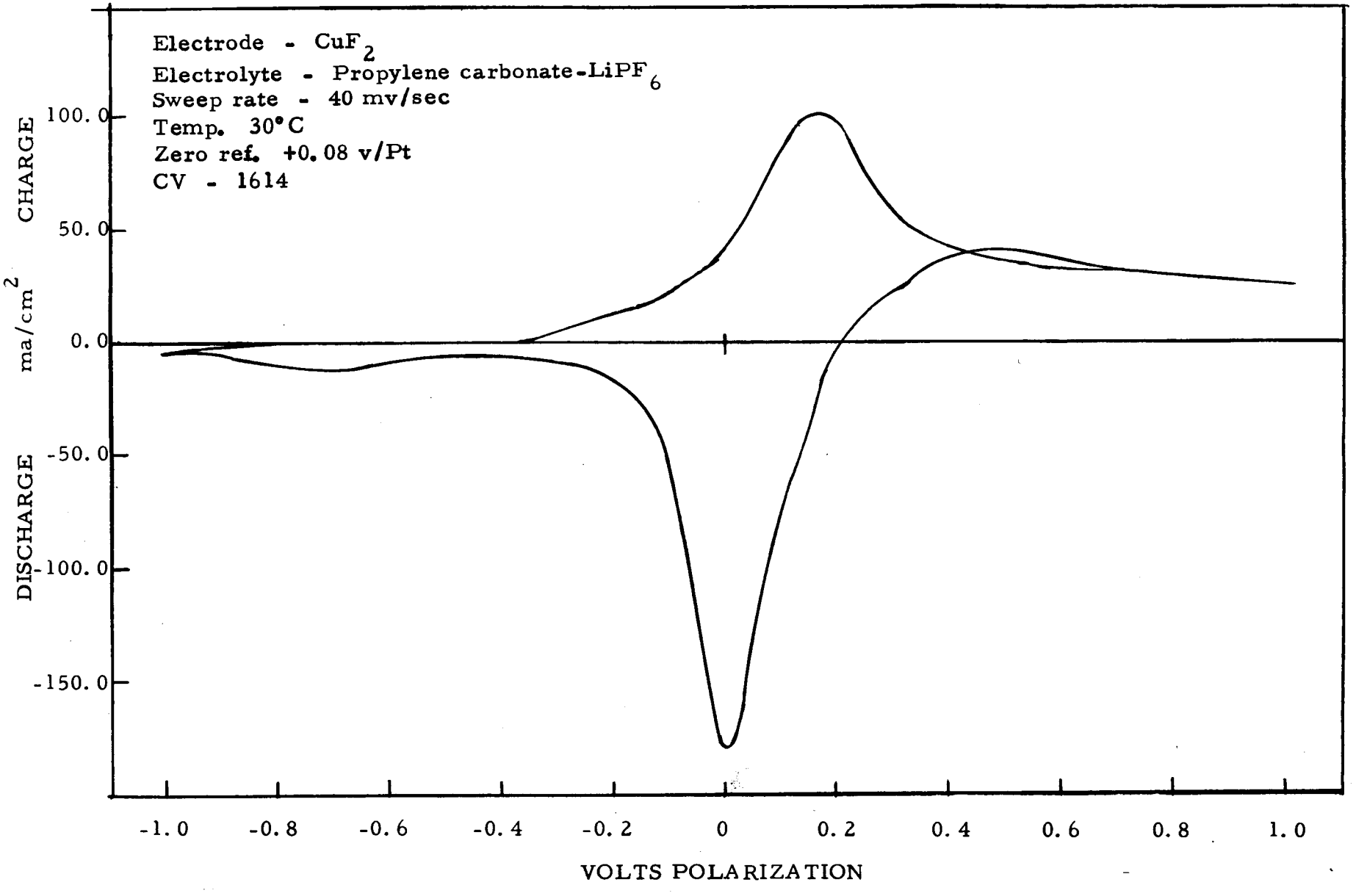
Electrode - CuF_2
Electrolyte - Propylene carbonate-$LiPF_6$
Sweep rate - 40 mv/sec
Temp. 30°C
Zero ref. +0.08 v/Pt
CV - 1614
CHARGE
DISCHARGE
ma/cm^2
100.0
50.0
0.0
-50.0
-100.0
-150.0
-1.0
-0.8
-0.6
-0.4
-0.2
0
0.2
0.4
0.6
0.8
1.0
VOLTS POLARIZATION

Figure 22

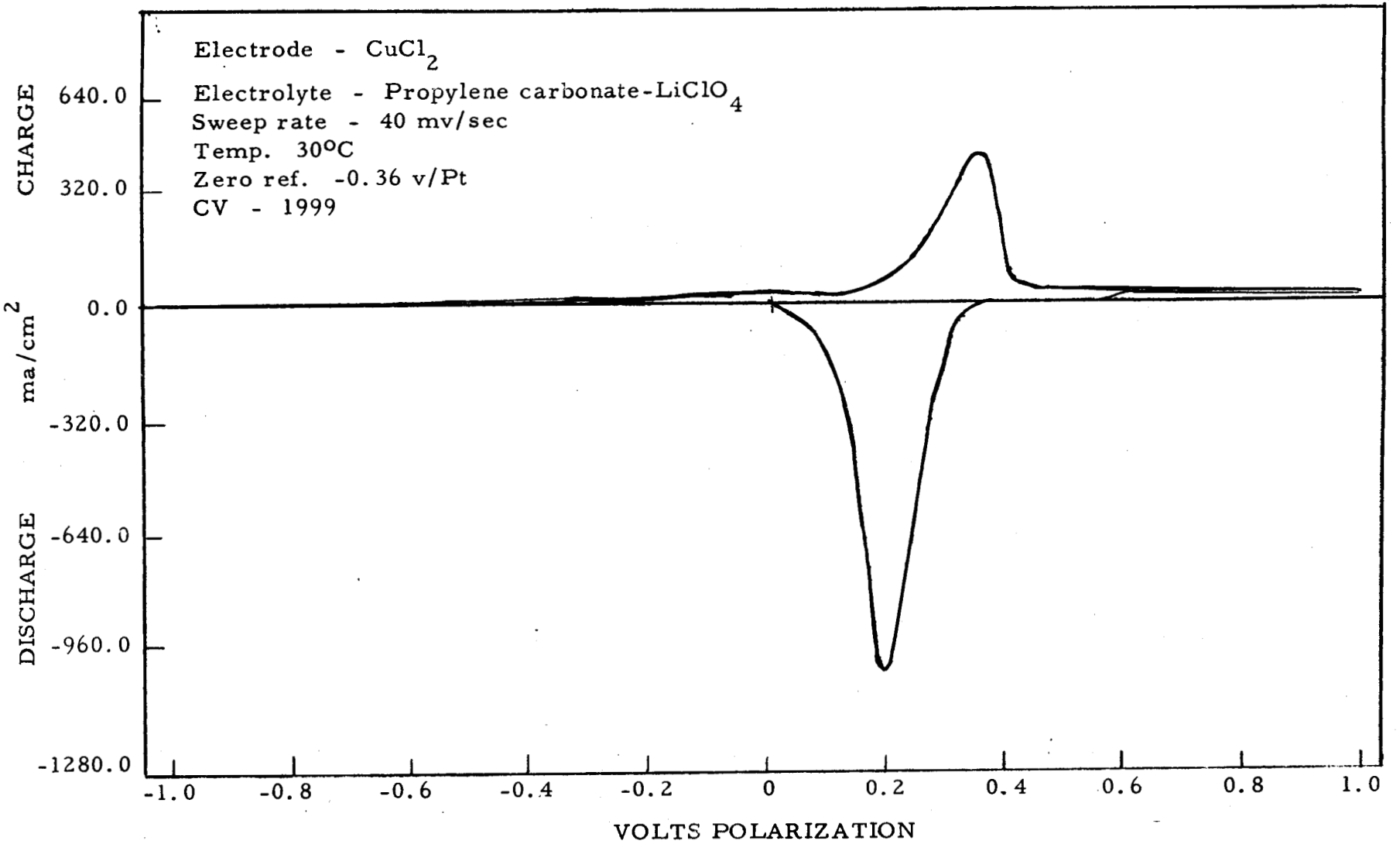
Electrode - $CuCl_2$
Electrolyte - Propylene carbonate-$LiClO_4$
Sweep rate - 40 mv/sec
Temp. 30°C
Zero ref. -0.36 v/Pt
CV - 1999
CHARGE
DISCHARGE
ma/cm^2
640.0
320.0
0.0
-320.0
-640.0
-960.0
-1280.0
-1.0
-0.8
-0.6
-0.4
-0.2
0
0.2
0.4
0.6
0.8
1.0
VOLTS POLARIZATION

Figure 23

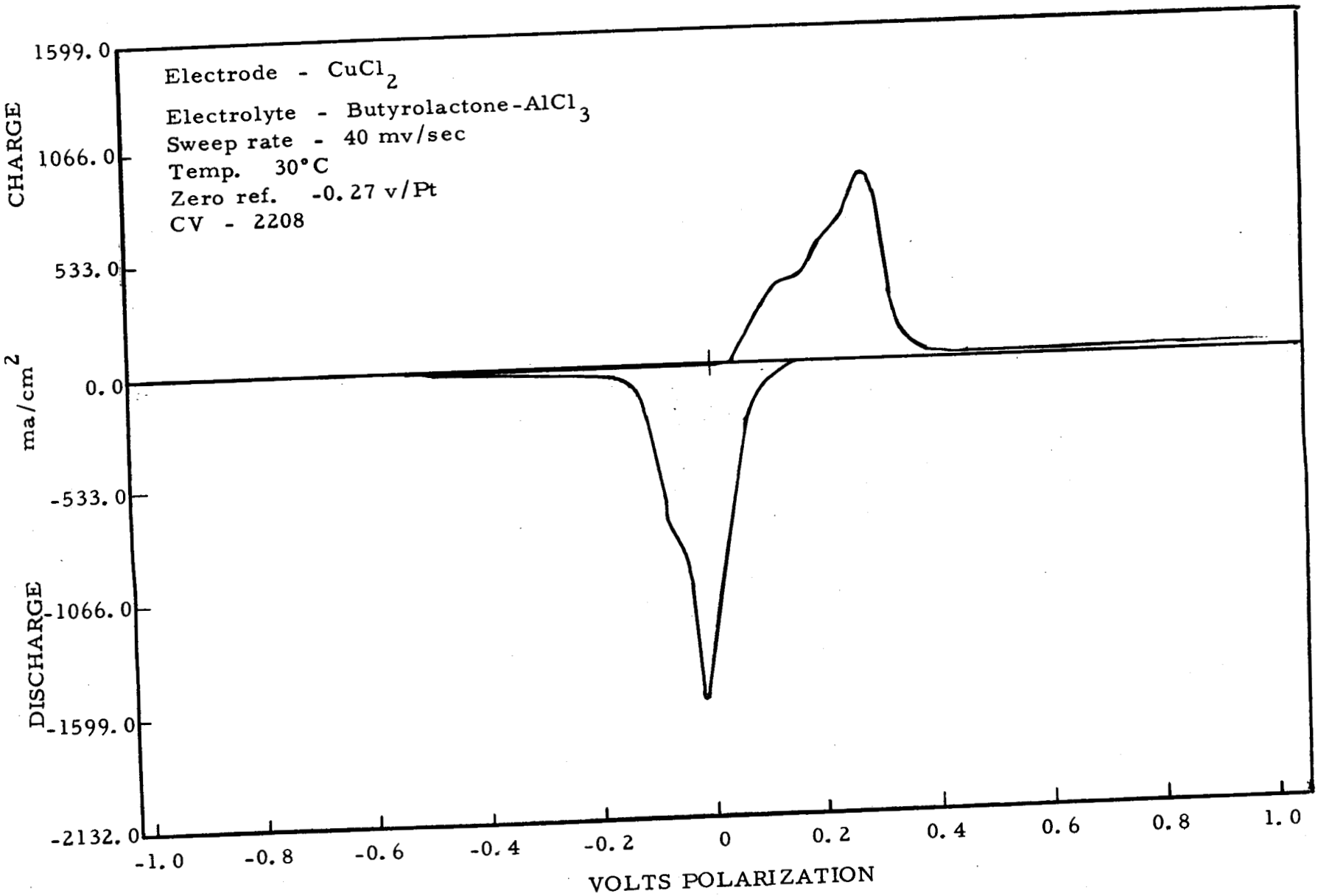
Electrode - $CuCl_2$
Electrolyte - Butyrolactone-$AlCl_3$
Sweep rate - 40 mv/sec
Temp. 30°C
Zero ref. -0.27 v/Pt
CV - 2208
CHARGE
DISCHARGE
ma/cm^2
1599.0
1066.0
533.0
0.0
-533.0
-1066.0
-1599.0
-2132.0
-1.0
-0.8
-0.6
-0.4
-0.2
0
0.2
0.4
0.6
0.8
1.0
VOLTS POLARIZATION

Figure 24

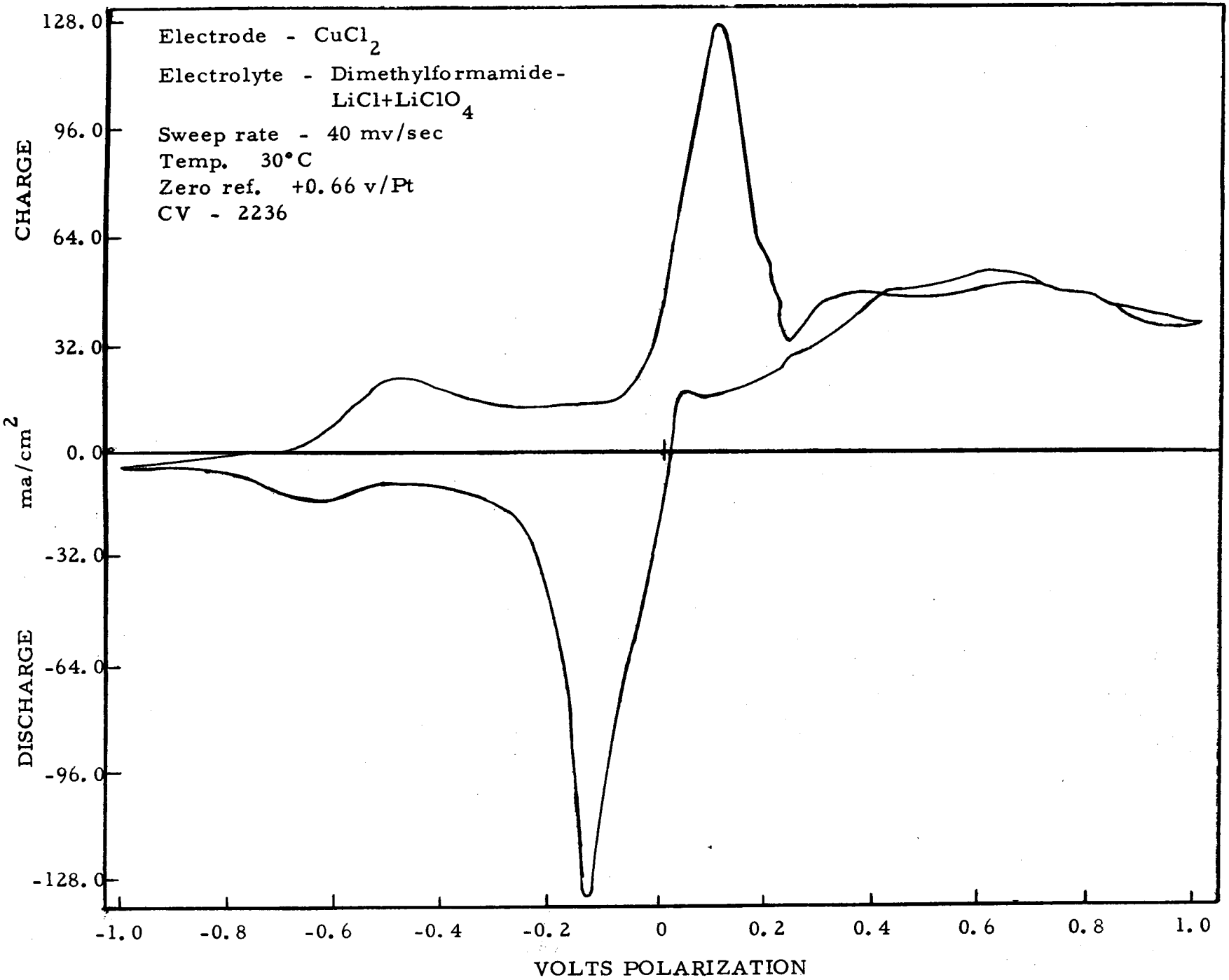
Electrode - $CuCl_2$
Electrolyte - Dimethylformamide-
$LiCl+LiClO_4$
Sweep rate - 40 mv/sec
Temp. 30°C
Zero ref. +0.66 v/Pt
CV - 2236
CHARGE
DISCHARGE
ma/cm^2
128.0
96.0
64.0
32.0
0.0
-32.0
-64.0
-96.0
-128.0
-1.0
-0.8
-0.6
-0.4
-0.2
0
0.2
0.4
0.6
0.8
1.0
VOLTS POLARIZATION

Figure 25

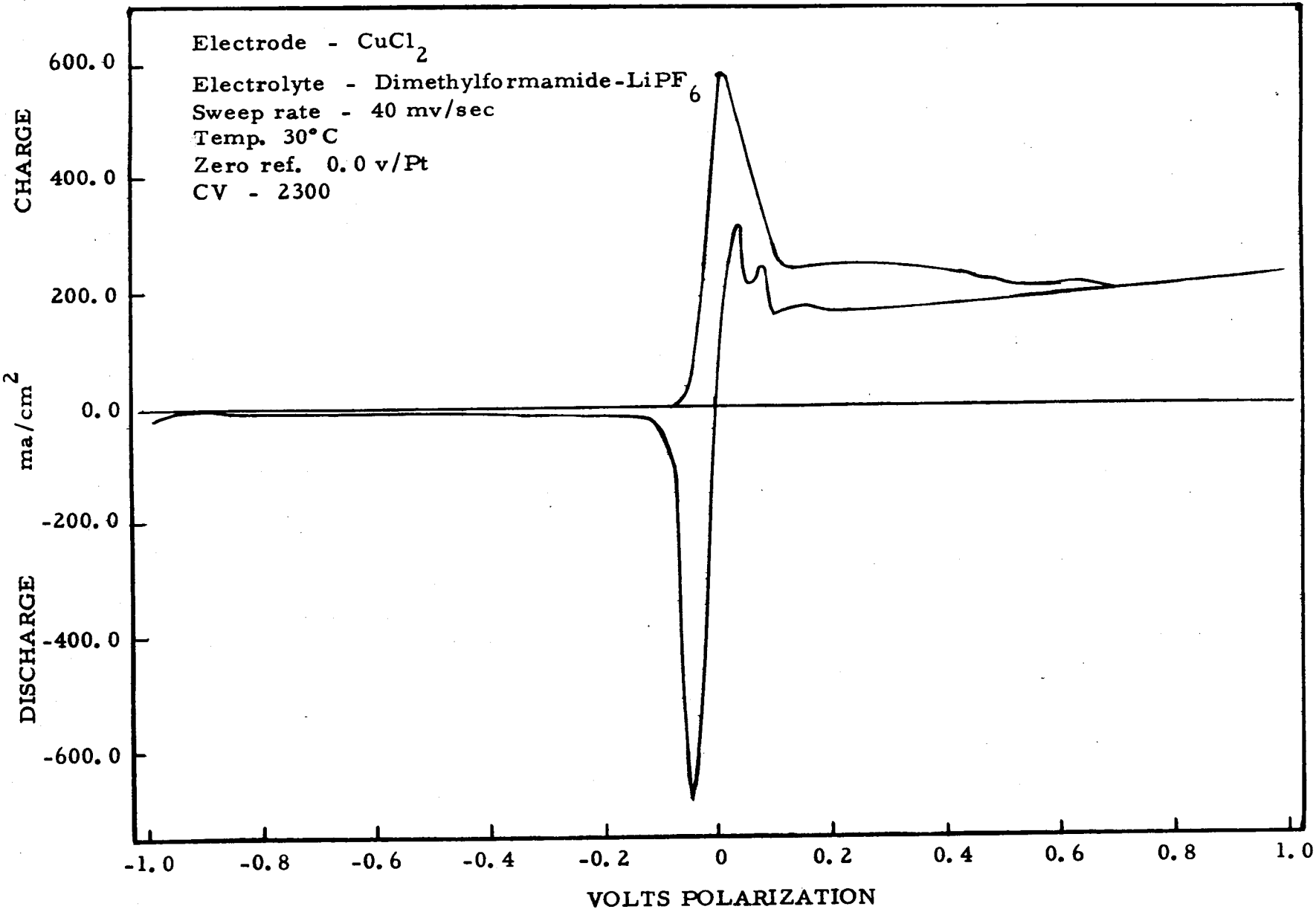
Electrode - $CuCl_2$
Electrolyte - Dimethylformamide-$LiPF_6$
Sweep rate - 40 mv/sec
Temp. 30°C
Zero ref. 0.0 v/Pt
CV - 2300
CHARGE
DISCHARGE
ma/cm^2
600.0
400.0
200.0
0.0
-200.0
-400.0
-600.0
-1.0
-0.8
-0.6
-0.4
-0.2
0
0.2
0.4
0.6
0.8
1.0
VOLTS POLARIZATION

Figure 26

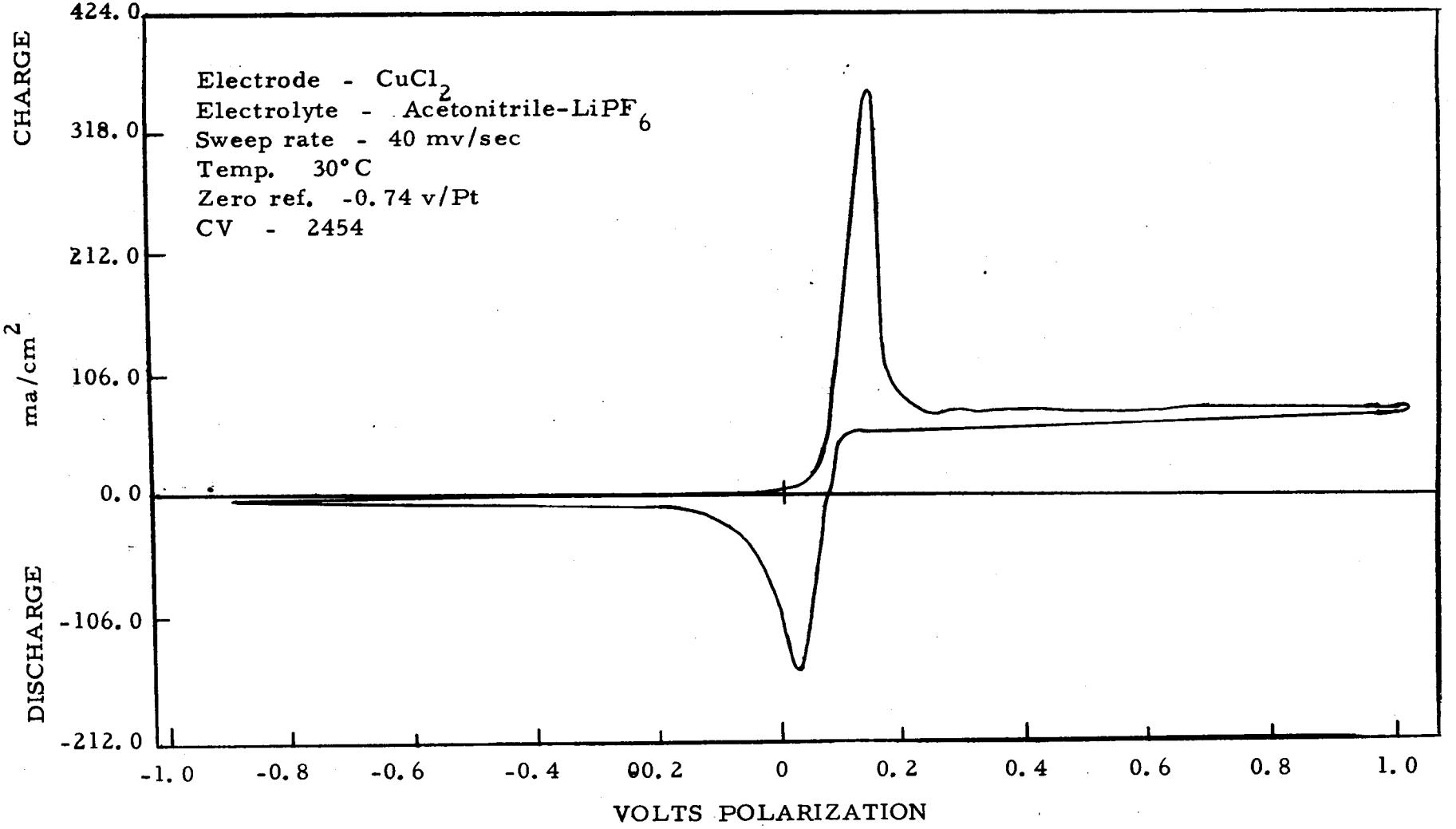
424.0
318.0
212.0
106.0
0.0
-106.0
-212.0
CHARGE
DISCHARGE
ma/cm 2
Electrode - CuCl2
Electrolyte - Acetonitrile-LiPF6
Sweep rate - 40 mv/sec
Temp. 30°C
Zero ref. -0.74 v/Pt
CV - 2454
-1.0
-0.8
-0.6
-0.4
-0.2
0
0.2
0.4
0.6
0.8
1.0
VOLTS POLARIZATION

Figure 27

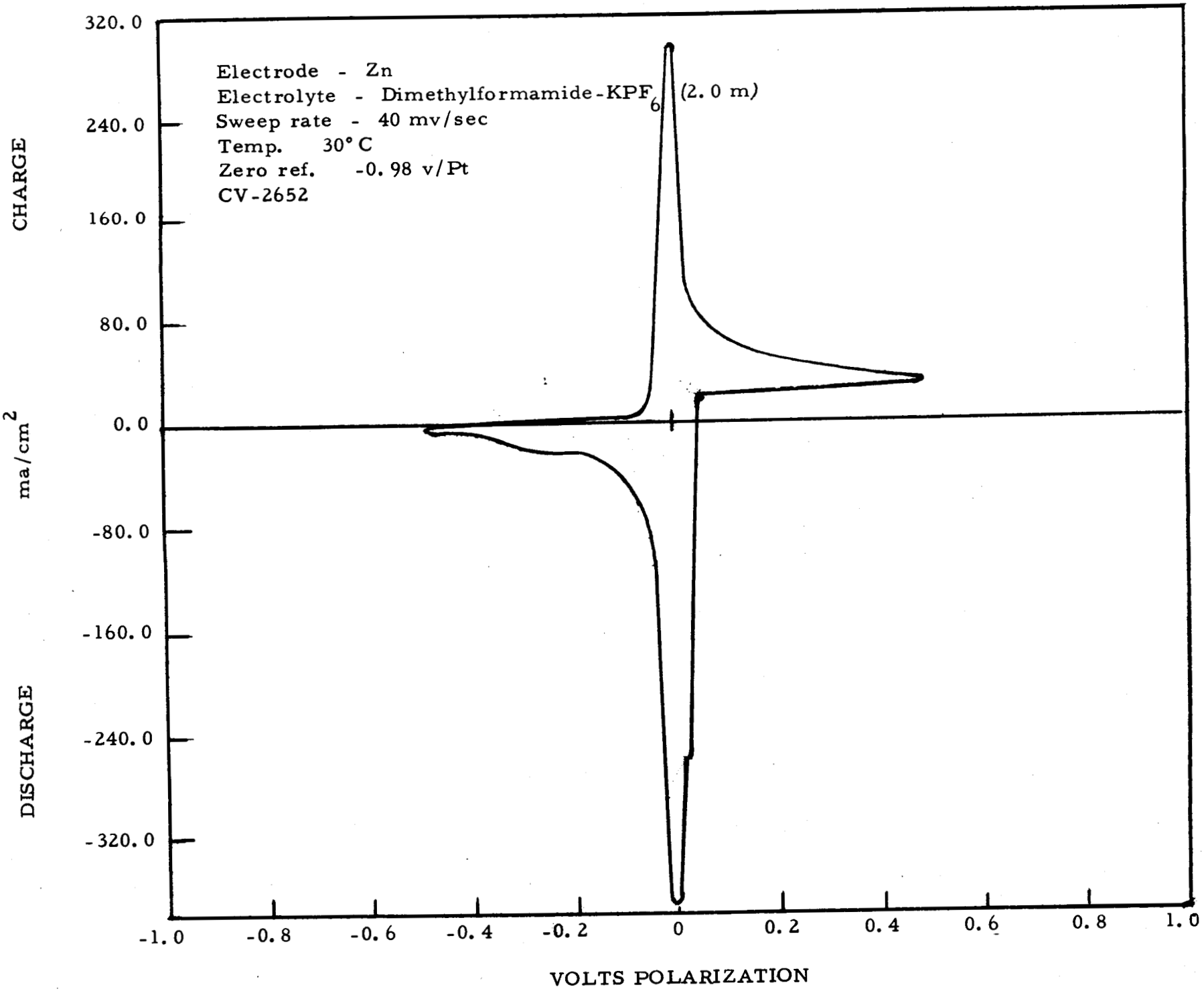
Electrode - Zn
Electrolyte - Dimethylformamide-KPF_6 (2.0 m)
Sweep rate - 40 mv/sec
Temp. 30° C
Zero ref. -0.98 v/Pt
CV-2652
320.0
240.0
160.0
80.0
0.0
-80.0
-160.0
-240.0
-320.0
CHARGE
DISCHARGE
ma/cm^2
-1.0
-0.8
-0.6
-0.4
-0.2
0
0.2
0.4
0.6
0.8
1.0
VOLTS POLARIZATION

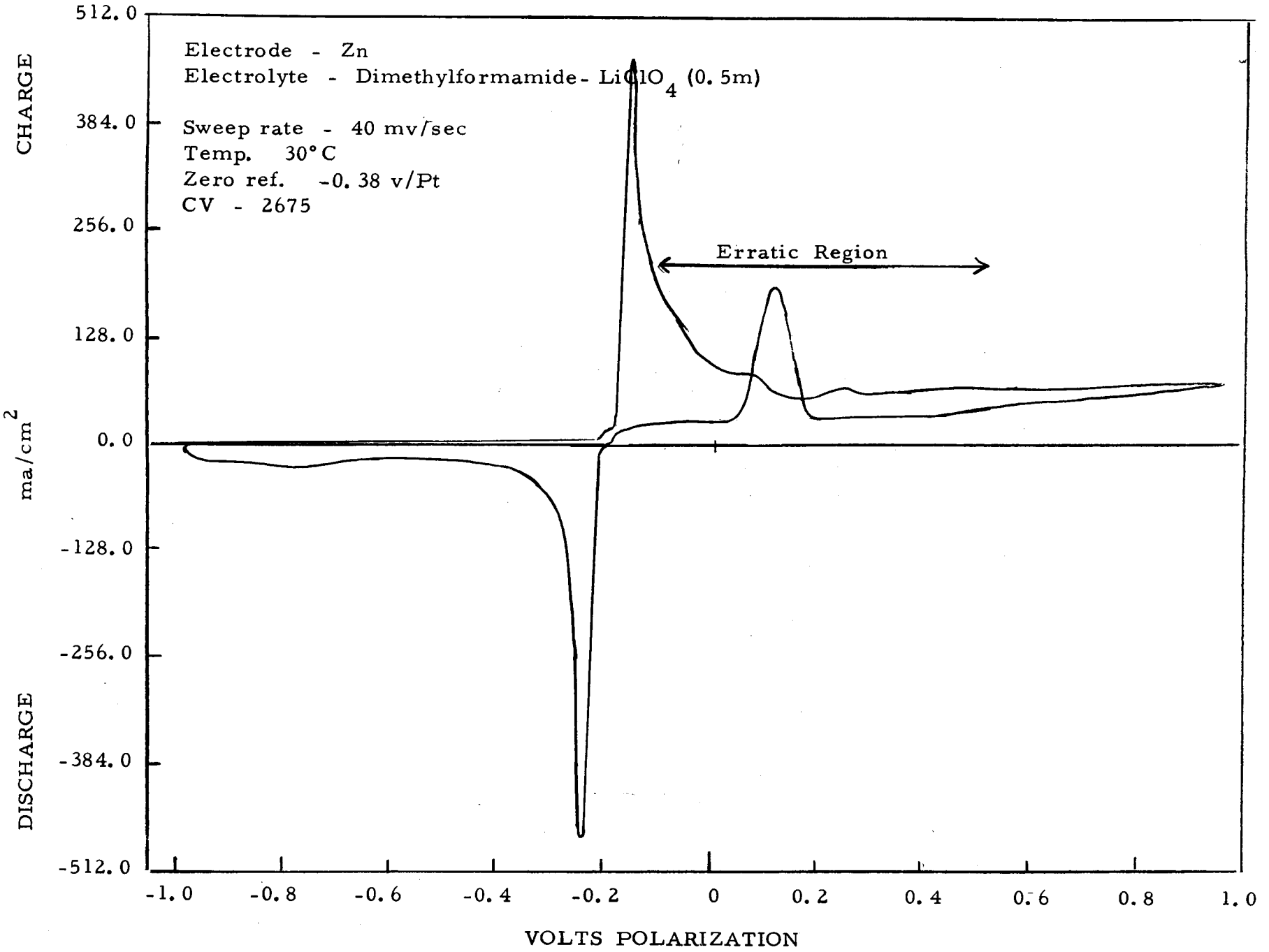
Electrode - Zn
Electrolyte - Dimethylformamide- $LiClO_4$ (0.5m)
Sweep rate - 40 mv/sec
Temp. 30°C
Zero ref. -0.38 v/Pt
CV - 2675
Erratic Region
CHARGE
DISCHARGE
ma/cm^2
512.0
384.0
256.0
128.0
0.0
-128.0
-256.0
-384.0
-512.0
-1.0
-0.8
-0.6
-0.4
-0.2
0
0.2
0.4
0.6
0.8
1.0
VOLTS POLARIZATION

Figure 29

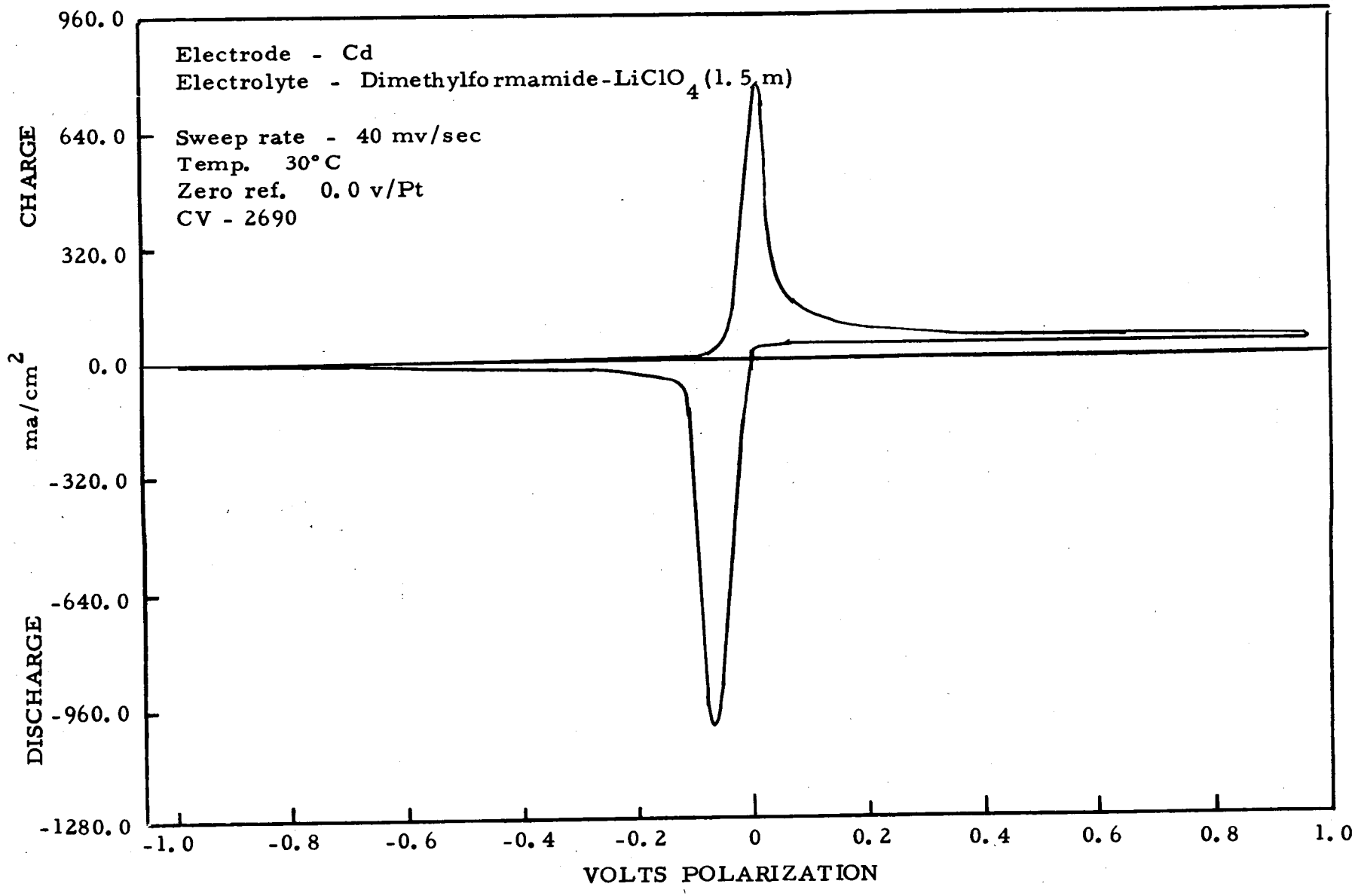
Electrode - Cd
Electrolyte - Dimethylformamide-$LiClO_4$ (1.5 m)
Sweep rate - 40 mv/sec
Temp. 30° C
Zero ref. 0.0 v/Pt
CV - 2690
960.0
640.0
320.0
0.0
-320.0
-640.0
-960.0
-1280.0
CHARGE
DISCHARGE
ma/cm^2
-1.0
-0.8
-0.6
-0.4
-0.2
0
0.2
0.4
0.6
0.8
1.0
VOLTS POLARIZATION

Figure 30

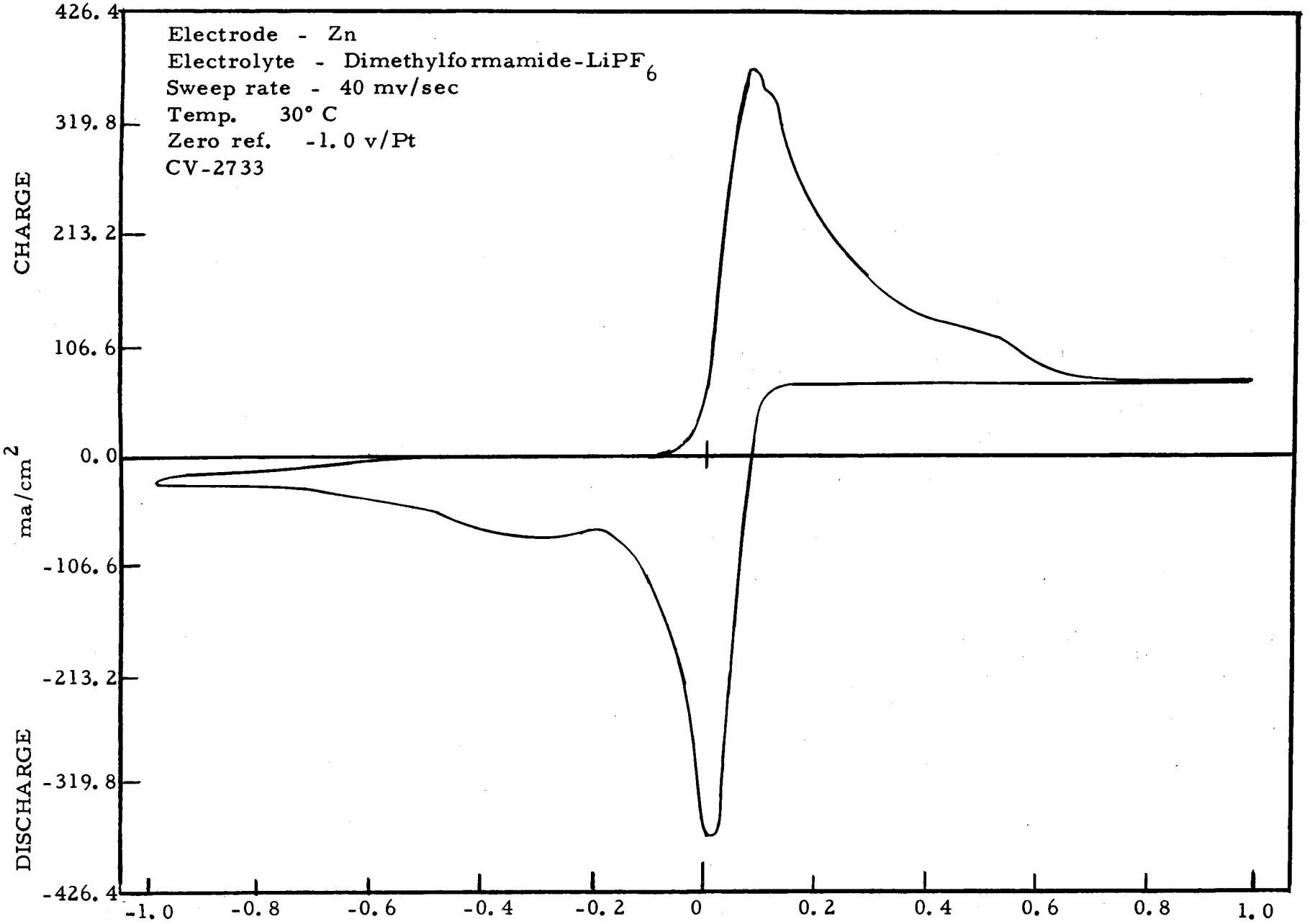
Electrode - Zn
Electrolyte - Dimethylformamide-LiPF6
Sweep rate - 40 mv/sec
Temp. 30° C
Zero ref. -1.0 v/Pt
CV-2733
426.4
319.8
213.2
106.6
0.0
-106.6
-213.2
-319.8
-426.4
CHARGE
DISCHARGE
ma/cm2
-1.0
-0.8
-0.6
-0.4
-0.2
0
0.2
0.4
0.6
0.8
1.0
VOLTS POLARIZATION

Figure 31

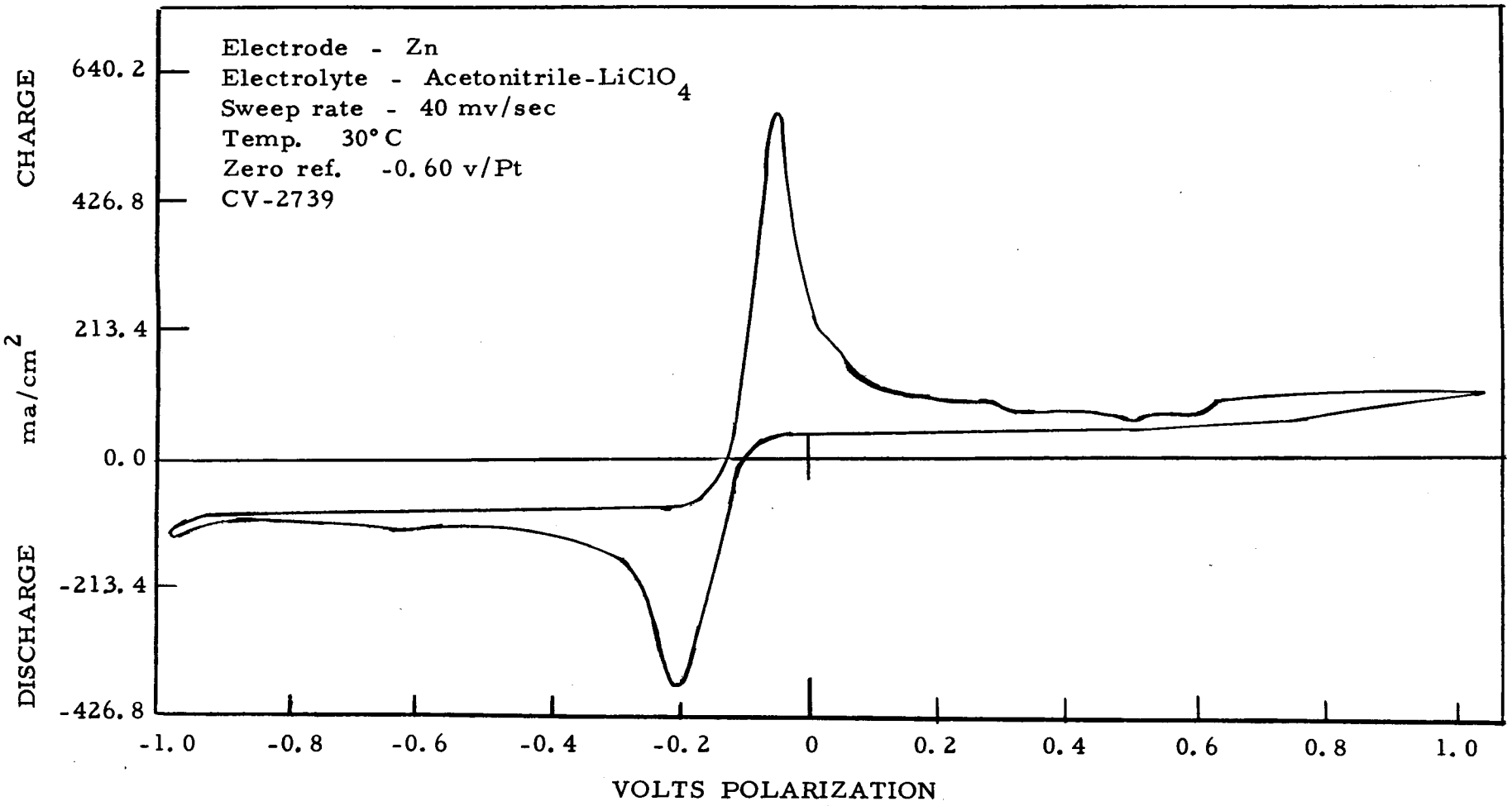
Electrode - Zn
Electrolyte - Acetonitrile-LiClO4
Sweep rate - 40 mv/sec
Temp. 30° C
Zero ref. -0.60 v/Pt
CV-2739
CHARGE
DISCHARGE
ma/cm2
640.2
426.8
213.4
0.0
-213.4
-426.8
-1.0
-0.8
-0.6
-0.4
-0.2
0
0.2
0.4
0.6
0.8
1.0
VOLTS POLARIZATION

Figure 32

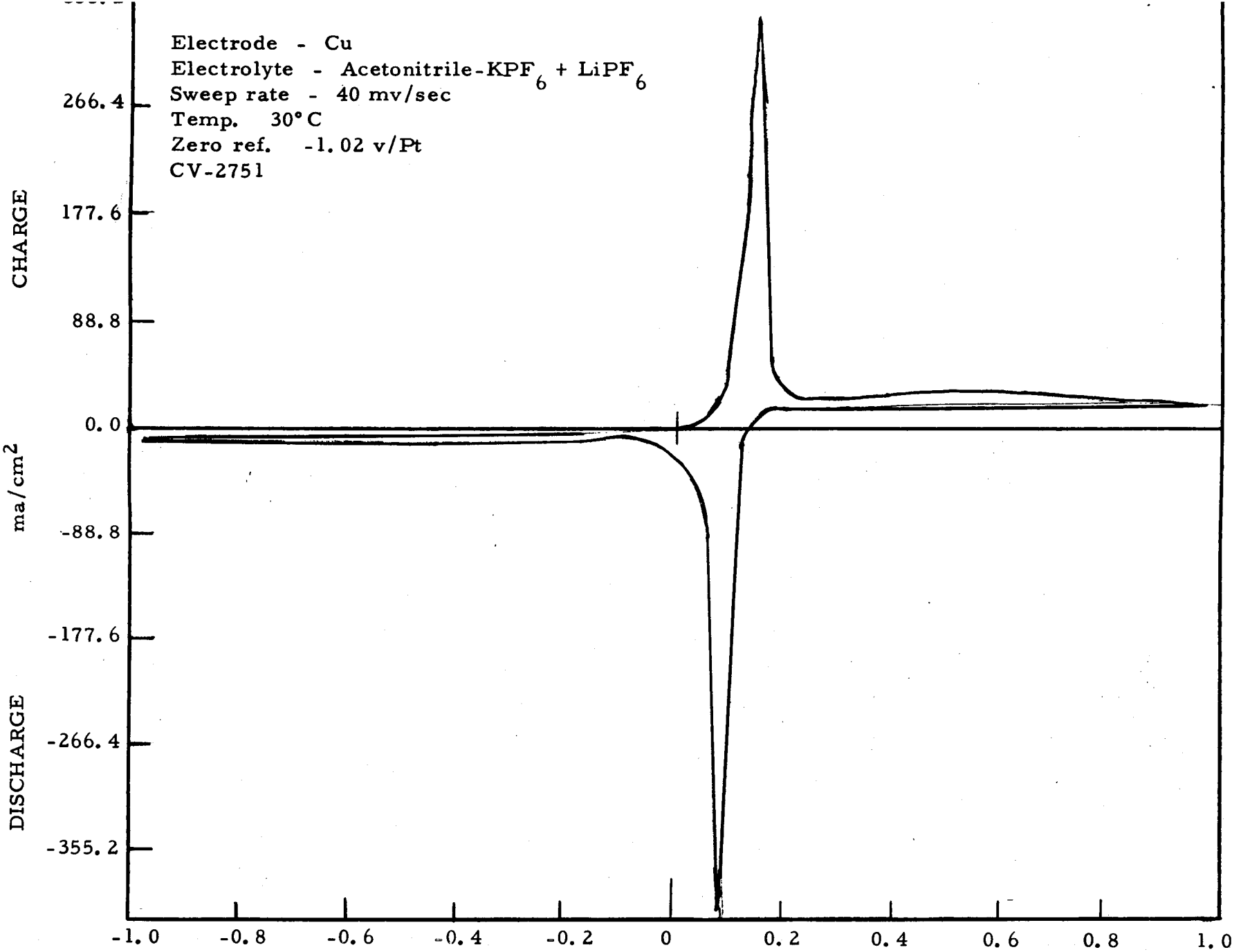
Electrode - Cu
Electrolyte - Acetonitrile-KPF6 + LiPF6
Sweep rate - 40 mv/sec
Temp. 30° C
Zero ref. -1.02 v/Pt
CV-2751
CHARGE
DISCHARGE
ma/cm2
266.4
177.6
88.8
0.0
-88.8
-177.6
-266.4
-355.2
-1.0
-0.8
-0.6
-0.4
-0.2
0
0.2
0.4
0.6
0.8
1.0
VOLTS POLARIZATION

Figure 33

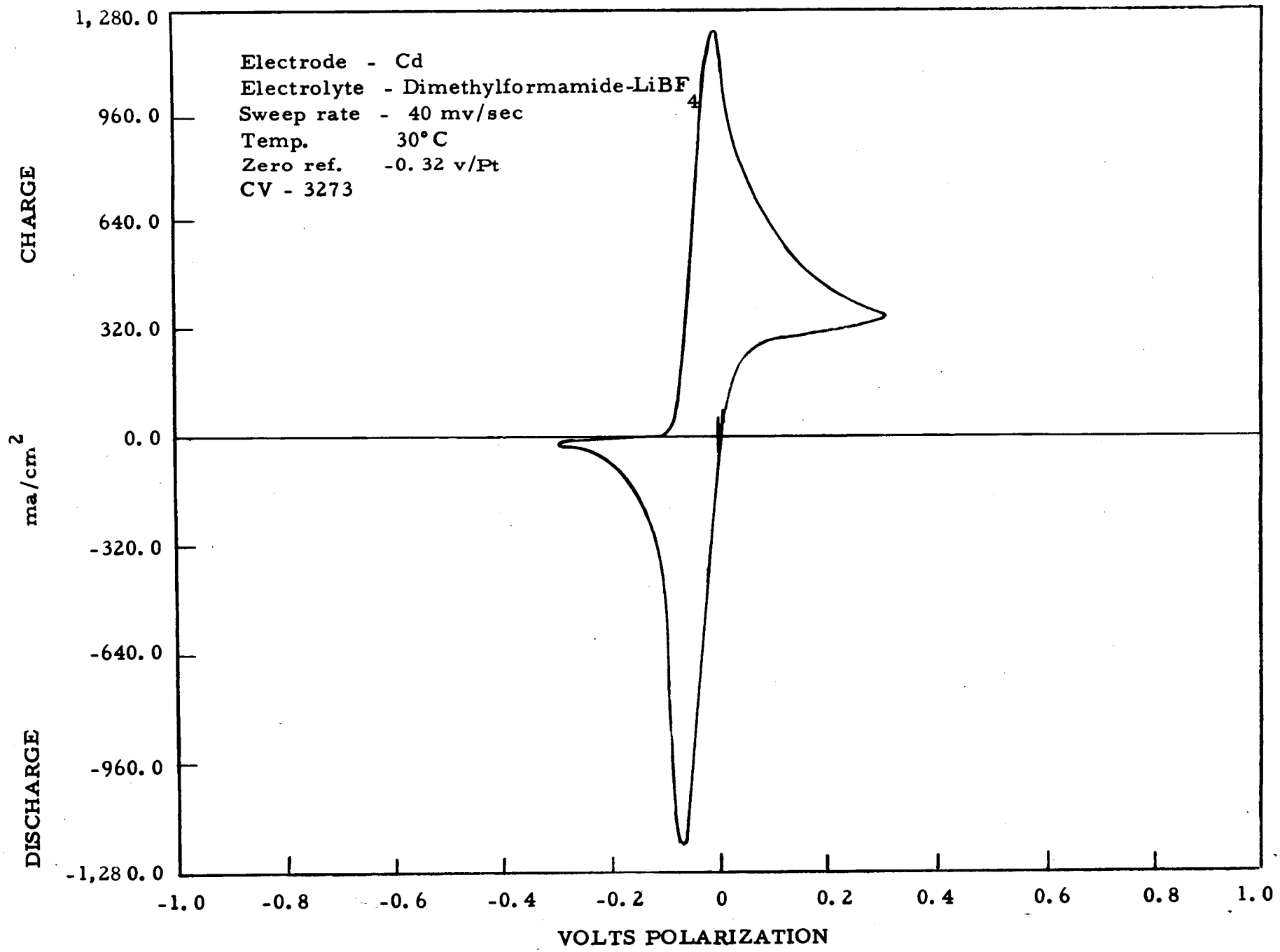
Electrode - Cd
Electrolyte - Dimethylformamide-LiBF4
Sweep rate - 40 mv/sec
Temp. 30° C
Zero ref. -0.32 v/Pt
CV - 3273
1,280.0
960.0
640.0
320.0
0.0
-320.0
-640.0
-960.0
-1,280.0
CHARGE
DISCHARGE
ma/cm2
-1.0
-0.8
-0.6
-0.4
-0.2
0
0.2
0.4
0.6
0.8
1.0
VOLTS POLARIZATION

Figure 34

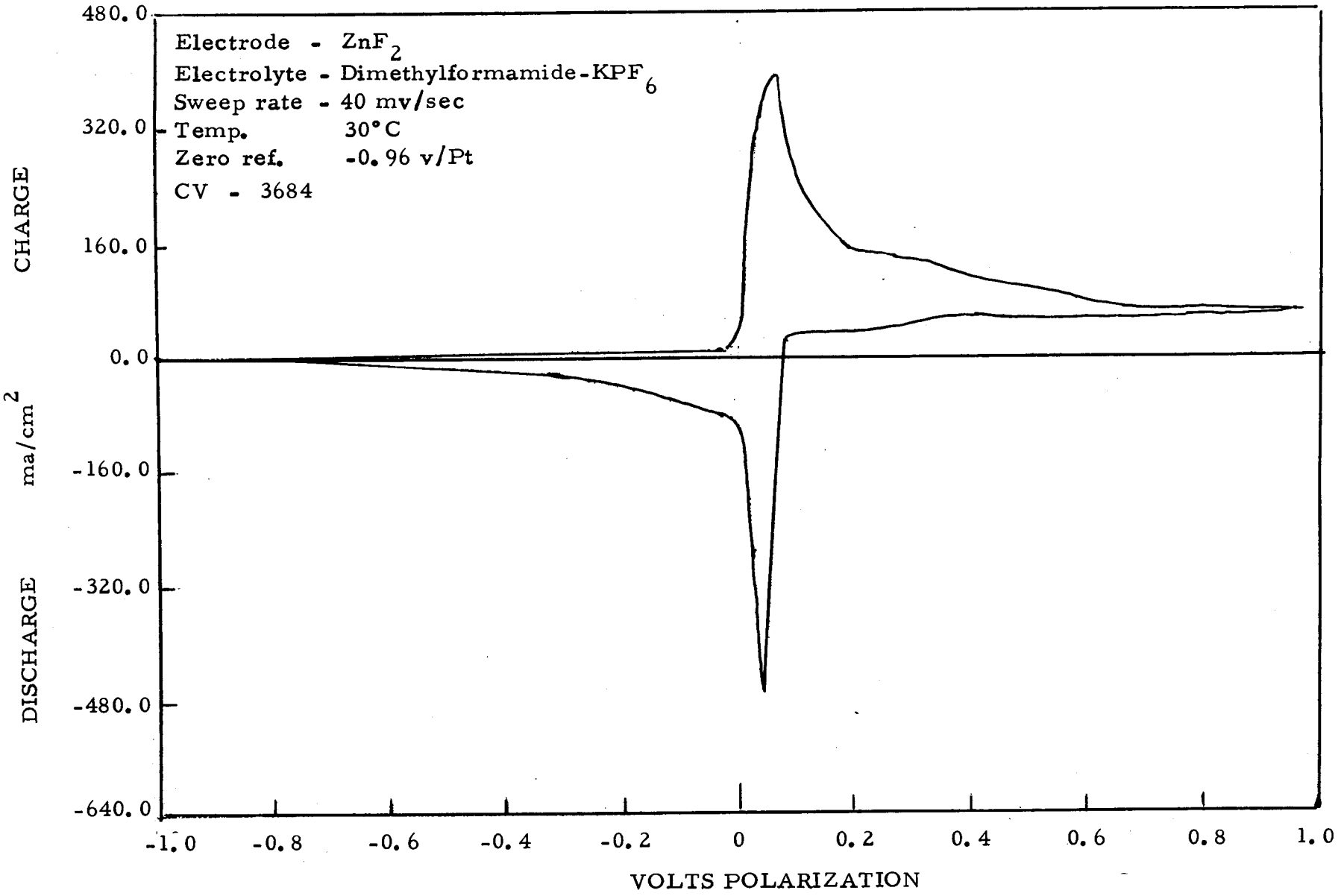
Electrode - ZnF_2
Electrolyte - Dimethylformamide-KPF_6
Sweep rate - 40 mv/sec
Temp. 30°C
Zero ref. -0.96 v/Pt
CV - 3684
480.0
320.0
160.0
0.0
-160.0
-320.0
-480.0
-640.0
CHARGE
DISCHARGE
ma/cm^2
-1.0
-0.8
-0.6
-0.4
-0.2
0
0.2
0.4
0.6
0.8
1.0
VOLTS POLARIZATION

Figure 35

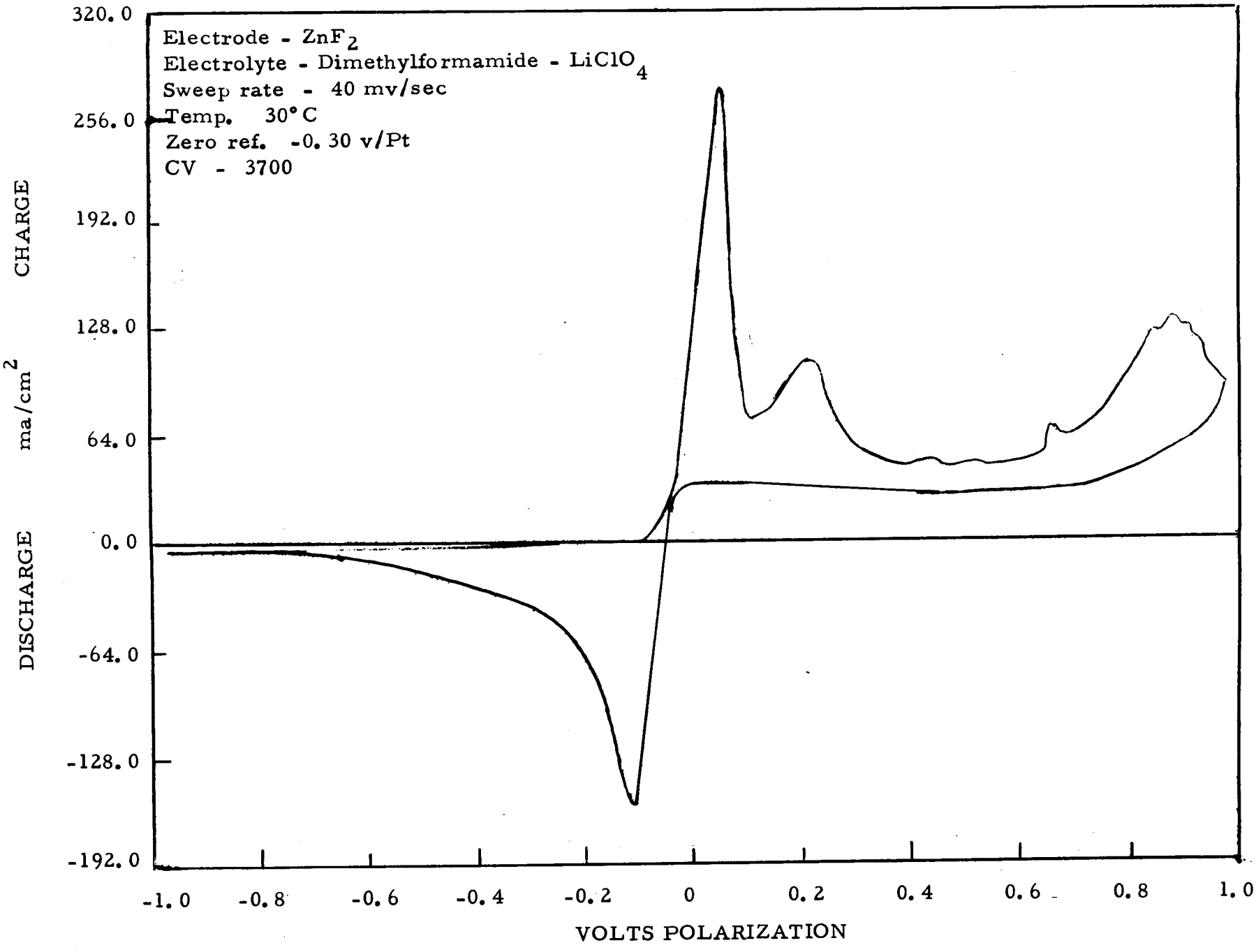
Electrode - ZnF_2
Electrolyte - Dimethylformamide - $LiClO_4$
Sweep rate - 40 mv/sec
Temp. 30° C
Zero ref. -0.30 v/Pt
CV - 3700
320.0
256.0
192.0
128.0
64.0
0.0
-64.0
-128.0
-192.0
CHARGE
DISCHARGE
ma/cm^2
-1.0
-0.8
-0.6
-0.4
-0.2
0
0.2
0.4
0.6
0.8
1.0
VOLTS POLARIZATION

Figure 36

TABLE XII

THE TEN BEST RECOMMENDED SYSTEMS
IN TERMS OF PEAK CURRENT DENSITY*

System	CV	Cathodic C. D. amps/cm^2	Anodic C. D. amps/cm^2	ΔVp ** volts	S_c
CuF_2/DMF-$LiPF_6$	1525	1.86	1.06	0.04	2573
$CuCl_2$/BL-$AlCl_3$	2208	1.60	0.91	0.30	1350
Cd/DMF-$LiBF_4$	3273	1.22	1.22	0.06	1400
AgO/BL-LiCl+$AlCl_3$	1081	1.04	0.62	0.23	955
$CuCl_2$/PC-$LiClO_4$	1999	1.01	0.40	0.20	847
Cd/DMF-$LiClO_4$	2690	0.78	1.04	0.08	1267
$CuCl_2$/DMF-$LiPF_6$	2300	0.70	0.59	0.04	1080
Zn/DMF-KPF_6	1048	0.59	0.45	0.32	333
ZnF_2/DMF-KPF_6	3684	0.49	0.40	0.01	559
Zn/DMF-$LiClO_4$	2675	0.47	0.47	0.09	563

* In order of decreasing peak discharge c. d.

** ΔVp - Peak displacement

S_c - Cathodic sweep index $= \dfrac{(\text{peak c. d.})^2 \times 100}{\text{sweep rate} \times \text{coul/cm}^2}$

BL - Butyrolactone
DMF - Dimethylformamide
PC - Propylene carbonate

TABLE XIII

BEST RECOMMENDED SYSTEMS IN TERMS OF PEAK C. D., PEAK DISPLACEMENT, AND SWEEP INDEX*

System	CV	Cathodic C. D. amps/cm^2	Anodic C. D. amps/cm^2	ΔV_p ** volts	S_c ***
CuF_2/DMF-$LiPF_6$	1525	1.86	1.06	0.04	2573
Cd/DMF-$LiBF_4$	3273	1.22	1.22	0.06	1400
Cd/DMF-$LiClO_4$	2690	0.78	1.04	0.08	1267
$CuCl_2$/DMF-$LiPF_6$	2300	0.70	0.59	0.04	1080
ZnF_2/DMF-KPF_6	3684	0.49	0.40	0.01	559
Zn/DMF-$LiClO_4$	2675	0.47	0.47	0.09	563

* In order of decreasing peak discharge c. d.

** ΔV_p - Peak displacement

*** S_c - Sweep index = $\dfrac{(\text{peak c. d.})^2 \times 100}{\text{sweep rate} \times \text{coul/cm}^2}$

DMF - Dimethylformamide

III. ELECTRODE COMPATIBILITY

A. INTRODUCTION

Although 24 systems represent only a small percentage of the total number screened, this quantity is nevertheless a large number to evaluate in an extensive cell development program. It is therefore necessary to decrease this to a workable value by a process of elimination. The most obvious approach is to eliminate those cathodic materials least compatible with their electrolyte counterpart. It is recognized that the degree of compatibility of a given material is probably a function of its method of preparation and physical state. Since, however, electrochemical characterization was done using wire electrodes, this same form should be screened in terms of compatibility.

Generally, compatibility tests are made by observing solution color changes, and analysis of the solution for dissolved electrode material. The prime consideration, however, is the capacity retention of a battery as a function of wet-stand during either its operating or shelf life. (In the case of secondary batteries whose electrochemical systems permit restoration of active material by charging, then the consideration of a suitable membrane becomes an important practical consideration).

Capacity retention of the wire electrodes was chosen as the basis for determining the relative compatibility of the recommended systems. Essentially, the procedure consists of charging the electrodes and allowing them to remain at open circuit for various stand time intervals, after which they are discharged. Compatibility was then measured by comparing the amount of discharge obtained after a given stand time interval with that obtained at zero stand time.

B. EXPERIMENTAL

1. Standard Compatibility Test

The electrode was preconditioned by sweep cycling at 40 mv/sec over a 2-volt range (±1.0 v relative to the ocv) for a maximum of ten cycles, by which time reproducible sweep curves were obtained. It was then completely discharged galvanostatically at 1 ma/cm^2 to assure the absence of cathodic material. The electrode was then charged by a single anodic sweep which was cut off just prior to entry into the cathodic region, at which point it was again discharged at 1 ma/cm^2. The length of this discharge was expressed in terms of millicoulombs (mcoul) delivered per cm^2 of electrode area at zero stand time.

The same procedure was repeated, but allowing the electrode to stand in the charged condition for progressively longer periods of time, after which it was discharged at 1 ma/cm^2. The number of mcoul/cm^2 delivered after various stand times was then compared with that delivered at zero stand time, and expressed as a percentage of the latter. Test stand times of 15 minutes, 1 hour, 24 hours, and 1 week were to be selected, or until the system suffered a loss of discharge 50% or greater relative to the initial discharge at zero stand time.

2. Effect of Charge Method on Compatibility

In addition to charging the electrodes by anodic sweep, electrodes were also charged galvanostatically and potentiostatically for various time periods. Electrode pretreatment, prior to charging at constant potential, involved cycling the electrode at positive and negative values of the applied potential several times to obtain an active surface. Pretreatment for constant current measurements involved cycling by sweep voltammetry several times at 200 mv/sec. In one instance, constant current charge was employed without pretreatment.

For tests made with silver electrodes in aqueous KOH solution, a minimum of three zero stand time discharge measurements were taken for each test run (a test run comprises a set of measurements performed at various time intervals on a given cell). Zero stand time reproducibility was better than 10% for the sweep charge method. Reproducibility of the zero stand time for constant current charging was better than ±1% for the low charge density electrodes, and within 10% for the high charge density electrodes.

The Wenking TR61 potentiostat was used in the galvanostatic mode for the constant current measurements. The sweep and constant potential charge methods were performed using the operational amplifier equipment described in an earlier report (Ref. 3, p. 93).

C. RESULTS AND DISCUSSION

1. Standard Compatibility Test

Seven systems, comprising zinc, cadmium, copper, and silver difluoride in dimethylformamide or propylene carbonate solutions of KPF_6, $LiPF_6$, $LiBF_4$ or $LiClO_4$, were subjected to the standard compatibility test. Since all systems suffered greater than 50% loss of discharge after 15 minutes stand time, an additional 5-minute stand time interval was measured in all cases. A minimum of three zero stand time measurements was recorded in all tests. The reproducibility of the zero stand time varied with each system from a few percent to as much as 50% in one or two instances. Table XIV lists the zero stand time capacity (mcoul/cm^2 delivered at 1 ma/cm^2 immediately after completion of the sweep charge), and the percent of zero stand time capacity retained after 5 and 15 minutes of stand, for the systems evaluated.

2. Comparison with Silver Oxide in KOH

The rapid loss of capacity in less than 15 minutes of stand time, made it mandatory that these results be compared with a state-of-the-art battery

TABLE XIV

CAPACITY RETENTION AFTER 5
AND 15 MINUTES OF STAND TIME*

System	Zero Stand Time Capacity Millicoul/cm^2	% Retention After 5 min %	15 min %
Zn/DMF-KPF_6 (0.75 m)	204	-	1.5
Zn/DMF-KPF_6 (2.0 m)	256	-	1.0
Zn/PC-KPF_6 (0.75 m)	106	29.0	2.0
Zn/DMF-$LiClO_4$ (1.0 m)	89	0.0	0.0
Cd/DMF-$LiClO_4$ (1.0 m)	230	1.6	0.0
AgF_2/PC-$LiBF_4$ (0.5 m)	249	14.5	2.0
Cu/DMF-$LiPF_6$ (0.5 m)	276	17.0	4.0

* Electrodes charged by anodic sweep and discharged galvanostatically at 1 ma/cm^2.

DMF - Dimethylformamide
PC - Propylene carbonate

system. Measurements were therefore repeated with a silver wire electrode in an aqueous 8.0 m KOH solution. Not only was the capacity retention much greater (82% after 15 minutes stand time), but there appeared to be an improvement in compatibility (measured as capacity retention) by increasing the charge density, i.e., the number of coulombs/cm^2 of electrode surface. This is shown in Figure 37.. Curve A shows the capacity retention of a silver oxide electrode formed by constant current charge of 1 ma/cm^2 for 30 minutes (equivalent to 1800 mcoul/cm^2). The charge density obtained by discharging the electrode at 1 ma/cm^2 at zero stand time, is 1500 mcoul/cm^2. (This is equivalent to 83.5% utilization efficiency). Curve B, with a charge density of only 230 mcoul/cm^2 shows a greater loss of capacity, such that after 15 hours of stand time, only 30%of the original silver oxide (at zero stand time) remains, compared with 65%for the higher charge density (1500 mcoul/cm^2). Although Curve C represents silver oxide formed by sweep charge, the charge density of 170 mcoul/cm^2 results in a still lower capacity retention, which is more marked during the initial hours.

Even though the results shown in Figure 37 indicate enhancement of compatibility for the high charge density electrodes, additional experiments in solutions saturated with charged-state reactants should be carried out before any definite conclusion can be made.

3. Effect of Charging Method

Based on the observation that silver electrodes exhibit greater capacity retention by increasing the initial charge density, a limited effort was made to increase the charge density of the wire electrodes, using charging methods other than by sweep charging. Zinc electrodes were charged in DMF-KPF_6 and PC-KPF_6 under constant current and constant potential conditions, and then discharged at 0.1 and 1.0 ma/cm^2. Only in the case of PC-KPF_6 under potentiostatic charging, was there an increase

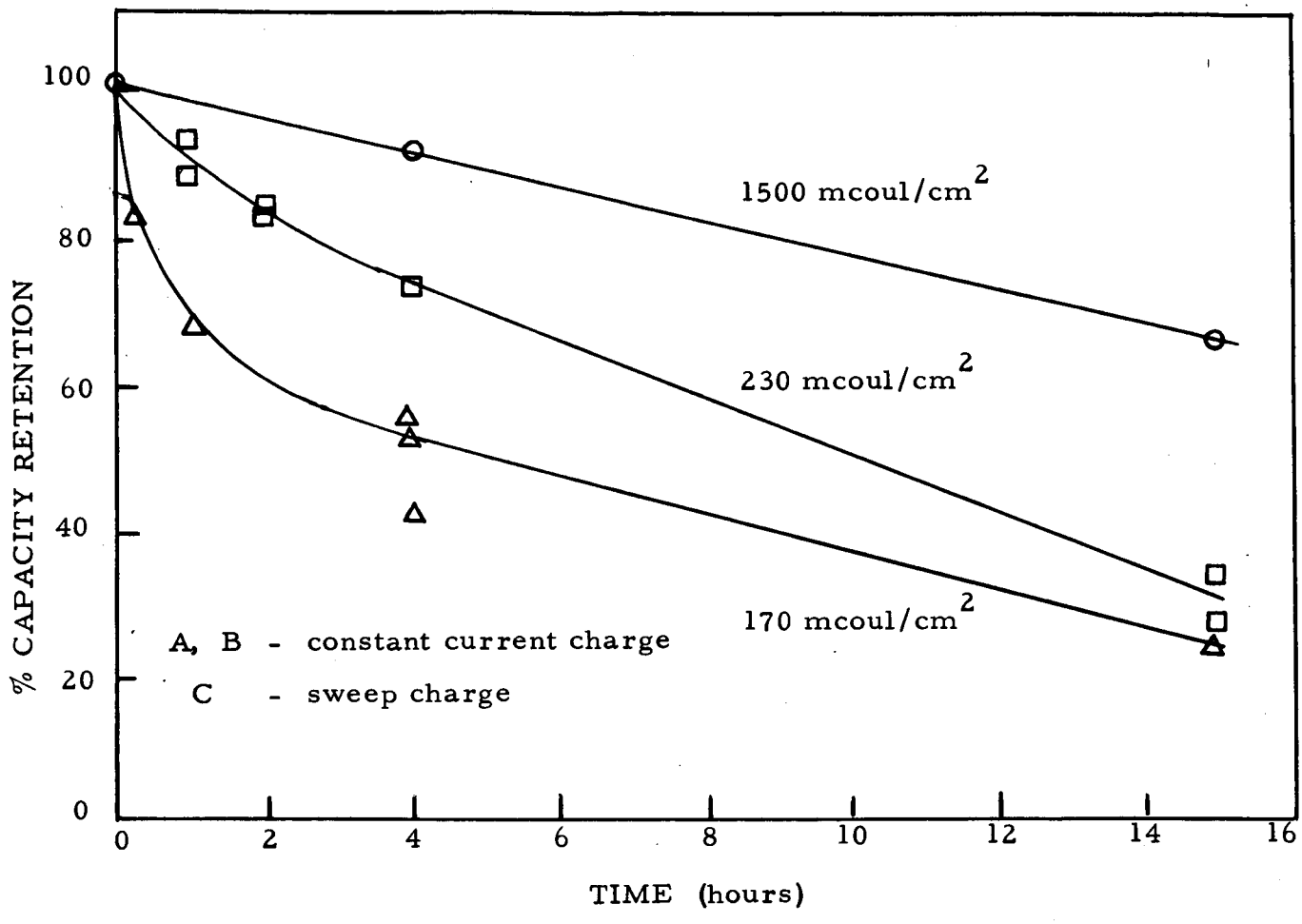

Figure 37. Capacity retention as a function of stand time and charge density for a silver electrode in 8.0 m KOH.

in charge density. In all cases, galvanostatic charging gave lower charge densities. These electrodes had been charged without preconditioning, however, in one case, where the electrode was given the standard pre-treatment (cyclic sweep at 200 mv/s), there was a decided increase in charge density over the non-treated electrodes.

None of the charging methods tested resulted in significant improvement of capacity retention. An apparent improvement in retention was observed when discharge was carried out at the lower current density (0.1 ma/cm^2).

4. Measurements in Saturated Solution

The observed loss of capacity during stand time leads one to the immediate conclusion that active electrode material must be dissolving in the electrolyte, and therefore the systems evaluated are not compatible. If electrode dissolution exists, then a given electrode should exhibit a much longer discharge time in a solution saturated with the electrode active material, than in one initially free of such material. A zinc electrode was therefore potentiostatically charged with continuous stirring for several hours in KPF_6 solution of dimethylformamide, until approximately 300 coulombs of zinc had reacted. Since the solution appeared cloudy, and clumps of dark grey material were evident at the bottom of the electrolysis cell, a saturated solution was indicated. In confirmation of this, the solution was analyzed polarographically, and the zinc ion concentration was found to be 5.9×10^{-3} M. The total electrolyte volume in the cell was 20 ml. If all 300 coulombs of zinc had been able to dissolve, this would have given a zinc concentration of 78.0×10^{-3} M, more than an order of magnitude larger than found by analysis, thus confirming solution saturation.

Using this solution (saturated with Zn ion introduced under charging conditions) a fresh zinc electrode was charged and discharged according to the standard procedure for determining compatibility. No improvement in charge retention was evident. These results suggest that the loss of

discharge on standing is not caused by solution of the electroactive material from the electrode surface. Related measurements on zinc-plated nickel wire demonstrated significantly larger capacity retention, suggesting that the physical nature of the electrode surface may be an important criterion of charge retention. If this is so, then compatibility measurements on smooth wire electrodes may not be valid.

IV. REFERENCES

1. Whittaker Corporation, Narmco R and D Division, Fifth Quarterly Report. NASA Contract 3-8509, NASA Report CR-72293, August 1967.

2. Whittaker Corporation, Narmco R and D Division, Sixth Quarterly Report, NASA Contract 3-8509, NASA CR-72349, November 1967.

3. Whittaker Corporation, Narmco R and D Division, First Quarterly Report, NASA Contract 3-8509, NASA Report CR-72069, August 1966.

DISTRIBUTION LIST

National Aeronautics and Space Admin.
Washington, D. C. 20546
Attn: E. M. Cohn/RNW
A. M. Greg Andrus/PC

National Aeronautics and Space Admin.
Goddard Space Flight Center
Greenbelt, Maryland 20771
Attn: T. Hennigan, Code 716.2
J. Sherfey, Code 735
P. Donnelly, Code 636.2
E. R. Stroup, Code 636.2

National Aeronautics and Space Admin.
Langley Research Center
Instrument Research Division
Hampton, Virginia 23365
Attn: J. L. Patterson, MS 234
M. B. Seyffert, MS 112

National Aeronautics and Space Admin.
Langley Research Center
Hampton, Virginia 23365
Attn: S. T. Peterson
Harry Ricker

National Aeronautics and Space Admin.
Lewis Research Center
21000 Brookpark Road
Cleveland, Ohio 44135
Attn: Library, MS 60-3
N. D. Sanders, MS 302-1
John E. Dilley, MS 500-309
B. Lubarsky, MS 500-201
H. J. Schwartz, MS 500-201
R. B. King, MS 500-201 (2cys.)
V. F. Hlavin, MS 3-14 (Final only)
M. J. Saari, MS 500-202
J. J. Weber, MS 3-19
Report Control, MS 5-5
Dr. J. S. Fordyce, MS 6-1

National Aeronautics and Space Admin.
Scientific and Tech. Information Facility
P. O. Box 33
College Park, Maryland 20740
Attn: Acquisitions Branch (SQT-34054)
(2 cys. + 1 repro.)

National Aeronautics and Space Admin.
George C. Marshall Space Flight Center
Huntsville, Alabama 35812
Attn: Philip Youngblood
R. Boehme, Bldg. 4487.BB,
M-ASTR-EC

National Aeronautics and Space Admin.
Manned Spacecraft Center
Houston, Texas 77058
Attn: W. R. Dusenbury, Propulsion
and Energy Systems
R. Cohen (KS 111)
R. Ferguson (EP-5)
F. E. Eastman (EE-4)

National Aeronautics and Space Admin.
Ames Research Center
Pioneer Project
Moffett Field, California 94035
Attn: J. R. Swain
A. S. Hertzog
J. Rubenzer, Biosatellite Project

Jet Propulsion Laboratory
4800 Oak Grove Drive
Pasadena, California 91103
Attn: A. Uchiyama

U. S. Army Engineer R and D Labs.
Fort Belvoir, Virginia 22060
Attn: Electrical Power Branch
SMOFB-EP

Commanding Officer
U. S. Army Electronics R and D Labs.
Fort Monmouth, New Jersey 07703
Attn: Power Sources Div.,
Code SELRA/PS

Research Office
R and D Directorate
Army Weapons Command
Rock Island, Illinois 61201
Attn: G. Riensmith, Chief

U. S. Army Research Office
Box CM, Duke Station
Durham, North Carolina 27706
Attn: Dr. W. Jorgensen

U. S. Army Research Office
Chief, R and D
Department of the Army
3 D 442, The Pentagon
Washington, D. C. 20546

Harry Diamond Laboratories
Room 300, Bldg. 92
Conn. Ave and Van Ness St., NW
Washington, D. C. 20438
Attn: N. Kaplan

Army Materiel Command
Research Division
AMCRD-RSCM-T-7
Washington, D. C. 20315
Attn: J. W. Crellin

Army Materiel Command
Development Division
AMCRO-DE-MO-P
Washington, D. C. 20315
Attn: M. D. Aiken

U.S. Army TRECOM
Fort Eustis, Virginia 23604
Attn: Dr. R. L. Echols (SMOFE-PSG)
L. M. Bartone (SMOFE-ASE)

U. S. Army Mobility Command
Research Division
Watten, Michigan 48090
Attn: O. Renius (AMSMO-RR)

U. S. Army R and L Liaison Group
(9851 DV) APO 757
New York, New York 10004
Attn: B. R. Stein

Office of Naval Research
Department of the Navy
Washington, D. C. 20360
Attn: Head, Power Branch, Code 429
H. W. Fox, Code 425

Naval Research Laboratory
Washington, D. C. 20390
Attn: Dr. J. C. White, Code 6160

U. S. Navy
Marine Engineering Laboratory
Annapolis, Maryland 21402
Attn: J. H. Harrison

Bureau of Naval Weapons
Department of the Navy
Washington, D. C. 20360
Attn: W. T. Beatson, Code RAAE-52
M. Knight, Code RAAE-50

Naval Ammunition Depot
Crane, Indiana 47522
Attn: E. Bruess
H. Schultz

Naval Ordnance Laboratory
Department of the Navy
Corona, California 91720
Attn: W. C. Spindler, Code 441

Army Reactors, DRD
U. S. Atomic Energy Commission
Washington, D. C. 20545
Attn: D. B. Hoatson

Naval Ordnance Laboratory
Department of the Navy
Silver Springs, Maryland 20900
Attn: P. B. Cole, Code WB

Bureau of Ships
Department of the Navy
Washington, D. C. 20360
Attn: B. B. Rosenbaum, Code 340
C. F. Viglotti, Code 660

Space Systems Division
Los Angeles AF Station
Los Angeles, California 90045
Attn: SSSD

Air Force Cambridge Research Lab.(CRFE)
L. G. Hanscom Field
Bedford, Massachusetts 01731
Attn: Dr. Richard Payne

Flight Vehicle Power Branch
Aero Propulsion Laboratory
Wright-Patterson AFB, Ohio 45433
Attn: J. E. Cooper

Headquarters, USAF (AFRDR-AS)
Washington, D. C. 20546
Attn: Maj. G. Starkey
Lt. Col. W. G. Alexander

Rome Air Development Center, ESD
Griffis AF Base, New York 13442
Attn: F. J. Mollura (RASSM)

National Bureau of Standards
Washington, D. C. 20234
Attn: Dr. W. J. Hamer

Office DDR and E, USE and BSS
The Pentagon
Washington, D. C. 20310
Attn: G. B. Wareham

Institute for Defense Analyses
R and E Support Division
400 Army-Navy Drive
Arlington, Virginia 22022
Attn: R. Hamilton
Dr. G. C. Szego

U. S. Atomic Energy Commission
Auxiliary Power Branch (SNAP)
Division of Reactor Development
Washington, D. C. 20545
Attn: Lt. Col. G. H. Ogburn, Jr.

U. S. Atomic Energy Commission
Advanced Space Reactor Branch
Division of Reactor Development
Washington, D. C. 20545
Attn: Lt. Col. J. H. Anderson

Office of Technical Services
Department of Commerce
Washington, D. C. 20009

Aerojet-General Corporation
Von Karman Center
Building 312/Dept. 3111
Azusa, California 91703

Aeronutronic Division
Philco Corporation
Ford Road
Newport Beach, California 92660

Aerospace Corporation
P. O. Box 95085
Los Angeles, California 90045
Attn: Library

Burgess Battery Company
Foot of Exchange Street
Freeport, Illinois 61032
Attn: Dr. Howard J. Strauss

Aerospace Corporation
Systems Design Division
2350 East El Segundo Boulevard
El Segundo, California 90246
Attn: John G. Krisilas

Allis-Chalmers Manufacturing Company
Research Division Library
P. O. Box 512
Milwaukee, Wisconsin 53201

American University
Massachusetts and Nebraska Avenues NW
Washington, D. C. 20016
Attn: Dr. R. T. Foley, Chemistry Dept.

Arthur D. Little, Incorporated
Acorn Park
Cambridge, Massachusetts 02140
Attn: Dr. Ellery W. Stone

Atomics International Division
North American Aviation, Incorporated
8900 DeSoto Avenue
Canoga Park, California 91304
Attn: Dr. H. L. Recht

Battelle Memorial Institute
505 King Avenue
Columbus, Ohio 43201
Attn: Dr. C. L. Faust

Bell Laboratories
Murray Hill, New Jersey 07971
Attn: U. B. Thomas

The Boeing Company
P. O. Box 3707
Seattle, Washington 98124

Borden Chemical Company
Central Research Laboratory
P. O. Box 9524
Philadelphia, Pennsylvania 19124

C and D Batteries
Division of Electric Autolite Company
Conshohocken, Pennsylvania 19428
Attn: Dr. Eugene Willihnganz

Calvin College
Grand Rapids, Michigan 49506
Attn: Prof. T. P. Dirkse

Catalyst Research Corporation
6101 Falls Road
Baltimore, Maryland 21209
Attn: J. P. Wooley

ChemCell, Incorporated
150 Dey Road
Wayne, New Jersey 07470
Attn: Peter D. Richman

Delco-Remy Division
General Motors Corporation
2401 Columbus Avenue
Anderson, Indiana 46011
Attn: Dr. J. J. Lander

Douglas Aircraft Company, Incorporated
Astropower Laboratory
2121 Campus Drive
Newport Beach, California 92663

Dynatech Corporation
17 Tudor Street
Cambridge, Massachusetts 02138
Attn: R. L. Wentworth

Eagle-Pitcher Company
P. O. Box 47
Joplin, Missouri 64802
Attn: E. M. Morse

General Electric Company
Battery Products Section
P. O. Box 114
Gainesville, Florida 32601
Attn: Dr. R. L. Hadley

Elgin National Watch Company
107 National Street
Elgin, Illinois 60120
Attn: T. Boswell

Electric Storage Battery Company
Missile Battery Division
2510 Louisburg Road
Raleigh, North Carolina 27604
Attn: A. Chreitzberg

Electric Storage Battery Company
Carl F. Norberg Research Center
Wardley, Pennsylvania 19068
Attn: Dr. R. A. Schaefer

Electrochimica Corporation
1140 O'Brien Drive
Menlo Park, California 94025
Attn: Dr. Morris Eisenberg

Electro-Optical Systems, Incorporated
300 North Halstead
Pasadena, California 91107
Attn: E. Findl

Emhart Manufacturing Company
Box 1620
Hartford, Connecticut 06101
Attn: Dr. W. P. Cadogan

Englehard Industries, Incorporated
497 Delancy Street
Newark, New Jersey 07105
Attn: Dr. J. G. Cohn

Dr. Arthur Fleischer
466 South Center Street
Orange, New Jersey 07050

Grumman Aircraft
CPGS Plant 35
Beth Page, Long Island, New York 11101
Attn: Bruce Clark

General Electric Company
Research and Development Center
Schenectady, New York 12301
Attn: Dr. H. Liebhafsky
Dr. R. C. Osthoff, Bldg. 37.

General Telephone and Electronics Labs.
Bayside, New York 11352
Attn: Dr. Paul Goldberg

Globe-Union, Incorporated
900 East Keefe Avenue
Milwaukee, Wisconsin 53201
Attn: Dr. Warren Towle

Gould-National Batteries, Incorporated
Engineering and Research Center
2630 University Avenue, SE
Minneapolis, Minnesota 55418
Attn: D. L. Douglas

Gulton Industries
Alkaline Battery Division
212 Durham Avenue
Metuchen, New Jersey 08840
Attn: Dr. Robert Shair

Leesona Moos Laboratories
Lake Success Park, Community Drive
Great Neck, New York 11021
Attn: Dr. H. Oswin

Livingston Electronic Corporation
Route 309
Montgomeryville, Pennsylvania 18936
Attn: William F. Meyers

Hughes Aircraft Corporation
Centinela Avenue and Teale Street
Culver City, California 90230
Attn: T. V. Carvey

Hughes Aircraft Corporation
Building 366, MS 524
El Segundo, California 90245
Attn: R. B. Robinson

Hughes Research Labs. Corp.
2011 Malibu Canyon Road
Mailbu, California 90265
Attn: T. M. Hahn

ITT Federal Laboratories
500 Washington Avenue
Nutley, New Jersey 07110
Attn: Dr. P. E. Lightly

IIT Research Institute
10 West 35 Street
Chicago, Illinois 60616
Attn: Dr. H. T. Francis

Idaho State University
Department of Chemistry
Pocatello, Idaho 83201
Attn: Dr. G. Myron Arcand

Institute of Gas Technology
State and 34 Street
Chicago, Illinois 60616
Attn: B. S. Baker

John Hopkins University
Applied Physics Laboratory
8621 Georgia Avenue
Silver Springs, Maryland 20910

Lockheed Missiles and Space Co.
3251 Hanover Street
Palo Alto, California 94304
Attn: Library
Dr. G. B. Adams

Lockheed Missiles and Space Co.
Department 52-30
Palo Alto, California 94304
Attn: J. E. Chilton

Lockheed Missiles and Space Co.
Department 65-82
Palo Alto, California 94304
Attn: Larry E. Nelson

P. R. Mallory and Co., Inc.
Technical Services Laboratory
Indianapolis, Indiana 46206
Attn: A. S. Doty

P. R. Mallory and Co., Inc.
3029 East Washington Street
Indianapolis, Indiana 46206
Attn: Library

Marquardt Corporation
16555 Saticoy Street
Van Nuys, California 91406
Attn: Dr. H. G. Krull

Philco Corporation
Division of Ford Motor Company
Blue Bell, Pennsylvania 19422
Attn: Dr. Phillip Cholet

Radiation Applications, Inc.,
36-40 37th Street
Long Island City, New York 11101

Material Research Corporation
Orangeburg, New York 10962
Attn: V. E. Adler

Melpar
Technical Information Center
3000 Arlington Boulevard
Falls Church, Virginia 22046

Metals and Control Division
Texas Instruments, Inc.
34 Forest Street
Attleboro, Massachusetts 02703
Attn: Dr. E. M. Jost

Midwest Research Institute
425 Volker Boulevard
Kansas City, Missouri 64110
Attn: Dr. B. W. Beadle

Monsanto Research Corporation
Everett, Massachusetts 02149
Attn: Dr. J. O. Smith

North American Aviation, Inc.
Rocketdyne Division
6633 Canoga Avenue
Canoga Park, California 91303
Attn: Library

Ozark Mahoning Company
1870 S. Boulder Avenue
Tulsa, Oklahoma 74119
Attn: Dr. James Beal

Power Information Center
University of Pennsylvania
3401 Market Street, Room 2107
Philadelphia, Pennsylvania 19104

Tyco Laboratories, Inc.
Bear Hill
Hickory Drive
Waltham, Massachusetts 02154
Attn: W. W. Burnett

Radio Corporation of America
Astro Division
Highstown, New Jersey 08520
Attn: Seymour Winkler

Radio Corporation of America
P. O. Box 800
Princeton, New Jersey 08540
Attn: L. Schulman

Sandia Corporation
Box 5800
Albuquerque, New Mexico 87115
Attn: Technical Library (2 copies)

Sonotone Corporation
Saw Mill River Road
Elmsford, New York 10523
Attn: A. Mundel

Texas Instruments, Inc.
13500 North Central Expressway
Dallas, Texas 75222
Attn: Dr. Isaac Trachtenberg

Thomas A. Edison Research Lab.
McGraw Edison Company
Watchung Avenue
West Orange, New Jersey 07052
Attn: Dr. P. F. Grieger

TRW Incorporated
TRW Systems Group
One Space Park
Redondo Beach, California 90278
Attn: Dr. A. Krausz, Bldg. 60, Rm 1470

TRW Incorporated
23555 Euclid Avenue
Cleveland, Ohio 44117
Attn: Librarian

Union Carbide Corporation
Development Laboratory Library
P. O. Box 6056
Cleveland, Ohio 44101

Union Carbide Corporation
Parma Research Center
P. O. Box 6116
Cleveland, Ohio 44101
Attn: Library

University of California
Space Science Laboratory
Berkeley, California 94720
Attn: Dr. C. W. Tobias

University of Pennsylvania
Electrochemistry Laboratory
Philadelphia, Pennsylvania 19104
Attn: Prof. J. O'M Brockris

University of Toledo
Toledo, Ohio 43606
Attn: Dr. Albertine Krohn

Western Electric Company
Suite 802, RCA Building
Washington, D. C. 20006
Attn: R. T. Fiske

Westinghouse Electric Corporation
Research and Development Center
Churchill Borough
Pittsburgh, Pennsylvania 15235
Attn: Dr. A. Langer

Whittaker Corporation
Power Sources Division
3850 Olive Street
Denver, Colorado 80237
Attn: J. W. Reiter
Dr. E. Doucette

Whittaker Corporation
Narmco R and D Division
12032 Vose Street
North Hollywood, California 91605
Attn: Dr. M. Shaw

Yardney Electric Corporation
40-50 Leonard Street
New York, New York 10013
Attn: Dr. George Dalin